DOI:10.14753/SE.2018.2123

SUBCELLULAR DISTRIBUTION OF VOLTAGE-GATED ION CHANNELS IN THE HIPPOCAMPUS

PhD thesis

Tekla Kirizs M.D.

János Szentágothai Doctoral School of Neurosciences
Semmelweis University

Supervisor: Zoltán Nusser, D.Sc.

Official reviewers:
Anna L. Kiss, M.D., Ph.D.
Katalin Halasy, D.Sc.

Head of the Final Examination Committee:
Péter Enyedi, M.D., D.Sc.

Members of the Final Examination Committee:
Katalin Schlett, Ph.D.
Tibor Zelles, M.D., Ph.D.

Budapest, 2017

DOI:10.14753/SE.2018.2123

TABLE OF CONTENTS

DOI:10.14753/SE.2018.2123

DOI:10.14753/SE.2018.2123

1. The list of Abbreviations

+ - positive

* - $P < 0.05$

** - $P \leq 0.01$

*** - $P \leq 0.001$

aa. - amino acid

4-AP - 4-aminopyridine

AIS - axon initial segment

AMPA - α-amino-3-hydroxy-5-methyl-4-isoxazole propionate

Ank-G - Ankyrin-G

AP - action potential

associational/commissural - A/C

AZ - active zone

BSA - bovine serum albumin

Ca_v - voltage gated calcium channel

CB1 - cannabinoid receptor type 1

CCK - cholecystokinin

CNS - central nervous system

D - dimensional

E-face - exoplasmic-face

Elfn1 - extracellular leucine- rich repeat fibronectin-containing protein 1

EPSC - excitatory postsynaptic current

EPSP - excitatory postsynaptic potential

GABA - γ-aminobutyric acid

GAD - glutamate decarboxylase

GluR - ionotropic glutamate receptor

HA - hemagglutinin

HCN - hyperpolarization-activated cyclic-nucleotide-gated channels

I_A - A-type, K^+ current

I_D - α-dendrotoxin-sensitive delayed rectifier current

I_K - TEA and 4-AP sensitive dendrotoxin-insensitive delayed rectifier current

IMP - intramembrane particle

IN - interneuron

IPSC - inhibitory postsynaptic current

IPSP - inhibitory postsynaptic potential

K_v - voltage gated potassium channel

mGluR - metabotropic glutamate receptor

Na_v - voltage gated sodium channel

NGS - normal goat serum

NL-2 - Neuroligin-2

NMDA - N-methyl-D-aspartate

O-Bi cell - oriens-bistratified cell

O-LM cell - oriens-lacunosum-moleculare cell

P-face - protoplasmic-face

PA - picric acid

PALM - photoactivation localization microscopy

pan-NF - pan-Neurofascin

PB - phosphate buffer

PC - pyramidal cell

PFA - paraformaldehyde

PSD - postsynaptic density

Pr - release probability

PV - parvalbumin

SD - standard deviation

SDS - sodium dodecylsulphate
SDS-FRL - sodium dodecylsulphate-digested freeze-fracture replica labeling
SIM - structural illumination microscopy
SL - *stratum lucidum*
SLM - *stratum lacunosum-moleculare*
SO - *stratum oriens*
SP - *stratum pyramidale*
SR - *stratum radiatum*
STED - stimulation emission depletion microscopy
TBS - Tris-buffered saline
TEA - tetraethylammonium
VGAT - vesicular GABA transporter

2. Introduction

2.1. Differential expression and subcellular distribution of ion channels underlies functional heterogeneity

Our brain's ability to process, store and retrieve information about the continuously changing internal and external world, and to effectively perform widely different functions, is supported by a remarkable diversity of its building blocks (neurons) and an astonishingly complex dynamic connectivity (synaptic) between them. Already at the turn of the 20th century, the pioneering work of Camillo Golgi[1], Santiago Ramon'y Cajal[2] and Rafael Lorent de No[3] began to reveal the complexity and diversity of neuronal morphology. Later on, with the development of modern molecular and electrophysiological techniques, the molecular and functional diversity of neurons was also recognized.

A prominent example of the molecular diversity of nerve cells is the expression of many members of the large ion channel superfamily (*e. g.* more than 100 subunits of K^+ channels[4]) with a staggering number of distinct types of ion channels in their plasma membranes[5]. Among these, voltage- and ligand-gated ion channels are of particular significance due to their powerful role in controlling the activity of neurons (Figure 1). For example, voltage-gated ion channels (*e. g.* Na^+ (Na_v), K^+ (K_v), Ca^{2+} (Ca_v) channels)[4,5] are responsible for the generation and propagation of action potentials (APs)[6], which are believed to be the elementary units of rapid signaling of nerve cells. More than fifty years ago Hodgkin and Huxley demonstrated that APs arise from subsequent changes in the membrane's permeability to Na^+ and K^+ ions[7]. Later on, the presence of ion-selective channels in neuronal membranes was proved by patch-clamp recordings[8] measuring ionic currents flowing through individual ion channels[9]. It was shown that ion channels present in the axon initial segment (AIS) of neurons (*e.g.* Na_v, $K_v1–3$, K_v7, Ca_v) will set the AP threshold and influence the AP generation and propagation along the neurites[10-12]. When the AP reaches the axon terminals, evokes the release of neurotransmitter containing vesicles, which will traverse the synaptic cleft and bind to postsynaptic ligand-gated ion channels (*e. g.* AMPA, NMDA, $GABA_A$ receptors)[13-17] transferring information from the presynaptic cell to the postsynaptic neuron. This process of synaptic transmission is governed by the activity of Ca_v, K_v and

Na_v channels[18] present in presynaptic axon terminals. On the postsynaptic side, the activation of ligand-gated ion channels induces local changes in the membrane potential that spread from their site of generation towards the soma and AIS, and are modified by dendritic ion channels (*e.g.* $K_v4.2$, Ca_v, Na_v, and HCN channels)[19-21]. It was also demonstrated that dendritically localized voltage-gated ion channels (Na_v) support the active 'back-propagation' of axonally generated APs into the dendritic tree, which will influence synaptic transmission, strength and synaptic integration[22].

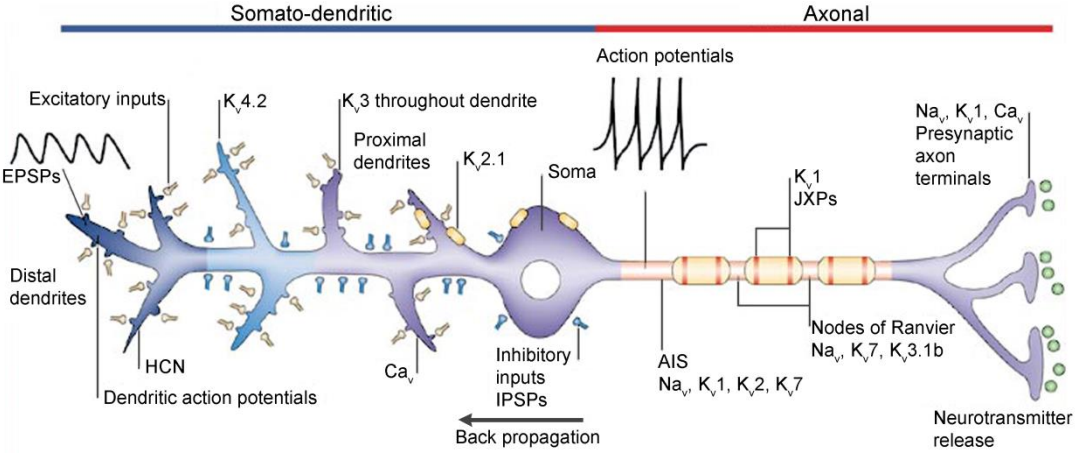

Figure 1. Subcellular compartment-specific distribution of voltage-gated ion channels and their main functional roles in a model neuron. Canonically, excitatory inputs (EPSPs–postsynaptic potentials; yellow boutons) activate AMPA, NMDA receptors and evoke local depolarization. Inhibitory inputs (IPSPs–inhibitory postsynaptic potentials; blue boutons) activate GABA type A ($GABA_A$) receptors, and evoke hyperpolarization. These signals spread to the soma, then to the AIS where APs are generated, if the evoked changes in membrane potantial exceed a treshold. In general, Na_v channels and a subset of K_v channels (K_v1, K_v2, $K_v3.1b$, K_v7) are present in the AIS, nodes of Ranvier, juxtaparanodes (JXPs) of adult myelinated axons where they contribute to the AP generation and propagation. When APs invade the presynaptic nerve terminals, activate Ca_v channels that increase intracellular Ca^{2+} levels thereby triggering neurotransmitter release. In contrast, dendritically localized Ca_v together with Na_v channels are involved in the generation of local dendritic APs. Dendritic K_v, Na_v and HCN channels shape the postsynaptic responses and control the backpropagation of somatic APs. *Modified from* [23].

Following the discovery of the astonishing molecular and functional diversity of ion channels, it became also evident that the functional heterogeneity of neurons is the consequence of the expression of distinct sets of ion channels. Moreover, in addition to the molecular structure of ion channels, their precise subcellular distribution and densities on the surface of nerve cells add another layer of complexity to their functional

impact (reviewed *e.g.* in [23-26]). A particularly revealing example is presented by the $Ca_v2.1$ voltage-gated Ca^{2+} channel subunit (P/Q-type) in cerebellar Purkinje cells[27]. Dendritically localized $Ca_v2.1$ channels play a role in inducing dendritic spikes after climbing fiber[28] or strong parallel fiber activation[29], and in the amplification of excitatory inputs in the distal dendrites[30]. In contrast, when localized to presynaptic axon terminals, these channels induce the Ca^{2+} influx necessary for neurotransmitter release[31].

Currently it is accepted that the combinatorial effect of genetic/molecular diversity and differential subcellular distribution of ion channels provides the basis for the large number of functionally distinct cell types[24,32]. Computational modelling and dynamic clamp studies of Ivan Soltesz and his colleagues also suggested that the diversity of neuronal types in a network has functional relevance, as modifications in heterogeneity influence the behavior of neuronal networks[33-36]. There is now evidence, which indicates that altered neuronal heterogeneity is a common mechanism contributing to various neurological (*e.g.* epilepsy) and psychiatric disorders (*e.g.* schizophrenia)[37].

Altogether, it is no wonder that tremendous efforts have been dedicated to identify the molecular diversity of ion channels and their expression patterns in the mammalian brain (*e.g.* the Allen Brain Atlas). With the experiments presented in this dissertation, I aimed to extend the current knowledge on ion channel distribution, and thereby contribute to the understanding of the complex interplay of channel subtypes underlying signal processing and computation in various neuronal circuits.

2.2. Techniques for studying the subcellular distribution of ion channels

Several approaches have been used to study the subcellular localization of ion channels in the central nervous system (CNS). Since the development of axonal and dendritic patch-clamp techniques[38], a large amount of experimental data have been obtained with this method, revealing the densities of several ligand- and voltage-gated ionic currents in different subcellular compartments of many cell types[39-46]. A great advantage of this technique is that it provides information about the functional state of the studied channels, although the molecular structure (*i.e.* subunit composition) of the channels can not be explored using patch-pipette recordings. Moreover, small axon

terminals, dendritic spines, nodes of Ranvier are still inaccessible for patch-pipette recordings. This is despite the fact that, in addition to relatively large subcellular compartments such as somata, AISs[22,47], main apical dendrites[40,41] and large axon terminals (*e.g.* calyx of Held, mossy terminals of the CA3 region)[48-50], recently this technique has been successfully applied to investigate ion channels in small-diameter dendrites (*e.g.* tuft dendrites)[45] and somewhat smaller boutons as well (*e.g.* stellate cell axon terminals)[51-53].

Immunohistochemistry with subunit specific antibodies can also be used for studying the subcellular distribution of metabotropic and ionotropic receptors. The fluorescent method is the most widely used immunohistochemical method, where fluorophore-coupled secondary antibodies are used to visualize the antigen-antibody complexes. This method has high sensitivity, allows the colocalization of multiple proteins simultaneously; but as the reactions are analyzed with light microscopy, it has a diffraction-limited resolution of more than 200 nm. This is in the size range of spines, active zones (AZs) and postsynaptic densities (PSDs), rendering this method inadequate for the subcellular localization of proteins.

Recently, fluorescence light microscopic techniques capable of nanometer-scale resolution have been developed (stimulation emission depletion (STED), structural illumination microscopy (SIM), single molecule localization microscopy: stochastic optical reconstruction microscopy (STORM) and photoactivation localization microscopy (PALM); reviewed in [54-58]). However, unlike electron microscopy, in case of these techniques visualization of cellular membranes, which is particularly powerful for identifying synapses, requires labeling with antibodies. In addition, multicolor-imaging is still problematic.

Immunogold electron microscopy[59] has a resolution of ~20–30 nm and is indispensable for high-resolution localization and quantification of molecules. The most widely used pre-embedding immunogold method has high sensitivity, but the immunoreaction occurs in thick sections. As antibodies do not evenly penetrate in the sections, quantitative comparison of the signals of profiles localized in different regions is very difficult. Furthermore, the pre-embedding method hardly detects receptors located within the PSD because of the penetration problem and as a result false-negative labeling at synaptic sites is common[60,61]. In the post-embedding method, the

immunoreaction occurs evenly on the surface of ultrathin sections of resin-embedded tissue so problems of penetration are overcome. As synaptic and non-synaptic molecules are labeled with the same sensitivity, this method is more suitable for protein quantification[62]. However, sensitivity can be rather low in that only antigen molecules exposed on the surface of the section are accessible by antibodies[63,64].

The sodium dodecylsulphate-digested freeze-fracture replica labeling (SDS-FRL; reviewed in [65-67]) technique overcomes the mentioned limitations of electron microscopic techniques. The method was originally developed by Fujimoto[68] to visualize two-dimensional (2D) distribution of integral membrane proteins in cellular membranes of rapidly frozen tissue. It is a high-resolution technique which has exceptional sensitivity, with a labeling efficiency reportedly approaching 100% in multiple cases[69,70]. The technique requires the studied tissue to be rapidly frozen under

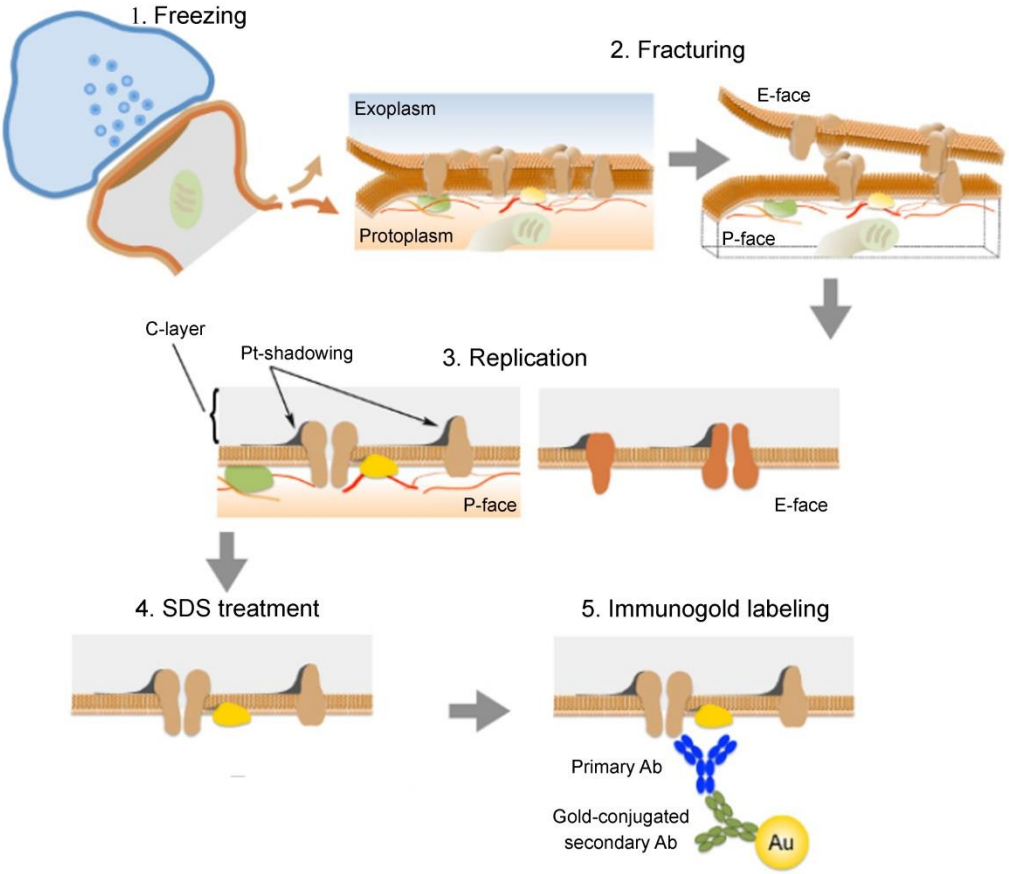

Figure 2. Illustration of the key steps of the SDS-FRL. 1. High pressure freezing of the tissue. 2. The freeze-fracture process splits the lipid bilayer exposing the fracture faces. Proteins in the plasma membrane are allocated onto either E-face or P-face. 3. The specimen is evaporated by carbon–platinum–carbon. 4. The SDS treatment removes cellular components not trapped by the replica. 5. Proteins of interest are

visualized by immunogold reactions. Ab, antibody; Au, gold; C, carbon; Pt, paltinum. *Modified from* [71].

high pressure and then fractured at low temperatures (Figure 2). The fracturing process is random, but the plane of the fracture often passes through the hydrophobic center of membrane lipid bilayers, splitting them into half-membrane leaflets. The membrane half located adjacent to the protoplasm is called protoplasmic-half, while the exposed view of the membrane is called protoplasmic-face (P-face). The membrane half closer to the extracellular space is called exoplasmic-half with the exposed exoplasmic-face (E-face). Integral membrane proteins—revealed as intramembrane particles (IMPs) by freeze-fracture process—that originally spanned the bilayer, are attached either to the E-face or to the P-face. The exposed fracture faces then are covered by evaporating thin layers of carbon, then platinum and again carbon to provide them stability and contrast for electron microscopic visualization. Afterwards, the tissue beneath the replica is dissolved with SDS, leaving only the transmembrane proteins in the membrane halves, which can be selectively labeled in subsequent immunogold reactions. Proteins attached to the E-face can be labeled with antibodies recognizing their extracellular domains, whereas proteins of the P-face can be visualized with antibodies raised against intracellular epitopes.

It is important to acknowledge that the SDS-FRL also has certain limitations[71,72]. First, identification of the different profiles based on morphological features is often difficult. There are only a few structures recognizable based on pure morphology: *e.g.* PSDs of the excitatory synapses are clearly indicated by clusters of IMPs (Figure 3B and D) on the E-face[73-75] of replicas; gap junctions have several distinctive morphologies in replicas such as close packed uniform 8–9 nm diameter IMPs on P-faces and uniform 8–9 nm diameter pits on E-faces[76-78]. Therefore it is frequently necessary to label marker proteins to facilitate identification of the fractured membranes. The availability of different sizes of gold particle conjugated to secondary antibodies enables double- or multiple labelings of proteins in replicas. However, multiple labeling is not without problems and should be performed with caution. If the labeled antigens are present in the same subcellular compartment such as PSD, AZ etc., due to steric hindrance, it is likely that their labeling density will be lower than that observed in single labeling experiments. The ‘mirror replica method’[79] offers an

alternative way to perform colocalization of multiple proteins in the same compartment. With this method, replicas are generated from both matching sides of the fractured

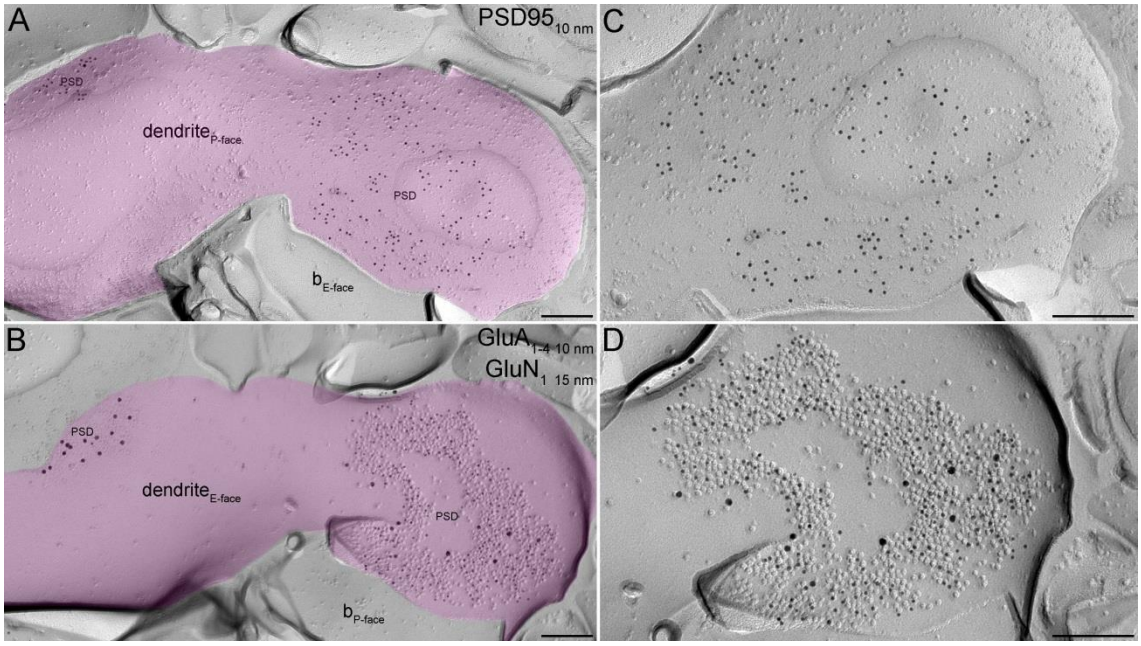

Figure 3 Simultaneous detection of multiple proteins in PSDs with the 'mirror replica method'. (A and B) Complementary E- and P-face images of the same dendritic membrane segment (pseudocolored lilac). The P-face of the putative IN dendrite was labeled for PSD95 (A), whereas the E-face was double-labeled with an antibody labeling the $GluN_1$ subunit (15 nm gold on B) and another one, which recognizes all four subunits of GluA receptors (10 nm gold on B). The PSD95 labeling on the P-face is concentrated over sub-areas of the dendritic membrane that are also labeled for $GluA_{1-4}$ and $GluN_1$ on the complementary E-face of the replicas. All labeling is restricted to PSDs indicated by IMP clusters on the E-face. (C and D) High magnification view of one of the PSDs from (A) and (B), respectively. b, bouton. *Scale bars, 200 nm.*

tissue surfaces, which have a corresponding E- and P-face of exactly the same membranes. Provided suitable antibodies are available, the immunolabeling of our proteins can be performed on separate, but complementary replicas (Figure 3). In addition, if no antibodies are available for the identification of certain profiles or cell-types, transgenic mice or viral vectors expressing membrane markers (*e.g.* membrane-targeted green fluorescent protein or tagged channelrhodopsin; Figure 4) in cell type-specific manner offer additional tools to facilitate identification of the fractured membranes. Viral vectors also carry the possibility of anterograde or retrograde tracing enabling the molecular analysis of specific inputs or outputs of specific cell populations[71].

The second limitation is the consequence of the fracturing itself, which occurs randomly. This makes it impossible to target specific cells, structures or physiologically characterized cells, and can also lead to sampling bias, *e.g.* in synapse collection, because membranes that have different curvatures fracture with different probability (*e.g.* shafts versus spines)[71,72].

Finally, the partition of membrane proteins with either the P-face or the E-face is unpredictable: certain proteins are preferentially allocated, while others are allocated to both faces, as was shown for the glutamate receptor $GluD_2$ in parallel fiber synapses of Purkinje cells in the CB[72] and for $GABA_A$ receptor γ2 in perisomatic synapses of CA1 and PCs[80]. Therefore, the allocation of proteins to the P-face or E-face, particularly for quantitative studies, should be carefully examined using antibodies that are reactive to intracellular and extracellular domains[71,72,75].

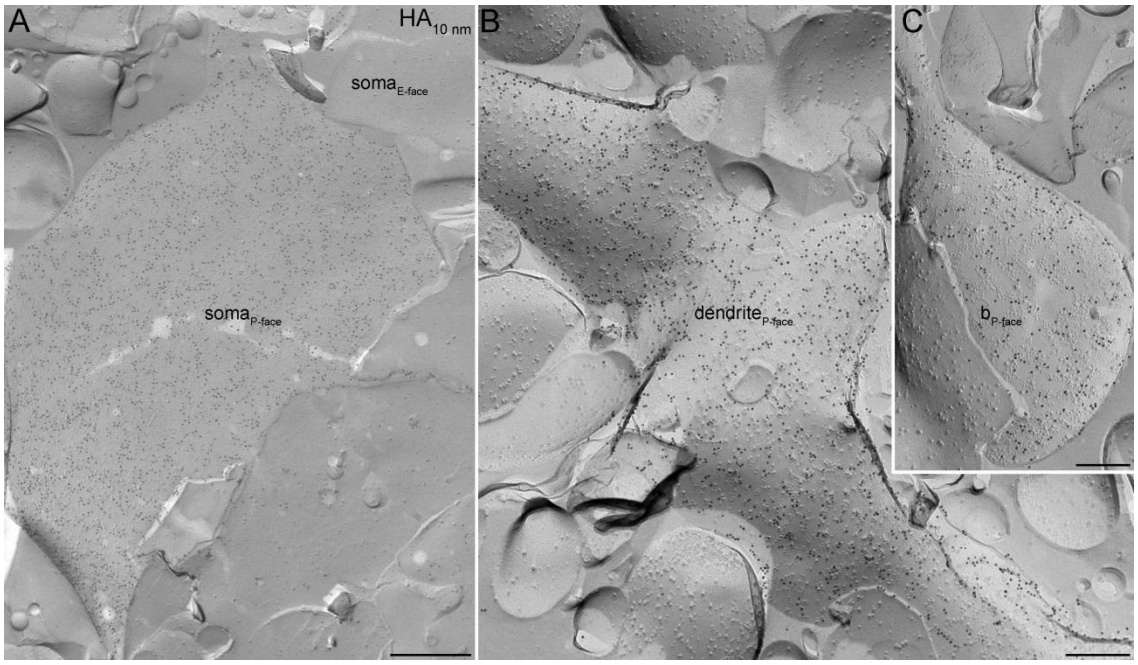

Figure 4. Example for SDS-FRL localization of a virally expressed membrane-targeted protein. (A–C) Hemagglutinin (HA)-tagged channelrhodopsin expression was virally transduced in mouse cortical neurons. The immunolabeling of the HA-tag was present on putative somatic (A), dendritic (B) and axonal (C) plasma membranes. b, bouton. *Scale bars, 500 nm (A); 200 nm (B and C).*

Altogether, the SDS-FRL is a high-resolution technique with exceptional sensitivity, and limitations that can be overcome by careful and prudent design of experiments. I adopted this technique to study the distribution of different K_v and Ca_v

channel subunits in the hippocampal region of the rat brain to further our knowledge on ion channel localization, which may also promote the construction of accurate neuronal models.

2.3. Synaptic organization of the hippocampus

Already there is a large amount of data regarding the distribution of ion channels and their functional relevance in the hippocampus, as this brain region has been the subject of many functional, structural and molecular investigations. In modern neuroscience, the hippocampus serves as a model for studying many key properties of neuronal circuits and nerve cells. This is attributable to its fundamental role in some forms of memory and learning[81,82], as well as to the relatively simple laminar organization of its neurons, coupled with highly organized laminar distribution of many of its inputs[83]. Importantly, the information obtained from this brain region can be effectively extrapolated to the anatomically and functionally far more complex neocortex. In the following, I will provide a concise morphological and functional overview of the hippocampus.

2.3.1. Principal cells of the hippocampus

The hippocampus (*Cornu Ammonis*, CA) is part of a group of structures, called hippocampal formation, which also includes the dentate gyrus and subiculum. The hippocampal formation has a laminar organization that arises because its principal cells are confined to a single layer (*stratum*): the granule cells of the dentate gyrus are organized into the *stratum granulosum*, while the pyramidal cells (PCs) of the Ammon's horn constitute the *stratum pyramidale* (SP). The hippocampus has been divided into subregions termed CA1, CA2 and CA3 regions based on the size and appearance of the PCs[3]. The layers above and below the principal cell layer contain functionally equivalent segments of the principal as well as local interneurons (INs). The main afferent fibers and the recurrent collaterals of principal cells are also organized in a laminar fashion, in a way that the incoming information enters and then leaves the hippocampal formation through a trisynaptic circuit (Figure 5). In the first step, afferent fibers of the perforant path[84,85] carrying polymodal sensory information from the entorhinal cortex synapse onto the dendrites of granule cells of the dentate

gyrus. The axons of granule cells, called mossy fibers, enter the CA3 region, where they terminate on complex spines, called thorny excrescenses, located on proximal dendrites of PCs[86] in the *stratum lucidum* (SL). Finally, the axons of the CA3 PCs, the Schaffer collaterals project either to ipsilateral or contralateral CA1 region, and establish synapses on the basal and apical dendrites of CA1 PCs in the *stratum oriens* (SO) and *stratum radiatum* (SR), respectively. The main extrinsic projections of the CA1 PCs are to the subiculum and to the layer V of the entorhinal cortex. Later additional excitatory

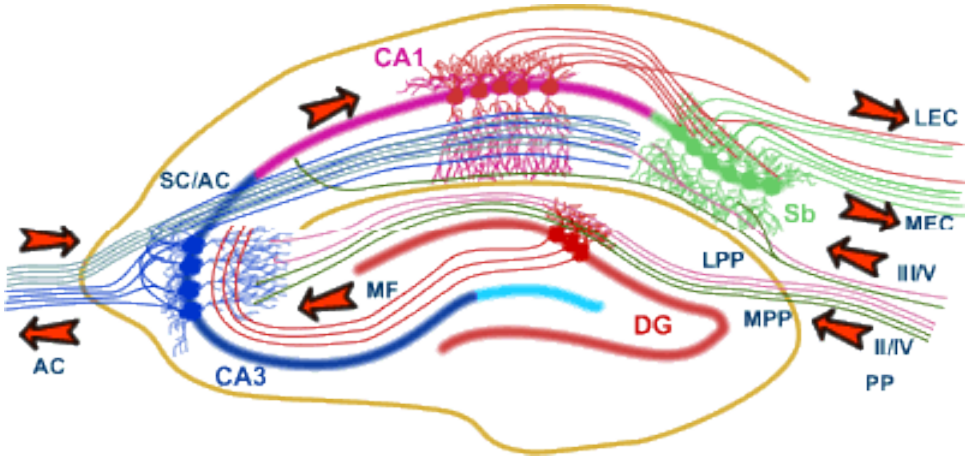

Figure 5. The trisynaptic circuit of the hippocampal formation. The main input of the hippocampal formation is carried by axons of the perforant path (PP), which convey polymodal sensory information from the entorhinal cortex (EC). Perforant path axons form synapses on granule cells of the dentate gyrus (DG) and PCs of the hippocampus (CA3 to CA1). Granule cells project via the mossy fibers (MF) to CA3 PCs which, in turn, project to ipsilateral CA1 PCs via the Schaffer collaterals (SC) as well as to the contralateral CA1 region via the associational/commissural pathway (A/C). CA1 PCs send axons to the PCs of the subiculum (Sb), which send axons back to the EC. *Adapted from University of Bristol, Centre for Synaptic Plasticity (http://www.bristol.ac.uk/synaptic/pathways/).*

pathways were described challenging this classical unidirectional trisynaptic circuit and turn it into a complex network. For example, perforant path axon fibers, in addition to granule cells, also contact PCs in the *stratum lacunosum-moleculare* (SLM) of CA1–CA3 regions and the subiculum[85]. Furthermore, CA3 cells also excite each other through an extensive recurrent network of associational/commissural (A/C) inputs originating from CA3 PCs on both sides of the hippocampus[87-89]. The CA3 PCs were also shown to send back several collaterals to the dentate gyrus[90], refuting the theory of unidirectional information flow in the hippocampal formation.

2.3.2. Glutamatergic synaptic transmission

The principal cells of the hippocampal formation, like the majority of principal cells in the CNS, release L-glutamate as neurotransmitter[91-93]. Neurotransmitters are released from vesicles at AZs of presynaptic cells, when an AP invades the axon terminal and opens voltage gated Ca^{2+} channels. Then, the influx of Ca^{2+} ions activates the closely positioned Ca^{2+} sensors (synaptotagmins) and triggers neurotransmitter release[94].

The released glutamate diffuses into the synaptic cleft and binds to postsynaptic ionotropic receptors (GluRs: AMPA, NMDA, and kainate receptors)[13,16,17] that act via opening of an ion channel permeable to Na^+, K^+ and Ca^{2+}. The resulting postsynaptic responses can be measured in the postsynaptic cell as an excitatory postsynaptic current (EPSC) or potential (EPSP). The size and kinetics of these responses display tremendous variability[95] due to differences, among others, in the type of glutamate receptors, their subunit composition, number, density and precise location in relation to the release site (also see chapter 2.5.1.). Glutamate can also act on postsynaptic G-protein coupled metabotropic receptors (mGluRs)[96], which have a role in tuning postsynaptic neuronal excitability[96]. Furthermore, both GluRs and mGluRs are present and can act presynaptically by modulating the neurotransmitter release in response to subsequent incoming APs[97-99].

The most widely accepted model of synaptic transmission between neurons is the quantal model pioneered by Katz and his colleagues[100]. According to this model, neurotransmitters are released in discrete quanta in a probabilistic manner from presynaptic axon terminals, and the efficacy of the synaptic transmission between pre- and postsynaptic neurons is determined by the number of release sites between the pre- and postsynaptic cells, the probability with which vesicles are released (*Pr*), and the size of the postsynaptic response caused by the neurotransmitter released from a single synaptic vesicle (termed quantal size). Many of these factors are highly variable at hippocampal glutamatergic synapses[101-104] despite the apparent uniformity of PCs.

Moreover, synaptic efficacy or strength is not static between individual neurons, but can dynamically change over time in an activity-dependent manner. Short-term synaptic plasticity[105,106] represents an increase (facilitation)[107] or decrease (depression) in synaptic strength, which lasts from hundreds of milliseconds to seconds. In contrast,

long-term plasticity (long-term potentiation (LTP) and long-term depression (LTD)) can last hours, days or even years[108-110]. Short- and long-term plasticity not only operate on different time-scale, but have distinct underlying mechanisms and functional relevance.

2.3.3. GABAergic cells of the hippocampus

The outlined excitatory network is precisely regulated by a rich diversity of local INs[111,112], which represent 10–15%[113,114] of all hippocampal cells. INs traditionally have exclusively local axonal arbor, but some of them may have extrahippocampal or commissural projections. Most INs receive inputs from the same extrinsic afferents that innervate their target principal cells, in turn they reduce the firing of the principal cells in a feed-forward regulatory manner. In case of the feed-back inhibition, the INs are activated by the recurrent collaterals of the principal cells. The weight of these two inputs may vary significantly between distinct IN types. In contrast to the relatively uniform principal cells, INs display great diversity[111,115,116]. Many IN classes have been defined on the basis of morphology, physiological properties, molecular expression profiles, and their selective innervation of distinct subcellular domains of postsynaptic cells. In addition, these IN types show AP firing at different preferred phases of PC activity during network oscillations *in vivo*[115-121] and also in *in vitro*[122,123] preparations. In the following, I will provide a brief description of the main morphological and functional characteristics of hippocampal INs relevant to this dissertation.

Perisomatic-targeting INs[124] consist of two non-overlapping IN subtypes, which have different functional roles: the basket cells target the somatic and proximal dendritic region (reviewed in [125-128]), while axo-axonic cells innervate the AIS of PCs[129-131]. Based on neurochemical content and firing properties, basket cells are divided into two groups. One basket cell type expresses the calcium-binding protein parvalbumin (PV)[132,133] and $K_v3.1b$ voltage-gated K^+ channel subunit[134,135], and exhibits fast, non-accommodating firing patterns[136]. The other type of basket cell displays regular-firing pattern with accommodating APs[136]. They expresses the neuropeptide cholecystokinin (CCK)[137] as well as type 1 cannabinoid receptor (CB_1) at high levels in their axons and terminals[138]. The CB_1 suppresses the GABA release upon activation by postsynaptically released endocannabinoids evoked by depolarization and Ca^{2+} entry[139]. Cell bodies of PV-positive (PV^+) are usually located within or immediately adjacent to the SP[132,136,140],

while CCK-containing INs have their somata primarily in dendritic layers[136,141]. Perisomatic INs have a radial dendritic arbor, usually spreading over all layers of the hippocampus, indicating that they might participate both in feed-forward and feed-back inhibitory circuits. Recently, it was shown that PV^+ basket cells confer preferential inhibition to PCs with distinct sublayer positions and long-distance targets, while CCK^+ basket cells do not show any selectivity between PC subpopulations[142]. While it is clear that basket cells inhibit their target neurons, the discharges of axo-axonic cells, in addition to their usual inhibitory effect[143], can also excite PCs under certain circumstances[144]. Axo-axonic cells also express PV[133] and K_v3 channels[134,135].

Several types of INs innervating the dendritic domain of PCs have been described. Among these, the oriens-lacunosum-moleculare (O-LM) cells of the CA1 area have their somata, horizontally-oriented spiny dendrites, and a few axon collaterals in the SO, while their axon is mostly distributed in the SLM innervating the apical dendritic tuft and presumably controlling the entorhinal cortical input[145]. In contrast in the CA3 area, dendritic tree of O-LM spans all layers except SLM. The distribution of dendrites in both CA subfields overlaps that of recurrent collaterals of local PCs, thereby suggesting the O-LM cells as a feed-back inhibitory IN[111]. These cells express the neuropeptide somatostatin[141] and $mGlu_{1a}$ at uniquely high levels in their extrasynaptic membranes[146]. The glutamatergic[97] and GABAergic[147] input terminals contacting these cells express the $mGlu_7$.

Bistratified cells have their cell body within or near the SP with their dendrites arborizing in the SR and SO, while their axon is associated with Schaffer collaterals or A/C inputs in the SO and SR[148,149]. These cells expresses PV, somatostatin as well as K_v3 channels[134,135], and display fast-spiking characteristics[148,150]. Similarly, oriens-bistratified cells (O-Bi), have their axon arborization in the SO and SR, while their soma and horizontal dendrites are restricted to the SO[151]. They express somatostatin[151] and occasionally $mGlu_{1a}$[151,152].

2.3.4. GABAergic synaptic transmission

INs express GABA synthesizing enzyme, glutamate decarboxylase (GAD)[153], and release γ-aminobutyric acid (GABA)[154,155]. Similarly to glutamate, the released GABA acts on ionotropic ($GABA_A$)[14,15] and metabotropic receptors (GABA type B,

$GABA_B$)[156-159]. The activation of $GABA_A$ receptors in mature neurons leads to an inward flow of anions, and a fast hyperpolarizing postsynaptic response—the inhibitory postsynaptic current (IPSC) or potential (IPSP), mediating the so-called phasic inhibition[160]. In addition, low GABA concentrations in extracellular space can activate $GABA_A$ receptors outside the synapse, generating the so-called tonic currents[160]. In contrast, activation of $GABA_B$ receptors stimulates intracellular G-protein signaling cascades that modulate ion channels (*e. g.* $K_{ir}3$, Ca_v) and adenylate cyclase activity, and as a result has differential slow modulatory effect on pre- and postsynaptic neuronal compartments (reviewed in [156-158]).

2.4. Distinct distribution patterns of different ion channels in the hippocampus

As outlined in the previous chapters, the activity of any individual neuron is shaped by excitatory and inhibitory inputs arriving from other cells. This picture is complicated by the fact that the impact of these inputs, the integration of the conveyed information and the transformation into output signals is governed by the orchestrated action of several types of ion channels that are expressed in different patterns on the surface of the neuron. Although there are still many gaps in our knowledge, a huge amount of data is available regarding the distribution of ion channels in hippocampal neurons. I therefore shall focus on a few selected ion channels, such as voltage-gated Na^+, K^+ and Ca^{2+} channels.

2.4.1. Distribution of voltage-gated Na^+ channels in the hippocampus

Na_v channels have been detected in axonal and dendritic compartments of hippocampal PCs by *in vitro* electrophysiology[161]. It was shown that their presence in high densities in the AIS lowers the threshold for AP initiation and gives rise to a fast, regenerative inward current during the rising phase of the AP[11]. In addition, in the nodes of Ranvier Na_v channels ensure the efficient AP conduction[162]. Na_v channels are also present in the somato-dendritic region of PCs, where they support the active back-propagation of axonally generated APs into the dendrites[163], as well as contribute to nonlinear synaptic integration and dendritic Na^+ spike initiation and propagation[39,164-167]. Adult hippocampal neurons express three Na_v subunits ($Na_v1.1$, $Na_v1.2$, and $Na_v1.6$)[168], but the lack of subunit-specific drugs precludes the identification of the

subunits responsible for axonal and somato-dendritic Na^+ currents. Therefore, immunohistochemistry with subunit-specific antibodies was used to address this issue in the CA1 area. The $Na_v1.1$ subunit was detected in the small axons and AISs of GABAergic INs[69],while the $Na_v1.2$ subunit in the AIS of PCs and VGLUT-1 putative axonal profiles[69]. Nodes of Ranvier, AISs[69,169] were intensely labeled for the $Na_v1.6$ subunit, while proximal apical dendrites of CA1 PCs were weakly immunoreactive. The high-resolution SDS-FRL technique was employed to explore the presence of the $Na_v1.6$ subunit in small subcellular compartments, and to quantify their densities in distinct subcellular compartments. This method revealed a characteristic subcellular distribution pattern of $Na_v1.6$ subunit in the axo-somato-dendritic compartments of PCs, with a dramatic drop (by a factor of 40 to 70) in density from nodes of Ranvier and AISs to somata, and a distance-dependent decrease in density along the proximo-distal axis of the dendritic tree without any detectable labeling in dendritic spines[69].

2.4.2. Distribution of voltage-gated K^+ channels in the hippocampus

K_v channels (41 subunits) comprise one of the four K^+ selective ion channel groups, together with the Ca^{2+}- and Na^+-activated K^+ channels of the K_{Ca} group (8 subunits), the constitutively active G protein- and ATP-regulated inwardly rectifying K^+ channels of the K_{ir} group (15 subunits), and the constitutively open or 'leak' K^+ channels of the tandem pore or K_{2P} group (15 subunits)[26].

Hippocampal PCs express a wide variety of K^+ channel subunits, which might reside in distinct axo-somato-dendritic compartments[26]. Indeed, electrophysiological experiments have identified K^+ currents in PC dendrites, including the transient A-type K^+ current (I_A) characterized by fast activation and rapid rates of inactivation, as well as the delayed rectifier K^+ current, which exhibits a delayed onset of activation followed by little or slow inactivation[170]. The latter one was further divided into two groups based on pharmacological properties: the I_K current can be blocked by low concentrations of tetraethylammonium (TEA) or high concentrations of 4-aminopyridine (4-AP)[171], while the I_D current is sensitive to α-dendrotoxin[170].

The I_A current is exclusively mediated by the low-voltage activated $K_v4.2$ channels in CA1 PCs[172]. It has a major role in a large variety of dendritic processes, including the regulation of dendritic electrogenesis[167], the AP back-propagation into the

dendrites[40,173], synaptic integration and plasticity[174-178]. Somatic and dendritic patch-clamp recordings from CA1 PCs revealed a sixfold increase in the density of I_A as a function of distance from proximal to distal main apical dendrites[40]. In contrast, SDS-FRL demonstrated only a 70% increase in the density of $K_v4.2$ subunit along the proximo-distal axis of main apical dendrites[179]. The $K_v4.2$ subunit was present in higher densities in dendritic spines than in shafts at the same distance from the soma[179]. Axonal compartments lacked the $K_v4.2$ subunit[179]. These results indicate that a large fraction of the $K_v4.2$ channels in the proximal dendrites do not conduct K^+. Posttranslational modifications or interactions with some auxiliary/associated proteins were suggested as possible mechanism for channel function modification[179].

The I_K current, mediated mainly by the high-voltage activated $K_v2.1$ channels, has also been revealed in the somato-dendritic region of CA1 PCs[171,180]. Interestingly, they are believed to regulate excitability and Ca^{2+} influx during periods of repetitive high-frequency firing, rather than regulating the repolarization of single APs[171,181]. Light microscopic immunohistochemical and functional studies demonstrated the presence of the $K_v2.1$ subunit in the somata, proximal dendrites and AISs of PCs[182-187], where it either forms clusters or has a uniform distribution depending on its phosphorylation state[181,188]. Increased neuronal activity induced by seizures or hypoxia-ischemia induces $K_v2.1$ dephosphorylation and the translocation of surface $K_v2.1$ from clusters to a uniform localization. This modulation is associated with changed channel gating properties (hyperpolarizing shift in the voltage-dependent activation) and a consequent increase in the amplitude of I_K currents, which might suppress the pathological hyperexcitability of central neurons[181,188]. Compared to the numerous studies exploring the $K_v2.1$ subunit localization in the perisomatic region of PCs, there is no data available regarding their localization in small subcellular compartments such as oblique dendrites, dendritic tufts, dendritic spines, nodes of Ranvier and axon terminals.

K_v have also been found in axons, where they set the threshold and sculpt the shape of the APs in addition to regulating repetitive firing properties of PCs[11,12,189-192]. The low-voltage activated delayed rectifier $K_v1.1$ channel is of particular significance, as dysfunctions or the absence of these channels have been associated with various types of neurological disorders including epilepsy[90] and episodic ataxia[193]. This is

consistent with functional studies showing the role of I_D current[170,194]—evoked by channels composed of $K_v1.1$, $K_v1.2$, or $K_v1.6$ subunits—in regulating axonal excitability and AP duration in hippocampal PCs. It was shown that inactivation of K_v1 channels in the AIS and proximal axon during slow subthreshold somato-dendritic depolarization generates a distance-dependent broadening of the axonal AP waveform[190], augmenting Ca^{2+} entry and facilitating neurotransmitter release[50,190]. Moreover, K_v1 channels in juxtaparanodal regions may act to reduce re-excitation of the node[195]. Light microscopic immunofluorescent and peroxidase reactions confirmed the presence of the $K_v1.1$ subunit in AISs, juxtaparanodal regions of myelinated axons of CA1 PCs and in the neuropil of the SO and SR of the CA1 area[169,196-198]. The neuropil signal in these regions is likely to originate from the labeling of pre-terminal axons and/or presynaptic axon terminals. Although $K_v1.1$ subunits can form heterotetrameric channels with the $K_v1.2$ subunits on the surface of neurons, the $K_v1.2$ subunit is barely detectable in the SO and SR of the CA1 area with light microscopic immunofluorescent reactions[169]. In contrast, AIS and juxtaparanodal axons of CA1 PCs were intensely labeled for the $K_v1.2$ subunit[169]. Both subunits were also localized in the AIS of INs[169], while the $K_v1.6$ subunit is predominantly expressed in INs[197]. Currently the presence of the $K_v1.1$ subunit at a low density in somato-dendritic compartments cannot be excluded based on the neuropil labeling in the SO and SR, especially because this subunit can also be localized to somato-dendritic regions as was shown in, *e.g.*, the ventral cochlear nucleus[199].

Finally, K_v3 channels reside in both somato-dendritic and axonal compartments of a subset of INs[134,135,200]. They mediate either delayed rectifier currents ($K_v3.1$ and $K_v3.2$) or I_A-type currents ($K_v3.3$ and $K_v3.4$), but can form heteromeric channels with intermediate gating characteristics[201]. Typically found in fast-spiking INs, K_v3 channels are important for AP repolarization and sustaining high-frequency firing[135,202-205]. Dendritic patch-clamp recordings demonstrated that K_v3 channels accelerate the decay time course of EPSPs, shortening the time period of temporal summation and promoting AP initiation with high speed and temporal precision[206,207]. Immunofluorescent reactions confirmed that the $K_v3.1b$ subunit is present in the somata, proximal dendrites and axon terminals of hippocampal INs. Furthermore, 90% of $K_v3.1b^+$ INs were PV^+[135], which are known to display fast-spiking characteritics[135]. Conversely, a large percentage

(82%) of PV^+ cells expresses the $K_v3.1b$ subunit[135]. Based on these findings $K_v3.lb$ is an ideal marker for PV^+ fast-spiking INs. Most $K_v3.3$-immunolabeled IN somata were also immunoreactive for PV, while a few of them contained somatostatin[208].

2.4.3. Distribution of voltage-gated Ca^{2+} channels in the hippocampus

A large body of data is available that demonstrates the presence of distinct types of Ca_v channels on hippocampal neurons, where these channels contribute to a wide range cellular processes, including dendritic electrogenesis, synaptic plasticity, neurotransmitter release, activation of Ca^{2+}-dependent enzymes and second messenger cascades, as well as gene expression[209,210].

Based on the pore-forming subunit, 10 types of Ca_v channels can be distinguished, which fall into three families according to their pharmacological and biophysical properties: (1) the high-voltage activated dihydropyridine-sensitive ($Ca_v1.1$–4, L-type) channels, (2) the high-voltage activated dihydropyridine-insensitive ($Ca_v2.1$, P/Q-type; $Ca_v2.2$, N-type; $Ca_v2.3$, R-type) channels and (3) the low-voltage-activated ($Ca_v3.1$–3, T-type) channels[211].

Dendritic patch-pipette recordings and Ca^{2+} imaging experiments demonstrated the presence of most, if not all, Ca_v channel types on CA1 PCs, which play important role in synaptic integration, synaptic plasticity, and neuronal excitability. Through these channels dendritic APs and synaptic inputs may elevate the intracellular Ca^{2+} concentration in the dendrites, which can result in release of neurotransmitters or other substances from dendrites or induction of synaptic plasticity[19]. In addition, dendritic Ca_v channels together with Na_v channels may produce amplification of distal synaptic inputs and minimize the attenuation that would otherwise occur as a consequence of passive cable properties[212]. Although the total Ca^{2+} channel density is fairly uniform across dendrites, the density of the individual channel subtypes varies between the proximal and distal regions of neurons[212]. For example, in the somata and proximal dendrites mainly N-type, P/Q-type, L-type channels contribute to the Ca^{2+} influx, whereas T-type and R-type channels are distributed in more distal dendrites[39,213-215]. Unfortunately, there are only a few studies showing immunohistochemical localization of Ca_v channels in the somato-dendritic region of hippocampal neurons. One light microscopic study showed weak immunosignal for the $Ca_v3.1$ T-type channel subunit in the somatic-

proximal dendritic region of CA1 and CA3 PCs, and stronger signal in the apical dendrites for the $Ca_v3.2$ and $Ca_v3.3$ subunits[216] with no detectable increase between the middle and distal regions of apical dendrites. The perisomatic region of most INs was also immunopositive for $Ca_v3.3$ or $Ca_v3.1$ or in some cases for $Ca_v3.2$[216,217]. It is worth mentioning, that the authors did not test the specificity of their immunoreactions neither in knockout animals (in which the protein of interest is specifically missing), nor by using two (or more) antibodies against different parts of the same protein[25].

The distribution of $Ca_v1.2$ and $Ca_v1.3$ L-type channel subunits was determined by pre- and post-embedding immunogold methods in CA1 PCs[218,219]. It was reported that both $Ca_v1.2$ and $Ca_v1.3$ subunits are distributed predominantly, but not exclusively in soma and dendritic processes at both PSDs and extrasynaptic sites[218,219]. Examination of the density of these Ca_v subunits along apical dendrites revealed no significant differences between proximal and distal regions[219]. However, thin dendrites and spines contained more gold particles than large diameter dendrites[219]. An elegant study, using super-resolution imaging, optogenetics and electrophysiological measurements demonstrated that $Ca_v1.3$ channels form functional clusters of two or more channels along the surface membrane of hippocampal neurons[220]. Clustered channels can be physically coupled via calmodulin in a Ca^{2+}-dependent manner, which will increase the activity of adjoined channels, facilitate Ca^{2+} currents and thereby increase firing rates in hippocampal neurons[220]. In addition, fluorescent immunolabeling revealed the $Ca_v1.2$ and/or $Ca_v1.3$ subunits in the somatic and proximal-dendritic regions of GABAergic INs, with PV^+ and somatostatin$^+$ INs mostly expressing the $Ca_v1.3$ subunit[217,221].

The $Ca_v2.3$ R-type channel was also observed postsynaptically in the somata, dendritic shafts, and spines of the putative CA1 PCs by pre-embedding immunogold labeling[222]. In dendritic spines immunogold particles were mainly observed in extrasynaptic plasma membranes, but as the used method is prone to false negative results, the presence of $Ca_v2.3$ at higher densities in PSDs cannot be excluded.

Ca_v channels are likely to be present also in the AISs of hippocampal PCs and INs. Although there is no available data for the hippocampus, PCs of the neocortex[223], Purkinje cells of the cerebellum[224] and INs of the dorsal cochlear nucleus[225] all express Ca_v channels in their AISs. In the first two cell types P/Q- and N-type channels, while in the third case T- and R-type channels are present. These channels can be activated by

both subthreshold and suprathreshold membrane potential depolarization, and play a role in controlling the pattern and waveform of generated APs[225], and thereby neurotransmitter release[223].

In contrast, there is clear functional and anatomical evidence demonstrating that Ca_v channels are present in axon terminals of hippocampal PCs and INs. In this subcellular compartment they mediate the Ca^{2+} influx necessary for neurotransmitter release[226] upon activation by APs and/or subthreshold depolarizing signals[227,228]. In hippocampal excitatory synapses, application of subtype-specific toxins showed that glutamate release relies primarily on the concerted action of ω-agatoxin IVA-sensitive P/Q-type and ω-conotoxin GVIA-sensitive N-type channels[229,230], the ratio of which varies markedly between terminals on the same axon[231]. In contrast, the majority of distinct IN types rely either on P/Q- or N-type channels[232,233], and only a small subset of them uses both subtypes[234] for GABA release. The presence of the P/Q-type channels was confirmed on axon terminals of PCs and INs of the CA1 and CA3 area by the high-resolution SDS-FRL method. The $Ca_v2.1$ subunit was confined to the AZ of axon terminals and their numbers scaled linearly with the AZ area[235,236]. Moreover, gold particles labeling the $Ca_v2.1$ subunit were non-randomly distributed within AZs of both excitatory and $VGAT^+$ GABAergic axon terminals[235,236].

In contrast, the contribution of R-type channels to neurotransmitter release is more controversial[235,237,238]. Recently it turned out that the SNX482 drug, used to demonstrate the role of this channel in synaptic release, also reduces I_A-type K^+ currents[239]. Nevertheless, pre-embedding immunogold reactions showed that the $Ca_v2.3$ subunit is present in both excitatory and inhibitory boutons of the CA1 region[222]. The labeling occupied mostly extrasynaptic membranes, but the lack of labeling in AZs could be the consequence of insufficient penetration into the AZ as a consequence of technical limitation of the used pre-embedding method.

$Ca_v1.2$ and $Ca_v1.3$ L-type channel subunits have also been shown to be present on hippocampal axon terminals by pre- and post-embedding immunohistochemistry[218,219]. Electrophysiological recordings in the presence of the L-type channel specific dihydropyridine antagonists (nifedipine) excluded their role in fast synaptic transmission[230,240]. However, recently it was shown that certain properties attributed to L-type channels, such as slow activation and the lack of contribution to

single APs, reflect the state-dependent nature of the dihydropyridine antagonists used to study them, and not the kinetics of native L-type currents[241]. The authors also found that these channels open over a range of voltages and activate rapidly in response to a variety of stimuli including individual APs, which suggests that they could potentially contribute to fast transmitter release[241].

Regarding the axonal location of T-type channels in hippocampal PCs, there is minimal data available. Post-embedding immunogold experiments revealed that the $Ca_v3.1$ T-type channel subunit is not present in PC terminals[242], but there is no available information concerning the other two T-type channel subunits. Particularly, the presence of the $Ca_v3.2$ subunit needs to be checked, as this subunit was localized to the AZ of cortical PCs axon terminals where they regulate glutamate release in conjunction with HCN1 channels[243]. In contrast, the mentioned post-embedding reactions demonstrated the presence the $Ca_v3.1$ T-type channel subunit in hippocampal PV^+ basket terminals near the AZ[242]. It was shown, that the Ca^{2+} influx triggered by these channels augmented by Ca^{2+} from internal stores can mediate GABA release[242].

2.5. Input- and target cell type-dependent distribution of ion channels

Another fundamental issue regarding the subcellular distribution of ion channels is that excitatory and inhibitory synapses localized in the same subcellular compartment of a given neuron can display differences in the type, number, density and nanoscale distribution of their ion channels. As I will demonstrate in the two following chapters, the exact molecular composition of synapses is determined by the identity of the presynaptic input neuron and/or the cell type of the postsynaptic target neuron (input versus target cell type-dependent differences, Figure 6).

Figure 6. Input- and target cell type-dependent synaptic differences. (A) Input-dependent differences occur between synapses supplied to the same postsynaptic cell by distinct types of presynaptic neurons. (B) In case of target cell type-dependent differences, axon terminals of a single presynaptic neuron diverging onto distinct types of postsynaptic neurons display morphological (and/or functional) differences. *Modified from* [18].

2.5.1. Input- and target cell type-specific distribution of AMPA receptors

AMPA-type glutamate receptors are ubiquitously present in every nerve cell. Their majority is concentrated in PSDs of glutamatergic synapses, but they are also present at low densities in the extrasynaptic plasma membranes, and occasionally in presynaptic compartments. These receptors are homo- or heterotetramers built from combinations of subunits, which differ in their contribution to channel kinetics, ion selectivity, and receptor trafficking properties, hence creating great structural and functional heterogeneity[13,16,17].

Interestingly, Fujiyama et al. (2004) revealed that the subunit composition of AMPA receptors localized on presynaptic axon terminals contacting neostriatal neurons is influenced by the cell-type of the input cell[244]. While cortico-striatal axon terminals contain presynaptic $GluA_1$, $GluA_{2/3}$ and $GluA_4$ subunit-containing AMPA receptors, thalamo-striatal terminals are devoid of the $GluA_4$ subunit and express only $GluA_1$ and $GluA_{2/3}$ in their AZs[244]. Furthermore, in contrast to cortico-striatal axon terminals, the presynaptic AZ of cortico-cortical terminals is devoid all of the examined AMPA receptor subunits[244]. This demonstrates, in addition to the presynaptic cell, the identity of the postsynaptic cell also affects the molecular structure of synapses.

In addition to different subunit composition, the nanoscale distribution of AMPA receptors can also show input cell type-specific differences. Accordingly, high-resolution SDS-FRL experiments, employing an antibody that recognizes all four AMPA receptor subunits, revealed differences between the postsynaptic AMPA receptor distribution of retinogeniculate and corticogeniculate synapses formed on relay cells of the dorsal lateral geniculate nucleus[245]. It was shown that individual corticogeniculate synapses express similar number of AMPA receptors in a larger synaptic area than retinogeniculate synapses[245]. As AMPA receptors are arranged in microclusters in both synapse types, this resulted in larger intrasynaptic areas devoid of AMPA receptors in corticogeniculate synapses than those in retinogeniculate synapses[245]. Because AMPA receptor occupancy declines with distance from the site of vesicle fusion[246], it was hypothesized that these differences in the distribution of AMPA receptors could endow distinct functional properties to synapses. Numerical simulations, however, showed that AMPA receptor-mediated quantal responses were almost identical in retinogeniculate synapses, displaying homogeneous receptor

distributions, and in corticogeniculate synapses, having similar number of receptors in a clustered arrangement[245].

This does not exclude the possibility that in other cell types AMPA receptor distribution does not regulate the synaptic strength. Accordingly, a recent study suggested that presynaptic Rim1/2 clusters are aligned to postsynaptic areas densest in $GluA_2$ receptors, endowing increased synaptic strength compared to uniform distribution of postsynaptic receptors[247].

In the hippocampus the AMPA receptor distribution was examined by a quantitative immunogold method with the antibody that recognizes all four AMPA receptor subunits[248]. Two functionally distinct synapses of CA3 PCs were compared with regard to their AMPA receptor content. It was found that all mossy fiber synapses contacting PC complex spines in the SL were immunopositive for AMPA receptors[248]. In contrast, up to 17% of A/C synapses contacting PCs spines in the SR were immunonegative. Furthermore, mossy fiber synapses had less variability in their immunoparticle number and contained four times as many AMPA receptors as A/C synapses[248]. These results demonstrate that the number and the variability of synaptic AMPA receptors on CA3 PCs depend on the identity of the presynaptic input. The influence of postsynaptic cells on AMPA receptor expression was also tested by comparing the AMPA receptor content of A/C synapses contacting PCs spines and GABAergic interneuron dendrites in the SR of the CA3 area[248]. In contrast to spine-targeting A/C synapses, IN dendrite-contacting A/C synapses always contained immunoreactive AMPA receptors, the number of which showed less variability and was four times larger than in the former connection[248]. This experiment demonstrates that the AMPA receptor distribution is different in two distinct cell types that are innervated by a common afferent. Altogether, these results indicate that in hippocampal synapses the AMPA receptor distribution is governed by both pre- and postsynaptic elements[249].

2.5.2. Input- and target cell type-specific distribution of Ca_v channels

Currently a lot of research is focused on presynaptic Ca_v channels as differences in their distributions are assumed to underlie the heterogeneity in the temporal precision, efficacy and short-term plasticity of synaptic transmission[250-254]. The opening of these Ca_v channels mediates a local intracellular Ca^{2+} influx. Ca^{2+} then diffuses from

the source (Ca_v channels) to the vesicular sensor (synaptotagmins) and by activating it, triggers neurotransmitter release. As the Ca^{2+} signal generated by a single open Ca^{2+} channel declines steeply with distance[255-257], the spatial arrangement of Ca_v channels and readily-releasable vesicles on the nanoscale is a crucial determinant of the *Pr*, in addition to the number of channels, single-channel conductance, their open probability, the length of time until they are open, as well as the presence and properties of fast internal Ca^{2+} buffers (reviewed in [18,258-260]).

Distinct Ca_v channel distribution was implicated as a mechanism underlying target cell type-dependent differences in the *Pr* of glutamate release and the consequent differences in short-term plasticity, which are well established phenomena with numerous examples in cortical microcircuits. For example, single PCs generate different responses in two distinct types of inhibitory INs: somatostatin and $mGlu_{1a}$-expressing O-LM and O-Bi cells of the hippocampus and bitufted INs of the neocortex receive facilitating EPSCs with low initial P_r, whereas synaptic inputs onto fast-spiking PV-expressing INs (*e.g.*, basket, axo-axonic, bistratified cells in the hippocampus and multipolar cells in the cortex) display short-term depression and have high initial *Pr* [18,152,261-263]. Importantly, such target cell-type dependent divergence in presynaptic release properties is not restricted to glutamatergic afferents, as simultaneous triple recordings revealed that GABAergic axons can also exhibit distinct release properties in a target cell-specific manner[264,265].

It was shown that these target cell type-dependent differences in *Pr* are reflected in the amplitude of [Ca^{2+}] transients in the presynaptic boutons[261]. Moreover, simultaneous recordings between a presynaptic PC and two distinct types of IN revealed that the axon of a single PC can transmit different aspects of information coded in a complex spike train to distinct postsynaptic cell types[261,264,266-268], and that distinct types of short-term plasticity enable neuronal networks to perform complex computations[268].

A candidate protein bestowing different *Pr* and short-term plasticity to axon terminals was $mGlu_7$, a metabotropic glutamate receptor that shows postsynaptic target cell type-dependent differences in its presynaptic density[97]. However, a group III mGluR-specific antagonist failed to abolish the differences in short-term plasticity of synapses expressing or lacking $mGlu_7$[269]. More recently, Sylwestrak and Ghosh (2012)[270] identified the extracellular leucine- rich repeat fibronectin-containing protein

1 (Elfn1) as a key molecule in bestowing short-term facilitation. This protein is selectively expressed postsynaptically in O-LM cell somata and dendrites, and knocking down Elfn1 from somatostatin$^+$ INs led to an increase in the amplitude of the first EPSC of a train and a reduction in the degree of short-term facilitation. Nevertheless, the short-term plasticity of somatostatin$^+$ INs after Elfn1 knock-down is still facilitating, very different from that observed in PV$^+$ IN-targeting boutons. Although, to date, there are no data available regarding the mechanisms underlying the low initial *Pr* of these facilitating synapses, Rozov *et al.* (2001)[271] put forward an elegant hypothesis based on their experiments involving fast and slow Ca^{2+} buffers. They postulated that the low initial *Pr* of facilitating cortical PC synapses can be explained by a larger coupling distance between Ca_v channels and Ca^{2+} sensors on the readily-releasable vesicles compared with the high *Pr* PC synapses on fast-spiking INs. Assuming similar Ca^{2+} sensors and docked vesicle distributions, this would suggest a lower average Ca_v channel density within the AZs of low *Pr* synapses. To confirm or reject this hypothesis high-resolution immunolocalization experiments will need to be carried out to compare the Ca_v channel densities between high and low *Pr* boutons of the same axons.

Input cell type-dependent differences in the properties of synaptic release were also described[272,273], and similarly differences in Ca_v channel distribution were suggested as underlying mechanism[274]. For example, CCK and PV-expressing basket cells terminals contacting hippocampal PCs differ substantially in their mechanisms of coupling of APs and exocytosis[274] (reviewed in [124-126]). While PV$^+$ output synapses release GABA in a tightly synchronized manner in response to presynaptic APs, CCK$^+$ INs generate a less timed, highly asynchronous input. From these cells GABA is released for up to several hundred milliseconds after high-frequency stimulation. It was suggested, that the asynchronous release at the CCK$^+$ IN output synapses could be a consequence of loose coupling between Ca^{2+} source and sensor, that is to say a larger diffusional distance between Ca_v channels and synaptotagmins that trigger GABA release[274]. In contrast, tight coupling would promote synchronous release in PV$^+$ output synapses[274]. The loose coupling at CCK$^+$ IN synapses was confirmed by the fact that the diffusion of Ca^{2+} from Ca_vs to synaptotagmins takes sufficiently long time that the slow Ca^{2+} chelator, EGTA, could interfere with the coupling[274]. In contrast, the EGTA did not have an effect on the synchronous release of PV$^+$ IN output synapses[274]. This

conclusion was in line with the result of pharmacological experiments using subtype specific blockers, which suggested the involvement of different types of Ca_v channels at the two types of synapses: while $Ca_v2.2$ channels trigger synchronous and asynchronous release in CCK^+ IN output synapses[274,275], PV^+ IN synapses rely on P/Q-type channels for transmitter release[274]. It was suggested that $Ca_v2.1$ channels must be located in AZs, while $Ca_v2.2$ channels should be distributed throughout the presynaptic terminals to explain the differential coupling between Ca_v channels and Ca^{2+} sensors at the two types of synapses[274]. To validate these assumptions direct anatomical proof will be needed.

In conclusion, recent experiments revealed that all ion channels studied to date, including the ones not presented here (*e.g.* HCN1 subunit), show distinct subcellular distribution patterns on the surface of a given neuron type. This prediction is based mostly on data originating from patch-pipette recordings and light microscopic immunolocalization methods, and only partially on high-resolution quantitative data. Unfortunately, small subcellular compartments are inaccessible for patch-pipette recordings rendering their ion currents enigmatic, and low densities of ion channels could remain undetectable due to the limited sensitivity and resolution of light microscopic immunolocalization methods. Therefore, highly sensitive, quantitative, high-resolution immunolocalization experiments will need to be carried out to determine the presence and relative densities of additional ion channels in the different axo-somato-dendritic compartments of neurons, including small subcellular compartments such as oblique dendrites, dendritic tufts, dendritic spines, nodes of Ranvier and axon terminals.

Furthermore, ion channel distribution of synapses is governed by both pre- and postsynaptic elements, which can underlie functional heterogeneity of synaptic connections. Once again, highly sensitive, quantitative, high-resolution immunolocalization experiments will need to be performed to reveal correlations between the molecular structure and functional properties of synaptic connections, and thereby facilitate our understanding of how the tremendous molecular diversity is exploited by neuronal circuits.

DOI:10.14753/SE.2018.2123

3. Objectives

The functional impact of ion channels depends on their molecular structure as well as their precise subcellular location and densities on the axo-somato-dendritic surface of nerve cells. Despite extensive electrophysiological and anatomical investigations, the exact location and densities of most ion channels in small subcellular compartments are still unknown.

Therefore, the general aim of my work was to investigate the cell surface distribution of different voltage-gated K^+ and Ca^{2+} channels and to reveal potential input- and target cell type-dependent differences in ion channel distributions that might underlie distinct functions. To address the aims of my dissertation, I adopted the highly-sensitive, high-resolution electron microscopic SDS-FRL technique.

The specific aims in this study were:

(1) To determine the precise subcellular distribution pattern of two delayed-rectifier K^+ channel subunits ($K_v1.1$ and $K_v2.1$) in distinct axo-somato-dendritic compartments of CA1 PCs.

(2) To reveal target cell type-specific differences in the distribution and densities of voltage-gated Ca^{2+} channels in CA3 PC axon terminals.

(3) To determine input cell type-dependent differences in the distribution of voltage-gated Ca^{2+} channels in basket cell axon terminals of the hippocampal CA3 area.

Contributions:

The gold distribution analysis was performed with a software written by Miklós Szoboszlay.

DOI:10.14753/SE.2018.2123

4. Methods

All experiments were conducted in accordance with the Hungarian Act of Animal Care and Experimentation and with the ethical guidelines of the Institute of Experimental Medicine Protection of Research Subjects Committee.

4.1. Tissue preparation for fluorescent immunohistochemistry and SDS-FRL

Wistar rats (adult: postnatal day (P) 30–66, n = 11 male; young: P15–17, n = 8 male), transgenic mice expressing DsRed fluorescent protein under the CCK promoter (CCK-BAC/DsRedT3; P19–P25, n = 5 male), $CB_1^{+/+}$ (P18, P26, n = 2 female) and $CB_1^{-/-}$ (P18, n = 2 female, kindly provided by Prof. Andreas Zimmer[276]) mice were deeply anaesthetized with ketamine (0.5 ml/100 g). The animals were transcardially perfused with an ice cold 0.9% saline solution for one minute, then with an ice cold fixative. The brains were then quickly removed from the skull and placed in 0.1 M phosphate buffer (PB).

For light microscopic immunofluorescent reactions, animals were perfused with a fixative containing either 4% paraformaldehyde (PFA; Molar Chemicals) and 15v/v% picric acid (PA) in 0.1 M PB (pH = 7.3 for the $K_v1.1$ labeling) or with 2% PFA in 0.1 M Na acetate buffer (pH = 6[277] for the $K_v2.1$ labeling) for 15 minutes. Afterwards, 70 μm thick coronal sections were cut from the forebrain with a vibratome (VT1000S; Leica Microsystems), and were washed in 0.1 M PB. Brain sections from animals perfused with 4% PFA and 15 v/v% PA in 0.1 M PB were treated with 0.2 mg/ml pepsin (Dako) in 0.2 M HCl at 37°C for 18–20 minutes, and then were washed in 0.1 M PB.

For SDS-FRL, animals were perfused with a fixative containing 2% PFA and 15v/v% PA in 0.1 M PB for 15 minutes. Coronal or horizontal sections of 80 μm thickness were cut from the forebrain. Small tissue blocks from the dorsal CA1, dorsal and ventral CA3 were trimmed, and cryo-protected by overnight immersion in 30% glycerol.

Replicas from $Ca_v2.2^{+/+}$ (P18, n = 1) and $Ca_v2.2^{-/-}$ mice (9 months old mouse, n = 1, kindly provided by Prof. Yasuo Mori) were provided by Prof. Ryuichi Shigemoto[278].

4.2. Fluorescent immunohistochemistry

Following several washes in 0.1 M PB and then in Tris-buffered saline (TBS; pH = 7.4), sections were blocked in 10% normal goat serum (NGS; Vector Laboratories) made up in TBS, followed by overnight incubation in primary antibodies diluted in TBS containing 2% NGS and 0.1% Triton X-100. The used primary antibodies are listed in Table 1. After several washes in TBS, the sections were incubated in Cy3-conjugated goat anti-rabbit IgGs (1:500 or 1:1000; Jackson ImmunoResearch Laboratories) and Alexa488-conjugated goat anti-mouse IgGs (1:500; Life Technologies) made up in TBS containing 2% NGS for 2 hours. Sections were washed in TBS, then in 0.1 M PB before mounting on slides in Vectashield (Vector Laboratories). Images from the CA1 region were acquired using a confocal laser scanning microscope (FV1000; Olympus) with either a 20X (NA = 0.75) or a 60X (NA = 1.35) objective. Automated sequential acquisition of multiple channels was used. For low magnification, single confocal images, while for high magnification, single confocal images or maximum intensity z-projection (three confocal images with 0.3 μm separation) images were used.

4.3. SDS-FRL

Small blocks from the CA1 and CA3 areas were sandwiched between copper carriers and were frozen in a high-pressure freezing machine (HPM100; Leica Microsystems). Carriers then were inserted into a double replica table and fractured at -135°C in a freeze-fracture machine (BAF060; Leica Microsystems). The fractured faces were coated on a rotating table by carbon (2 or 5 nm) with an electron beam gun positioned at 90°, then shadowed by platinum (2 nm) at 60° unidirectionally, followed by a final carbon coating (20 nm). Tissue debris was ‘digested’ from the replicas in a solution containing 2.5% SDS and 20% sucrose in TBS at 80°C overnight. Following several washes in TBS containing 0.05% bovine serum albumin (BSA; Sigma), replicas were blocked in TBS containing 0.1–5% BSA for 1 hour, then incubated overnight at room temperature or for four days at 4˚C in the blocking solution containing the primary antibodies listed in Table 1. Replicas were then incubated for 2 hours in TBS containing 5% BSA and goat anti-rabbit IgGs coupled to 5, 10, 15 nm gold particles

DOI:10.14753/SE.2018.2123

Table 1. Primary antibodies used in the immunoreactions.
LM, light microscopy; aa., amino acid.

Protein target	Source; catalogue number	Species	Antigen	Final protein concentration (µg/ml) LM	Final protein concentration (µg/ml) SDS-FRL	Characterization reference
Ankyrin-G (Ank-G)	NeuroMab; 75-146	Mouse monoclonal, clone N106/36	aa. 990–2622 of human Ank-G	2		Lorincz and Nusser (2010)[69]
$Ca_v2.1$	Synaptic Systems; 152 203	Rabbit polyclonal	aa. 1921-2212 of rat $Ca_v2.1$		1.7–2	Holderith *et al.* (2012)[235]
$Ca_v2.1$	Frontier Institute; VDCCa1A-GP-Af810	Guinea pig polyclonal	aa. 361–400 of mouse $Ca_v2.1$		2	Holderith *et al.* (2012)[235], Indriati *et al.* (2013)[27]
$Ca_v2.2$	Synaptic Systems; 152 303	Rabbit polyclonal	aa. 1921–2212 of rat $Ca_v2.2$		2.5	this study
CB_1	Cayman Chemical; 10006590	Rabbit polyclonal	aa. 461–472 intracellular region of the human CB_1		1.2	this study
CB_1	Frontier Institute; CB1-GP-Af530	Guinea pig polyclonal	mouse CB_1, C-terminal 31 aa.		2	this study
$K_v1.1$	Frontier Institute; Kv1.1-Rb-Af400	Rabbit polyclonal	aa. 478–492 of mouse $K_v1.1$	1	2	Iwakura *et al.* (2012)[279], also this study
$K_v1.1$	NeuroMab; 75-105	Mouse monoclonal, clone K36/15	aa. 191–208 of rat $K_v1.1$	4		Tiffany *et al.* (2000)[280], Lorincz and Nusser (2008)[169], see also NeuroMab website
$K_v2.1$	NeuroMab; 75-014	Mouse monoclonal, clone K89/34	aa. 837–853 of rat $K_v2.1$	3.4	10 or 20	Trimmer (1991)[182], Antonucci *et al.* (2001)[281], also this study
$K_v2.1$	NeuroMab; 75-159	Mouse monoclonal, clone K39/25	aa. 211–229 of rat $K_v2.1$	3.6		Lim *et al.* (2000)[185]
$K_v3.1b$	Alomone Labs; APC-014	Rabbit polyclonal	aa. 567–585 of rat $K_v3.1b$		3.2–4	Barry *et al.* (2013)[282]
$mGlu_{1a}$	Frontier Institute; mGluR1a-GP-Af660	Guinea pig polyclonal	aa. 945–1127 of mouse $mGlu_{1a}$		2	Mansouri *et al.* (2015)[283]
$Na_v1.6$	Alomone Labs; ASC-009	Rabbit polyclonal	aa. 1042–1061 of rat $Na_v1.6$	8	1.6	Lorincz and Nusser (2008)[169]
Neuroligin-2 (NL-2)	Synaptic Systems; 129 203	Rabbit polyclonal	aa. 750–767 of rat NL-2		1	Briatore *et al.* (2010)[284]
pan-Na_v	Alomone Labs; ASC-003	Rabbit polyclonal	aa. 1501–1518 of rat $Na_v1.1$	4		Lorincz and Nusser (2010)[69]
pan-Neurofascin (pan-NF)	NeuroMab; 75-027	Mouse monoclonal, clone L11A/41	aa. 1066–1174 of rat NF-155		3.6 or 7.1	Schafer *et al.* (2004)[285], Van Wart *et al.* (2007)[286]
Rim1/2	Synaptic Systems; 140 203	Rabbit polyclonal	aa. 1–466 of rat RIM2		0.5	Holderith *et al.* (2012)[235]
SNAP-25	Synaptic Systems; 111 001	Mouse monoclonal	aa. 20–40 of rat SNAP-25		0.7	Von Kriegstein *et al.* (1999)[287]
Synapto-tagmin-2	Synaptic Systems; 105 123	Rabbit polyclonal	aa. 406–422 in rat synaptotagmin-2		1.3	Johnson *et al.* (2010)[288], this study
Vesicular GABA transporter (VGAT)	Synaptic Systems; 131 004	Guinea pig polyclonal	aa. 2–115 of rat VGAT		0.5	Gallart-Palau *et al.* (2014)[289]

(1:50–1:100; British Biocell International) or to 6 nm gold particles (1:30; AURION Immuno Gold Reagents & Accessories), goat anti-mouse IgGs coupled to 10 or 15 nm gold particles (1:50–1:100; British Biocell) or goat anti-guinea pig IgGs coupled to 10 or 15 nm gold particles (1:50–1:100; British Biocell or 1:30; AURION). Finally, replicas were rinsed in TBS and distilled water before being picked up on copper parallel bar grids. Specimens were analyzed with a transmission electron microscope (JEM-1011; JEOL Ltd). Images of identified profiles were taken with a Cantega G2 camera (Olympus Soft Imaging Solutions) at 10000–25000x magnification. Gold particle counting and area measurements were performed with iTEM software (Olympus Soft Imaging Solutions). All used antibodies recognized intracellular epitopes on their target proteins and consequently were visualized by gold particles on the P-face. Nonspecific background labeling was measured on E-face structures surrounding the measured P-faces, as described previously[69].

In most double-labeling reactions, a mixture of the two primary, then a mixture of the two secondary antibodies was applied. However, I also performed sequential double-labeling reactions (*e.g.* for K_v1.1 and pan-NF, K_v1.1 and SNAP-25 as well as for VGAT and CB_1) in which the anti-K_v1.1 or the anti-VGAT primary were applied overnight at room temperature. On the next day appropriate secondary antibodies were used to label the primary antibodies. After this the replicas were incubated overnight with the second primary antibody (anti-pan-NF, anti-SNAP-25 or anti-CB_1) and on the following day with the corresponding secondary antibody.

4.4. Testing the specificity of the immunoreactions

Specificity of the immunoreactions for K_v1.1 and K_v2.1 subunits was tested by using two antibodies raised against different non-overlapping epitopes of the respective proteins, which revealed identical labeling patterns in the CA1 region. In addition, the labeling pattern for the K_v1.1 in the CA1 area was identical to that published by Lorincz and Nusser (2008)[169] with the mouse anti-K_v1.1 antibody; the specificity of that immunoreaction was verified in *K_v1.1$^{-/-}$* mice. The labeling pattern revealed by the K_v2.1 antibodies was also consistent with published data[26,181-187].

The rabbit anti-Ca_v2.1 antibody provides identical labeling to that of the guinea pig anti-Ca_v2.1, the specificity of which was proven in Holderith *et al*. (2012)[235].

The specificity of the $Ca_v2.2$ immunolabeling was confirmed using tissue derived from *$Ca_v2.2^{-/-}$* mice, where immunogold particles for $Ca_v2.2$ were mostly abolished from P-face sections of axon terminals attached to somatic E-face membranes (0–3 gold particles in 189 profiles from n = 2 animals), whereas in *$Ca_v2.2^{+/+}$* mice these structures were strongly labeled for $Ca_v2.2$ (0–15 gold particles in 301 profiles, n = 2 animals). In addition, in *$Ca_v2.2^{+/+}$* mice, excitatory axon terminals (identified based on the presence of an AZ facing a PSD on E-faces) contained stronger $Ca_v2.2$ labeling (mean ± standard deviation (SD) = 3, range: 0–10 gold particles in 27 profiles), compared with *$Ca_v2.2^{-/-}$* mice (mean ± SD = 0.25, range: 0–3 gold particles in 51 profiles).

The specificity of the CB_1 immunolabeling was tested on replicas in $CB_1^{-/-}$ and *$CB_1^{+/+}$* mice. In single-labeling experiments, immunogold particles for CB_1 were abolished from axon terminals in every layer of the CA3 in the *$CB_1^{-/-}$* tissue (n = 2 mice). Double-labeling reactions for CB_1 using two different anti-CB_1 antibodies resulted in double-labeled axon terminals in *$CB_1^{+/+}$* mice, while on replicas from *$CB_1^{-/-}$* mice no labeled profiles were found. Furthermore, CB_1 labeling showed extensive colocalization with VGAT in *$CB_1^{+/+}$* mice (31 CB_1^+ out of 60 $VGAT^+$ boutons), but in *$CB_1^{-/-}$* mice all VGAT terminals (0 out of 53) were immunonegative for CB_1.

4.5. Quantification of immunogold particles labeling the $K_v1.1$ and $K_v2.1$ subunits in the rat CA1 region

Quantitative analysis of immunogold labeling for the $K_v1.1$ and $K_v2.1$ subunits was performed on CA1 PC somata, 11 different dendritic compartments, AISs and axon terminals in six[179] CA1 sublayers (n = 3 rats for each subunit). In addition to SO, SP, SR, and SLM (above 360 μm), the SR was divided into proximal SR (0–120 μm), middle SR (120–240 μm) and distal SR (240–360 μm) parts based on the distance from SP. The main apical dendrites, oblique dendrites, spines and axon terminals were grouped according to this criterion. The distance of an individual process (P) from the SP was calculated from the position of the SP and from the stage coordinate (x_0, y_0) of the process using the following equation:

$$\text{distance } (P(x_0, y_0)) = \frac{\left|(y2 - y1) \times x0 + (x1 - x2) \times y0 + x2 \times y1 - x1 \times y2\right|}{\sqrt{(y2 - y1)^2 + (x1 - x2)^2}}$$

The position of the SP was determined by an imaginary line connecting two end points of the SP with the coordinates x_1, y_1 and x_2, y_2. Oblique dendrites were identified based on their small diameter and the presence of at least one emerging spine from the dendritic shaft. Structures were only considered to be spines if they emerged from a dendritic shaft. Axon terminals were identified either (1) based on the presence of an AZ facing a PSD on the opposing E-face of a spine or dendrite; or (2) based on the presence of synaptic vesicles on their cross-fractured portions; or (3) the presence of a large number of gold particles labeling SNAP-25. Images of AISs of CA1 PCs were taken in SP and SO. To quantify the $K_v2.1$ subunit in the AISs, the $K_v1.1$ subunit (n = 3 rats) was used as molecular marker. The NL-2[80] was used to identify GABAergic synapses on PC somata and dendrites. In these experiments, the quantified ion channels were visualized with 10 nm gold-conjugated IgGs. On the figures, gold particle densities are presented as mean $\pm$ SD between animals. One-way ANOVA with Dunnett's *post hoc* test was used to compare the gold particle densities between distinct subcellular compartments, and significance was taken as $P < 0.05$. In all figures, $*P < 0.05$, $**P \leq 0.01$, $***P \leq 0.001$.

4.6. Quantitative analysis of immunogold particles labeling the $Ca_v2.1$ and $Ca_v2.2$ subunits in rat CA3 PC axon terminals contacting $K_v3.1b$ or $mGlu_{1a}$ immunopositive cells

To quantify the $Ca_v2.1$ and the $Ca_v2.2$ subunit densities in the AZs of axon terminals targeting $K_v3.1b^+$ or $mGlu_{1a}^+$ dendrites in the SO of the CA3 area, all experiments were performed using the 'mirror replica method'[79]. With this method, replicas are generated from both matching sides of the fractured tissue surface, allowing the examination of the corresponding E- and P-faces of exactly the same membranes.

One replica was immunolabeled for $K_v3.1b$ and $mGlu_{1a}$ to identify IN dendrites; its mirror surface was labeled for a Ca_v channel subunit and all subcellular structures (dendrites, AZs) were identified in both replicas. The AZs were delineated on the P-face based on the underlying high density of IMPs. Gold particles inside the synaptic area and up to 30 nm away from its edge were counted. Axon terminals containing Ca_v subunit labeling without an elevated density of IMPs were discarded from the analysis because this is a characteristic feature of inhibitory terminals. All AZs, fractured

partially or in their completeness, were quantified. When the synaptic area was not flat, the replica was tilted. To eliminate reaction-to-reaction variability in the Ca_v subunit labeling, synaptic, extrasynaptic bouton, and background Ca_v densities were normalized to the mean of the Ca_v densities measured in the AZs targeting $mGlu_{1a}^+$ profiles in each reaction. On the figures, gold particle densities of measured individual AZs are represented by circles, boxes indicate IQRs, and horizontal bars indicate medians. As the Shapiro-Wilk test showed that data was different from normal distributions, Kruskal–Wallis test (5 unpaired groups) with Mann-Whitney *U* test with Bonferroni adjustment was used to compare the Ca_v densities. Significance was taken as $P < 0.05$. In all figures, $*P < 0.05$, $**P \leq 0.01$, $***P \leq 0.001$.

4.7. Quantification of CB_1, Rim1/2, $Ca_v2.1$ and $Ca_v2.2$ subunits in axon terminals targeting the somatic region of PCs in the distal CA3 area of the rat and mouse hippocampus

To quantify the CB_1, Rim1/2, $Ca_v2.1$ and $Ca_v2.2$ subunit densities on axon terminals, electron micrographs of PC somatic E-face membranes with attached P-face axon terminal fragments were taken from SP of the distal CA3 area of a rat and two mice (data pooled). These attached P-face profiles showed large variability in sizes. I have restricted the analysis to those profiles that had an area > 0.01 and < 0.21 μm^2, corresponding to the range of AZ sizes obtained from 3D electron microscopic reconstructions performed by Noémi Holderith[290]. The gold particle densities were then calculated in these P-face membranes without assuming that the entire membrane is an AZ. The AZs of CB_1^+ boutons do not contain an elevated density of IMPs, therefore their delineation based on morphological criteria is not possible. Molecules that are confined to the AZ should therefore be used to identify AZs. Here I used Rim1/2 immunolabeling for this purpose and delineated potential AZs in my figures for illustrative purposes only. However, I refrain from performing quantitative analysis of, for example, CB_1 immunoreactivity in AZs, due to uncertainties in determining the borders of the AZs. I also provided indirect evidence for the potential enrichment of $Ca_v2.1$ and $Ca_v2.2$ in AZs in the following way. Using Rim1/2 labeling, I demonstrated that 31.7% and 23.6% of the P-face membrane fragments fractured to large E-face somatic membranes contain AZs in rats and mice, respectively. In $Ca_v2.1$ and $Ca_v2.2$

double-labeling experiments, this proportion was similar (43% and 19.8%). The quantitative analysis of these double-labeling reactions revealed that these two Ca_v channels are almost fully exclusive: 89% and 92% of the fractured membranes had either $Ca_v2.1$ or $Ca_v2.2$ labeling in rats and mice, respectively. I also delineated $Ca_v2.2$- and $Ca_v2.1$ rich areas of the boutons for illustrative purposes in my figures, but I have no evidence that these areas fully overlap with the AZs.

4.8. Analysis of immunogold particle distribution patterns within specific subcellular compartments

To investigate whether the distribution of a given protein within a certain subcellular compartment is compatible with a random process or not, I computed two measures using a software developed by Miklós Szoboszlay.

First, I calculated the mean of the nearest neighbor distances ($\overline{\mathrm{NND}}$) of all gold particles within the area in question and that of random distributed gold particles within the same area (same number of gold particles placed in the same area, 200 or 1000 repetitions). The $\overline{\mathrm{NND}}$s were then compared statistically using the Wilcoxon signed-rank test (after normality of sample distributions was assessed using the Shapiro-Wilk test). In our second approach, I computed a 2D spatial autocorrelation function ($g(r)$) for my experimental data and for their corresponding random controls based on previously published methods[291]. The $g(r)$ reports the probability of finding a second gold particle at a given distance r away from a given gold particle. For randomly distributed gold particles, $g(r) = 1$, whereas spatial inhomogeneities result in $g(r)$ values > 1 at short distances. In my experiments, I computed the $g(r)$ for $0 < r < 80$ nm and then their mean ($\overline{g(r)}$) was calculated and compared with those obtained from random distributions using the Wilcoxon signed-rank test (after normality of sample distributions was assessed using the Shapiro-Wilk test). Significance was taken as $P < 0.05$. In all figures, $*P < 0.05$, $**P \leq 0.01$, $***P \leq 0.001$.

DOI:10.14753/SE.2018.2123

5. Results

5.1. Subcellular distribution of two delayed-rectifier K^+ channel subunits in the hippocampal CA1 area

5.1.1. Distribution and specificity of $K_v1.1$ subunit immunoreactivity in the CA1 area

First, I investigated the distribution of the $K_v1.1$ subunit in the hippocampal CA1 area of adult rats using light microscopic immunofluorescent localizations. I tested the specificity of the $K_v1.1$ subunit immunoreactions by using two antibodies directed against different, non-overlapping parts of the $K_v1.1$ protein (see Table 1). The identical labeling pattern obtained with the two antibodies strongly suggests the specificity of the immunolabeling (Figure 7A–D). At low magnifications, an intense punctate neuropil labeling was seen in the SO and SR in agreement with published data[169,196-198], corresponding to either presynaptic terminals[198] or dendritic spines. At higher magnifications, AISs (Figure 7E and H) and the juxta-paranodal region of myelinated axons were also observed. Double-labeling experiments with known AIS markers such as Ank-G[292] and pan-Na_v[69] (Figure 7E–J) verified that the intensely labeled processes were indeed AISs. In order to unequivocally identify the origin of the punctate neuropil labeling of the SO and SR, and to assess the densities of the $K_v1.1$ subunit in 18 axo-somato-dendritic compartments of CA1 PCs, I turned to the SDS-FRL method.

5.1.2. Axonal location of the $K_v1.1$ subunit in hippocampal CA1 PCs

I started by investigating whether the AISs, which were the most intensely immunolabeled profiles in my immunofluorescent reactions, contained a high density of gold particles in my replicas. In the SP and SO, several elongated structures contained a high density of immunogold particles labeling the $K_v1.1$ subunit (Figure 8A–D). Only P-face profiles were intensely labeled, consistent with the intracellular location of the epitope recognized by this antibody (aa. 478–492). These structures were then molecularly identified as AISs by the high density of pan-NF labeling (Figure 8B and D). In AISs, gold particles consistently avoided the PSD of axo-axonic GABAergic

DOI:10.14753/SE.2018.2123

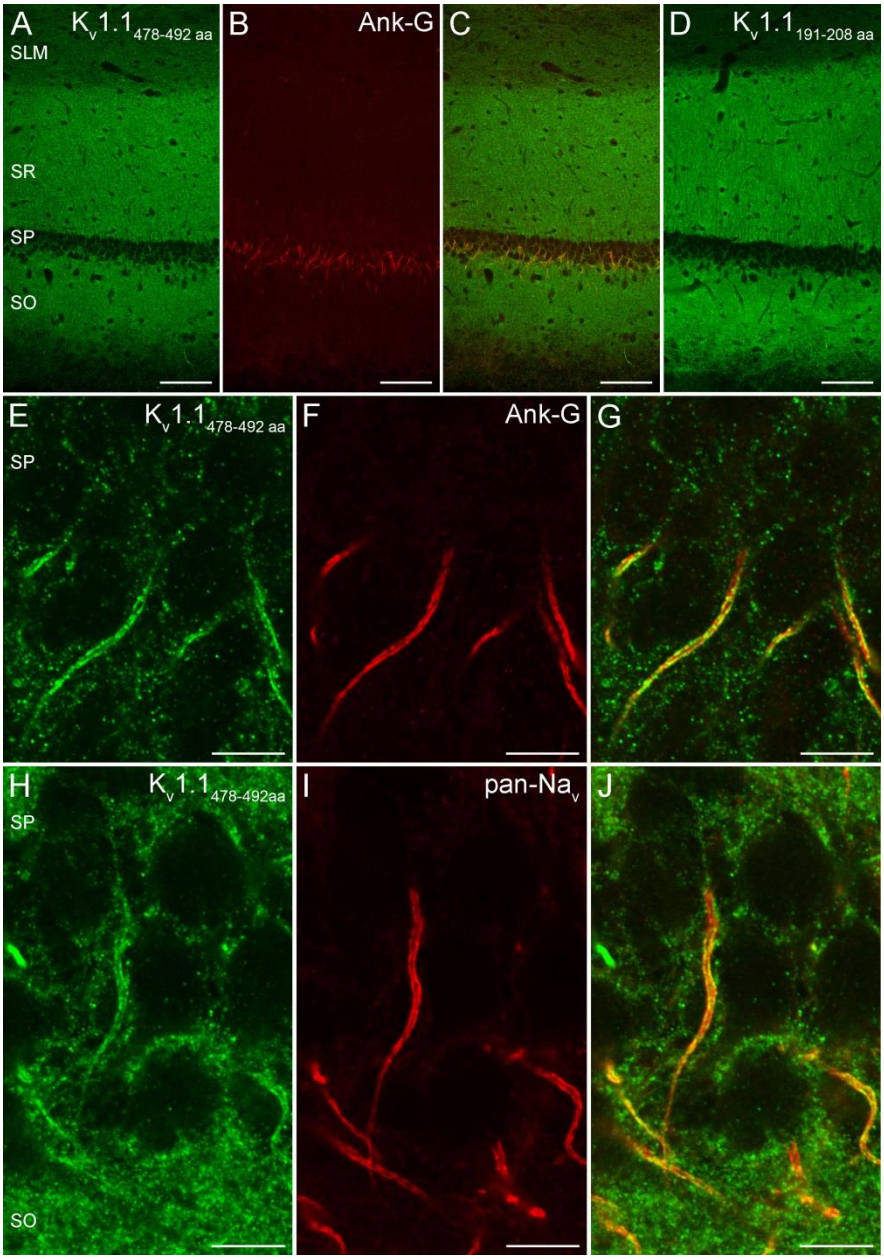

Figure 7. Distribution of the $K_v1.1$ subunit in the hippocampal CA1 area. (A–C) Low-magnification images of the CA1 area show a double-immunofluorescent reaction for the $K_v1.1$ subunit and the AIS marker Ank-G. An intense neuropil labeling can be observed with the antibody recognising aa. 478–492 of the $K_v1.1$ subunit (A). (D) Immunofluorescent reaction with an antibody raised against a different, non-overlapping part of the $K_v1.1$ subunit (aa. 191–208). The identical neuropil labeling obtained with the two different $K_v1.1$ antibodies (A and D) indicates that the immunoreaction is specific. (E–G) High-magnification images of the SP demonstrate the colocalisation of the $K_v1.1$ subunit and Ank-G in the AISs of PCs. (H–J) A double immunofluorescence reaction shows the colocalization of $K_v1.1$ subunit with pan-Na_v in strongly immunopositive AISs. *Scale bars, 100 µm (A–D); 10 µm (E–J).*

DOI:10.14753/SE.2018.2123

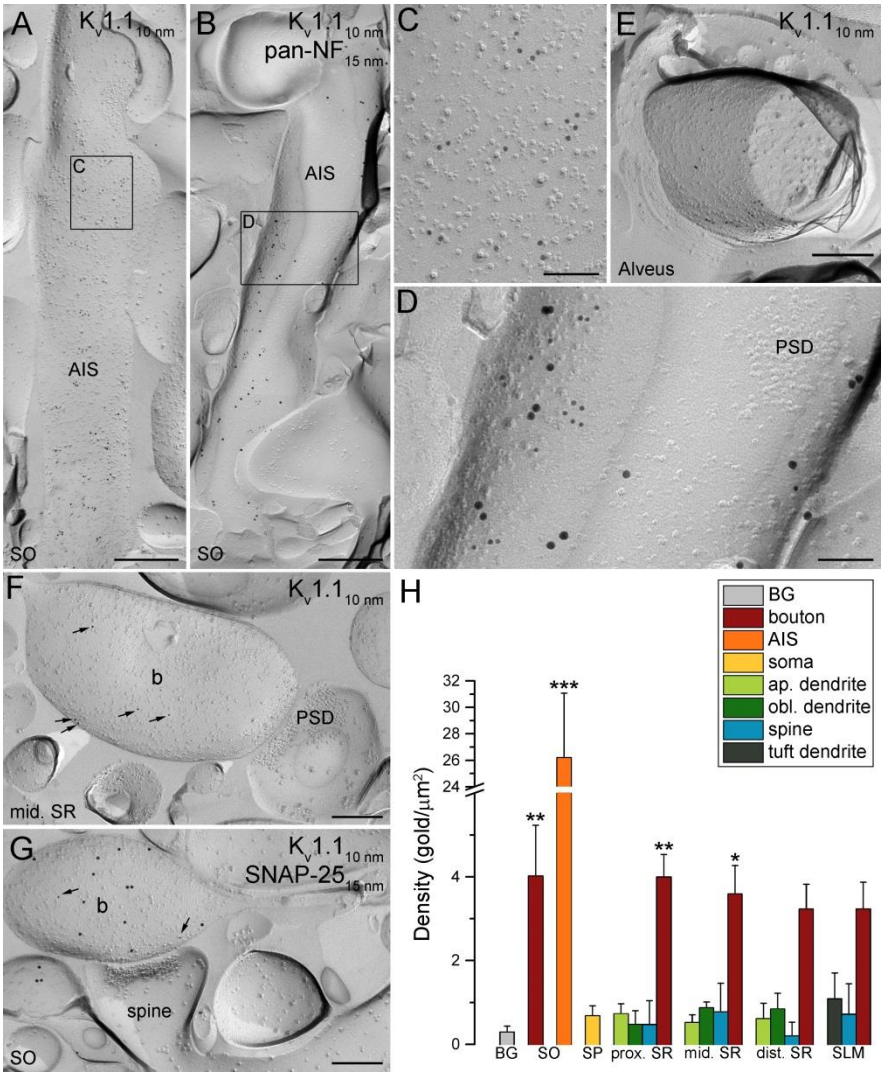

Figure 8. High-resolution immunogold localization of the K_v1.1 subunit in the CA1 area. (A) A large number of gold particles labeling the K_v1.1 subunit is observed on the P-face of an AIS. (B) Image of an AIS co-labeled for the K_v1.1 subunit (10 nm gold) and the AIS marker pan-NF (15 nm gold). (C and D) High-magnification views of the boxed regions shown in (A) and (B), respectively. Note that both the K_v1.1 subunit (10 nm gold) and pan-NF (15 nm gold) are excluded from the PSD of an axo-axonic synapse. (E) Gold particles labeling the K_v1.1 subunit are present on the P-face of a myelinated axon in the alveus. (F) The P-face of an excitatory bouton (b) innervating a putative spine is labeled for the K_v1.1 subunit (arrows). The PSD of the synapse is indicated by the accumulation of IMPs on the postsynaptic E-face. (G) A SNAP-25 (15 nm gold) immunopositive bouton, facing the PSD on the E-face of a spine, contains few gold particles for the K_v1.1 subunit (arrows; 10 nm gold). (H) Bar graphs illustrate K_v1.1 subunit densities (mean ± SD between n = 3 rats) in different axo-somato-dendritic compartments. Note that the AISs and the axon terminals in the SO and the proximal (prox.) and middle (mid.) parts of the SR contain significantly greater numbers of gold particles compared to background (BG; $P < 0.001$ One-way ANOVA, $P < 0.05$ Dunnett's *post hoc* test; n = 3 rats). ap., apical; obl., oblique; b, bouton. *Scale bars, 500 nm (A and B); 250 nm (E–G); 100 nm (C and D).*

synapses identified as dense IMP clusters[293] (Figure 8D). In the alveus, strongly $K_v1.1$ subunit immunoreactive profiles were found surrounded by cross-fractured myelin sheets (Figure 8E). These structures are likely to correspond to the juxta-paranodal region of myelinated axons that are strongly labeled in the immunofluorescent reactions.

Next, I assessed the origin of the neuropil labeling of the SO and SR. Small P-face membrane profiles containing an AZ and facing a PSD on the opposing spine or dendritic shaft membrane were consistently labeled (Figure 8F). Double-labeling experiments for the $K_v1.1$ subunit and SNAP-25, a member of the SNARE protein complex restricted to axon terminals[79], confirmed that these profiles were axon terminals (Figure 8G). These axon terminals contained a moderate number of gold particles, without any enrichment in the AZs. In P-face somatic and dendritic membranes (main apical and small oblique dendrites), gold particles were not more numerous than in the surrounding E-face membranes, which I consider as background labeling.

5.1.3. Densities of $K_v1.1$ immunogold particles in distinct axo-somato-dendritic compartments of CA1 PCs

After this qualitative assessment of the reactions, I calculated the densities of the $K_v1.1$ subunit in 18 distinct compartments by counting gold particles on P-face membranes and divided these numbers by the total measured membrane areas (Table 2). The background labeling was determined on the surrounding E-face plasma membranes and was found to be 0.3 ± 0.1 gold/μm^2 (mean ± SD; n = 3 rats). The gold particle density values were not significantly higher ($P < 0.001$ One-way ANOVA, $P = 0.999$ Dunnett's *post hoc* test; n = 3 rats) than background in somata, apical dendrites, tuft dendrites in the SLM, oblique dendrites and dendritic spines. In contrast, gold particle densities on axon terminals were significantly above background ($P < 0.001$ One-way ANOVA, $P < 0.05$ Dunnett's *post hoc* test; n = 3 rats; Figure 8H) in SO, proximal and middle SR. In distal SR and SLM gold particle densities on axon terminals were very similar, but the difference from background did not reach significance ($P < 0.001$ One-way ANOVA, $P = 0.07$ Dunnett's *post hoc* test; n = 3 rats). These densities on axon terminals were seven- to eightfold lower (ratios calculated after background subtraction;

$P < 0.001$ One-way ANOVA, $P < 0.001$ Dunnett's *post hoc* test; n = 3 rats) than that found in AISs.

Table 2. Densities of gold particles labeling $K_v1.1$ and $K_v2.1$ subunits in distinct subcellular compartments of CA1 PCs. Density values are provided in gold/μm^2 mean ± SD (between animals). In parentheses, the number denotes the number of counted gold particles. Bold indicates density values that are significantly above background. # indicates that the AIS densities were measured in separate, double-labeling experiments in which the AISs were molecularly identified with $K_v1.1$. In this reaction the background labeling was 0.6 ± 0.1 gold/μm^2.

Quantified subunit	$K_v1.1$	$K_v2.1$
SO bouton	**4.0** ± 1.2 (195)	1.1 ± 0.5 (47)
AIS	**26.2** ± 4.9 (2758)	**11.5** ± 1.8 (900) #
SP soma	0.7 ± 0.2 (704)	**10.3** ± 1.1 (10501)
SR proximal apical dendrite	0.7 ± 0.2 (98)	**9.4** ± 0.5 (3868)
SR middle apical dendrite	0.5 ± 0.2 (80)	1.6 ± 0.1 (377)
SR distal apical dendrite	0.6 ± 0.4 (107)	1.1 ± 0.1 (415)
SR proximal oblique dendrite	0.5 ± 0.3 (30)	1.4 ± 0.2 (126)
SR middle oblique dendrite	0.9 ± 0.1 (50)	1.0 ± 0.1 (95)
SR distal oblique dendrite	0.8 ± 0.4 (39)	1.2 ± 0.1 (97)
SR proximal spine	0.5 ± 0.6 (2)	1.2 ± 1.0 (10)
SR middle spine	0.8 ± 0.7 (4)	0.5 ± 0.9 (2)
SR distal spine	0.2 ± 0.3 (2)	1.1 ± 0.2 (8)
SR proximal bouton	**4.0** ± 0.5 (128)	1.4 ± 0.4 (42)
SR middle bouton	**3.6** ± 0.7 (158)	1.3 ± 0.2 (45)
SR distal bouton	3.2 ± 0.6 (137)	1.6 ± 0.6 (42)
SLM tuft dendrite	1.1 ± 0.6 (74)	1.4 ± 0.2 (221)
SLM tuft spine	0.7 ± 0.7 (10)	1.3 ± 0.2 (22)
SLM bouton	3.2 ± 0.6 (104)	1.1 ± 0.2 (42)
Background	0.3 ± 0.1 (97)	0.7 ± 0.1 (333)

5.1.4. Distribution and specificity of $K_v2.1$ subunit immunoreactivity in the CA1 area

For immunofluorescent localization of the $K_v2.1$ subunit in the CA1 area of adult rat, two antibodies recognizing non-overlapping epitopes of the protein were used to ensure that the immunosignal was the consequence of a specific antigen–antibody interaction. When the immunoreactions for the $K_v2.1$ subunit were analyzed at low magnification, strong immunolabeling of the SP and proximal part of the SR was observed (Figure 9A–D), in line with the results of previous work[181-186].

DOI:10.14753/SE.2018.2123

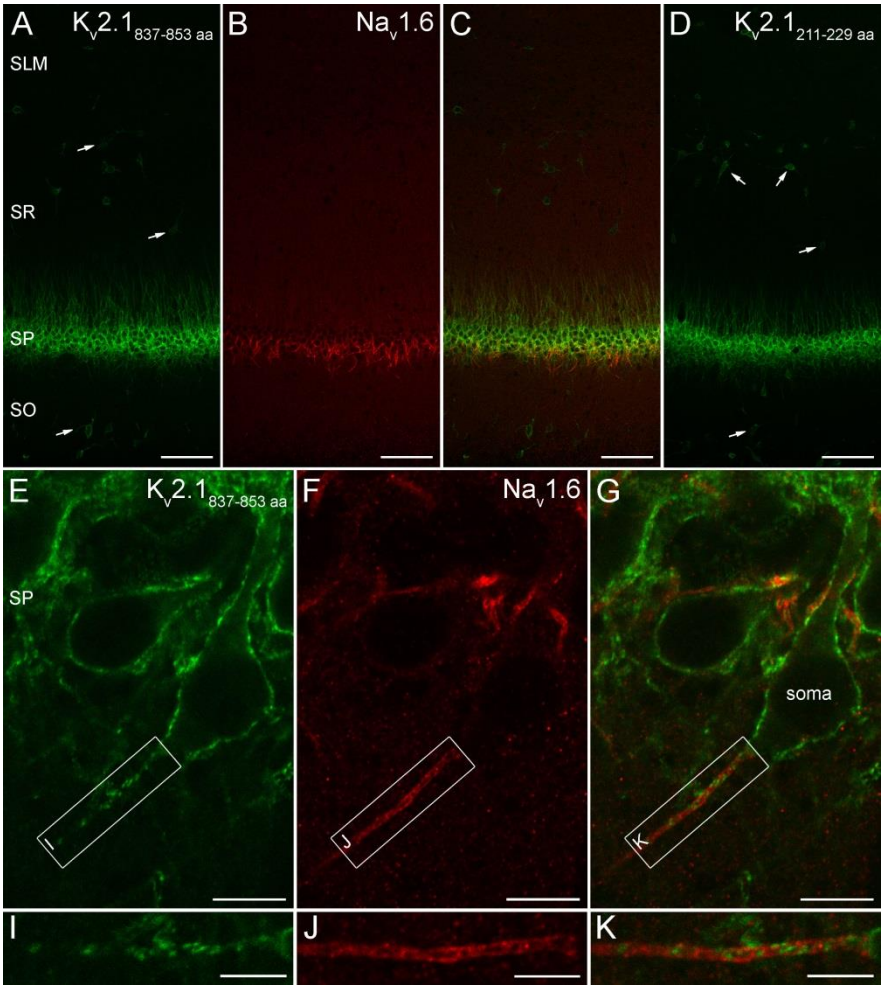

Figure 9. Immunofluorescent localisation of the $K_v2.1$ subunit in the CA1 region of the rat hippocampus. (A–C) Low-magnification view of the CA1 area double-labeled for the $K_v2.1$ (A) and the $Na_v1.6$ (B) subunits. (A and D) Identical immunofluorescent labeling pattern obtained with two antibodies recognising different, non-overlapping parts of the $K_v2.1$ subunit indicates that the immunoreaction is specific. Arrows point to the somata of INs. (E–G) High magnification images from the SP demonstrate that the immunolabeling for the $K_v2.1$ subunit is associated with somatic and proximal dendritic plasma membranes of CA1 PCs, as well as with AISs intensely labeled for the $Na_v1.6$ subunit. (I–K) Higher magnification views of the boxed areas in (E–G) show punctate, non-uniform labeling for the $K_v2.1$ subunit along the $Na_v1.6$ immunopositive AIS. *Scale bars, 100 µm (A–D); 10 µm (E–G); 5 µm (I–K).*

INs in all CA1 layers also showed somato-dendritic labeling (Figure 9A and D). High-magnification confocal microscopic images revealed plasma membrane-like labeling of somata, proximal apical and basal dendrites (Figure 9E). Double-labeling experiments for $K_v2.1$ and $Na_v1.6$ (Figure 9E–K) revealed a clustered $K_v2.1$ labeling of AISs, confirming the results of Sarmiere *et al.* (2008)[187]. Interestingly, high-

magnification single confocal images indicated that these $K_v2.1^+$ clusters did not overlap with the $Na_v1.6$ containing parts of AISs (Figure 9K).

5.1.5. High-resolution immunogold localization of the $K_v2.1$ subunit in the hippocampal CA1 area.

Using SDS-FRL, I detected immunogold labeling for the $K_v2.1$ subunit on P-face membranes, as expected from an antibody that recognizes an intracellular epitope (aa. 837–853). Strong $K_v2.1$ immunoreactivity of PC somata and proximal dendrites was observed (Figure 10A–F). The labeling consisted of scattered and clustered gold particles in the plasma membrane (Figure 10B and F). To test, whether the distribution

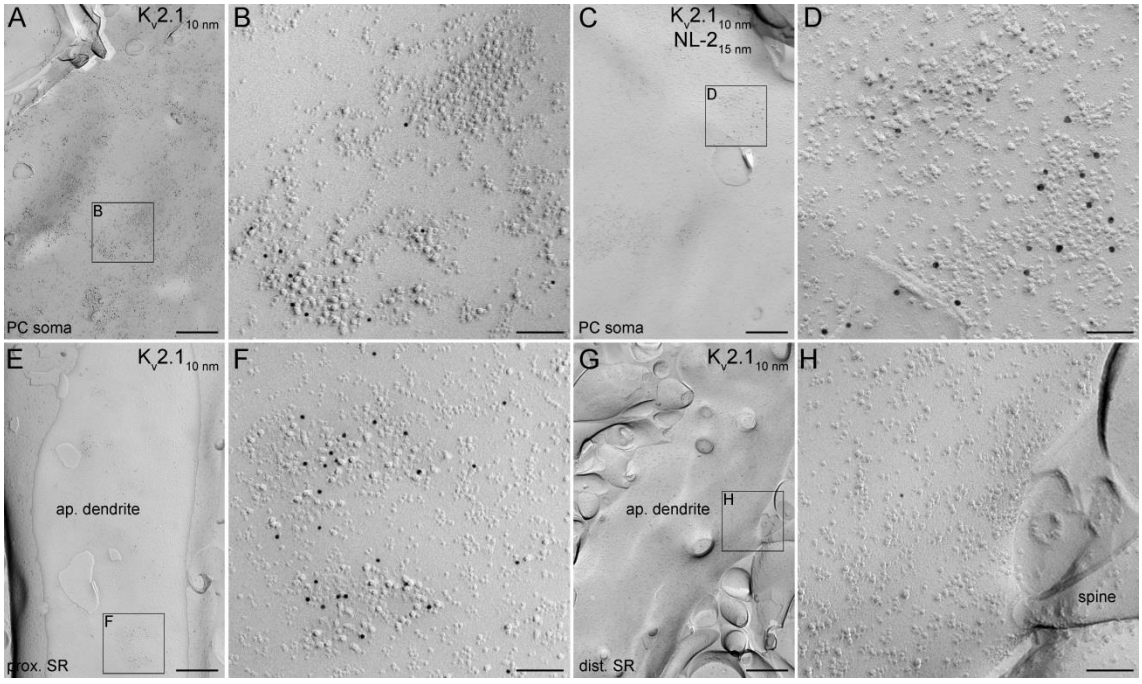

Figure 10. SDS-FRL localization of the $K_v2.1$ subunit on the somato-dendritic plasma membranes of CA1 PCs. (A) A low-magnification electron micrograph showing the P-face of a PC soma labeled for the $K_v2.1$ subunit (10 nm gold). (B) High-magnification view of the boxed area shown in (A). Immunogold particles labeling the $K_v2.1$ subunit are accumulated over a loose IMP cluster, whereas some nearby dense IMP cluster remains unlabeled. (C and D) Low (C) and high (D) magnification images of the P-face of a CA1 PC soma; 10 nm gold particles labeling the $K_v2.1$ subunit are associated with an IMP cluster distinct from the adjacent IMP cluster identified as an inhibitory synapse by the enrichment of NL-2 (15 nm gold). (E) Low-magnification image of the P-face of a thick apical dendrite (ap. dendrite) in the proximal SR (prox. SR) labeled for the $K_v2.1$ subunit. (F) Enlarged view of the boxed region shown in (E). Immunogold particles labeling the $K_v2.1$ subunit are concentrated over two IMP clusters, but scattered labeling is also present. (G and H) A distal (dist.) apical dendrite

contains very few gold particles labeling the $K_v2.1$ subunit. *Scale bars, 500 nm (A, C, E, and G); 100 nm (B, D, F, and H).*

of gold particles labeling the $K_v2.1$ subunit is compatible or not with a random process I used two measures implemented in an open source software by Miklós Szoboszlay (Figure 11). First, I computed $\overline{NND}$ of all gold particles within a somatic plasma membrane segment and that of random distributed gold particles within the same area (same number of gold particles placed in the same area, 200 repetitions). In my second approach, I calculated $\overline{g(r)}$ for the experimental data and for their corresponding random controls. Both measures indicated that the distribution of $K_v2.1$ subunit on CA1 PC soma is significantly different from random (Wilcoxon-signed rank test $P < 0.001$, n = 21 somata from 1 rat; Figure 11B and C).

I also observed that some of the $K_v2.1^+$ gold clusters were located over loose patches of IMPs, which might be GABAergic perisomatic synapses. To molecularly identify GABAergic synapses, I performed double-labeling experiments for $K_v2.1$ and NL-2, a specific marker of inhibitory synapses[80] (Figure 10C and D). These reactions revealed that the $K_v2.1$ subunit was absent from NL-2-containing areas, but occasionally the $K_v2.1^+$ and NL-2^+ clusters were close to each other. Distal apical dendrites (Figure 10G and H), oblique dendrites, dendritic spines and axon terminals rarely contained any gold particles. The non-uniform distribution of gold particles

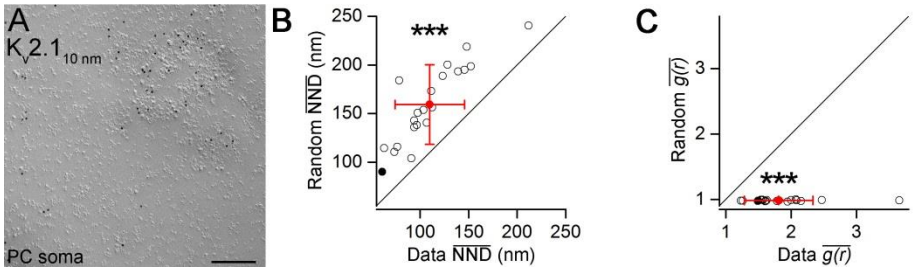

Figure 11. Non-random distribution of $K_v2.1$ subunit on CA1 PCs. (A) A P-face plasma membrane fragment of a CA1 PC cell labeled for the $K_v2.1$ subunit. (B and C) Comparison of the distribution of $K_v2.1$ labeling with random distributions (mean of n = 200 random) based on mean NND (B) and mean g(r) (C). Both measures indicate that the $K_v2.1$ labeling in these synapses is significantly different from random ($P < 0.001$ Wilcoxon-signed rank test; n = 21 somata). Open circles correspond to individual images, filled circles indicate the example shown in (A), the red symbols represent mean ± SD. *Scale bar, 200 nm.*

labeling for the $K_v2.1$ subunit was also characteristic for AISs (molecularly identified with either $Na_v1.6$ or $K_v1.1$; Figure 12A–D), but $K_v2.1$ clusters never overlapped with presumed axo-axonic synapses (Figure 12B and D) and also showed a segregation from the $Na_v1.6$ (Figure 12A and B) and $K_v1.1$ (Figure 12C and D) labeling.

Next, I performed a quantitative comparison of the $K_v2.1$ densities in 18 axo-somato-dendritic compartments of CA1 PCs (Table 2). The densities of immunogold particles for the $K_v2.1$ subunit in the somato-dendritic compartments and axon terminals were calculated from single-labeling experiments. Somata and proximal apical dendrites contained high densities of gold particles, which were significantly ($P < 0.001$ One-way ANOVA, $P < 0.001$ Dunnett's *post hoc* test; n = 3 rats; Figure 13A) higher than

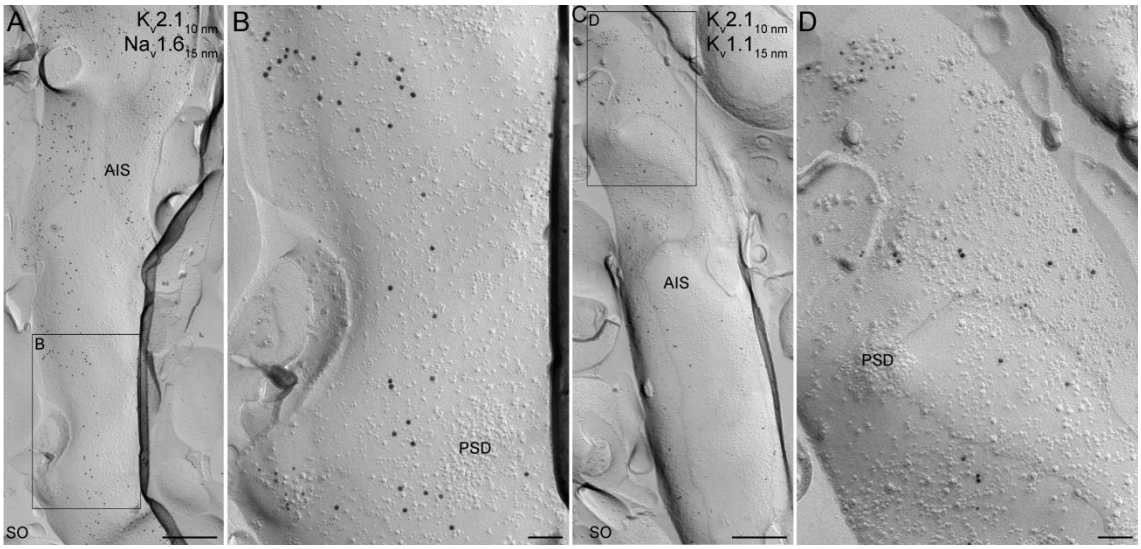

Figure 12. The $K_v2.1$ subunit is spatially segregated from $K_v1.1$ and $Na_v1.6$ subunits within the AISs of CA1 PCs. (A and B) Low-magnification (A) and high-magnification (B) images of the P-face of an AIS co-labeled for the $K_v2.1$ (10 nm gold) and $Na_v1.6$ (15 nm gold) subunits. The regions immunolabeled for the $K_v2.1$ and $Na_v1.6$ subunits seem mutually exclusive. (C and D) Low-magnification (C) and high-magnification (D) images of an AIS co-labeled for the $K_v2.1$ (10 nm gold) and $K_v1.1$ (15 nm gold) subunits. Gold particles labeling the $K_v2.1$ subunit are concentrated over an IMP cluster, but excluded from the PSD of a putative axo-axonic synapse. *Scale bars, 500 nm (A and C); 100 nm (B and D).*

background. The densities of the $K_v2.1$ subunit in apical dendrites in the middle and distal SR, SLM tuft dendrites, oblique dendrites, dendritic spines, and axon terminals were not significantly different from the nonspecific background labeling ($P < 0.001$ One-way ANOVA, $P > 0.26$ Dunnett's *post hoc* test; n = 3 rats). The density of the $K_v2.1$ subunit in AISs was calculated from double-labeling experiments with the $K_v1.1$

subunit. The strength of the $K_v2.1$ labeling of somata (11.4 ± 3.8 gold/μm^2) in these double-labeling experiments was very similar to that found in single-labeling reactions (P = 0.66, unpaired Student's t-test). AISs contained, on average, 11.5 ± 1.8 gold/μm^2, which did not differ significantly from the gold particle content of somata (P = 0.97, unpaired Student's t-test), but was significantly above the background (P < 0.01 One-way ANOVA, P < 0.01 Dunnett's *post hoc* test; n = 3 rats; Figure 13B).

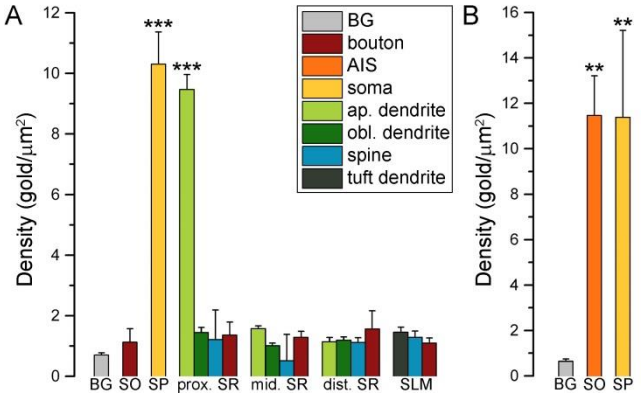

Figure 13. Densities of gold particles labeling the $K_v2.1$ subunit in different subcellular compartments of CA1 PCs. (A) Bar graphs show the $K_v2.1$ subunit densities (mean ± SD between animals) in different axo-somato-dendritic compartments. Significant densities of gold particles labeling the $K_v2.1$ subunit are found on the somata and proximal apical dendrites (ap. dendrites) of CA1 PCs (P < 0.001 One-way ANOVA, P < 0.001 Dunnett's *post hoc* test; n = 3 rats). (B) Gold particle density for the $K_v2.1$ subunit on the AISs of CA1 PCs was significantly different from the background (BG; P < 0.01 One-way ANOVA, P < 0.01 Dunnett's *post hoc* test; n = 3 rats). These data were obtained from double-labeling experiments for the $K_v2.1$ and $K_v1.1$ subunits. Gold particle densities for the $K_v2.1$ subunit on PC somata was similar in single- and double-labeling experiments (*cf.* A and B). obl., oblique; prox., proximal; mid., middle; dist., distal.

DOI:10.14753/SE.2018.2123

5.2. Target cell type-dependent localization of voltage-gated Ca^{2+} channels in CA3 PC axon terminals

5.2.1. $Ca_v2.1$ and $Ca_v2.2$ subunit densities in presynaptic AZs of CA3 PC axon terminals contacting $K_v3.1b$ and $mGlu_{1a}$ immunopositive dendrites

In the next set of experiments, I tested the hypothesis that different Ca_v channel densities in presynaptic AZs underlie different P_r values[271]. I chose CA3 PC local axon terminals in the SO of young rats as the subject of my study. These axons establish synapses onto fast-spiking PV-containing INs, which show high initial P_r and short-term depression, whereas next bouton of the same axon has low initial P_r and displays short-term facilitation when its postsynaptic target is $mGlu_{1a}$ and somatostatin expressing IN. The functional characterization of these synapses was performed by Tímea Éltes and Noémi Holderith in our laboratory[294]. I performed SDS-FRL to quantitatively compare the immunogold labeling for Ca_v subunits in presynaptic AZs that synapse onto distinct IN types. To achieve this, the postsynaptic targets of the axon terminals need to be identified. This requires the use of face-matched 'mirror replica' technique[79] and the molecular identification of the target IN types because the type of IN from small fractured membrane segments cannot be determined based on morphological features (Figure 15 and Figure 16). One replica was immunoreacted to identify IN dendrites; its mirror surface was labeled for a Ca_v subunit and all subcellular structures (dendrites, AZs) were identified in both replicas. The metabotropic $mGlu_{1a}$ receptor is a transmembrane protein that is expressed in the somato-dendritic plasma membrane of hippocampal INs and specific antibodies are available that can be used for replica labeling[283]. PV is a cytoplasmic protein that cannot be detected with SDS-FRL, so I identified somato-dendritic regions of fast-spiking PV^+ INs based on the presence of immunogold labeling for the $K_v3.1b$ voltage-gated K^+ channel subunit[134]. Both $mGlu_{1a}$ and $K_v3.1b$ antibodies recognize intracellular epitopes and thus label the P-face of dendritic plasma membranes. Many membrane segments are attached to these IN dendrites that represent the E-face of presynaptic axon terminals. Because my antibodies against Ca_v subunits recognize intracellular epitopes (label on the P-face), they cannot be used to localize these channels in these attached axonal E-face

membranes. The P-faces of these dendrite-attached presynaptic membranes are present in the mirror replicas. Because the release of glutamate from these axon terminals are mainly mediated by $Ca_v2.1$ and $Ca_v2.2$ subunits[294], I localized both subunits. The rabbit anti-$Ca_v2.1$ antibody used in the experiments provides identical labeling to that observed with another Ca_v antibody raised in guinea pig, which specificity was verified in tissue obtained from *$Ca_v2.1^{-/-}$* mice[235]. The specificity of the $Ca_v2.2$ immunolabeling was validated on hippocampal tissue of *$Ca_v2.2^{+/+}$* and *$Ca_v2.2^{-/-}$* mice (Figure 14A, B, D and E). The labeling pattern in *$Ca_v2.2^{+/+}$* mice tissue was similar to that observed in rats (Figure 14C and F).

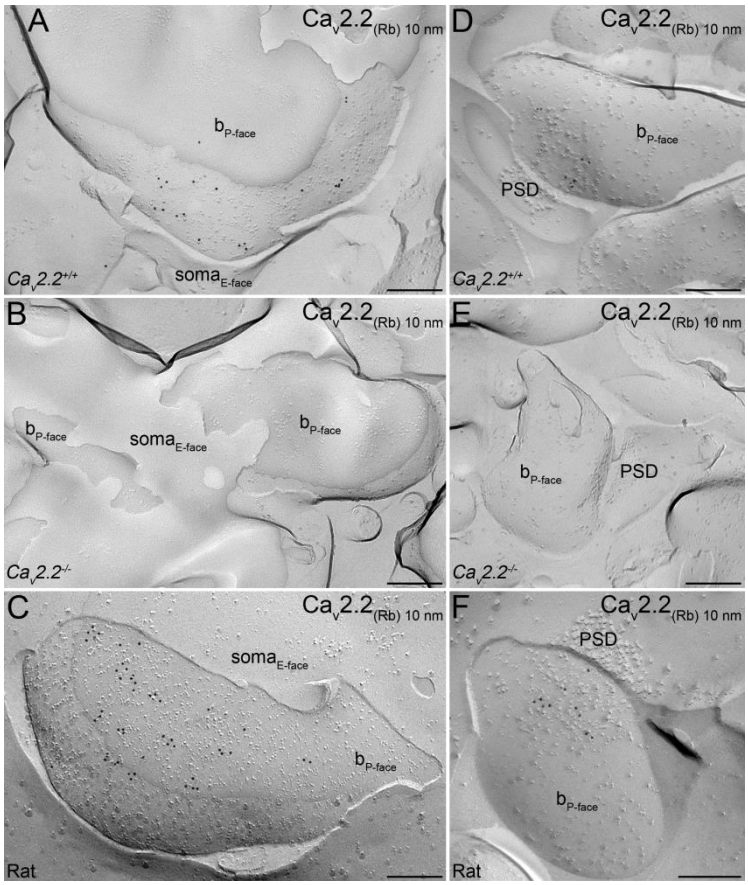

Figure 14. The $Ca_v2.2$ subunit immunolabeling is abolished in *$Ca_v2.2^{-/-}$* mice. (A–C) Perisomatic axon terminals are labeled for the $Ca_v2.2$ subunit in a *$Ca_v2.2^{+/+}$* mouse (A) and in a Wistar rat (C). In *$Ca_v2.2^{-/-}$* mice only non-labeled profiles were observed in the SP (B). (D–F) $Ca_v2.2$ labeling is concentrated in putative AZs facing a PSD on the opposing E-face in replicas from a *$Ca_v2.2^{+/+}$* mouse (D) and a Wistar rat (F). The $Ca_v2.2$ labeling was absent from AZs in *$Ca_v2.2^{-/-}$* mice (E). S*cale bars, 200 nm.*

In rats, the dendrite-attached P-face membrane segments were often labeled for the $Ca_v2.1$ subunit and the gold particles were concentrated over areas that had an elevated density of IMPs, corresponding to the AZs[79] (Figure 15A–N). The normalized density of gold particles within the AZs was significantly larger than that found in the surrounding E-face plasma membranes (defined as background; $P < 0.0001$ Kruskal–Wallis test, $P < 0.0001$ *post hoc* Mann-Whitney *U* test tests with Bonferroni correction),

DOI:10.14753/SE.2018.2123

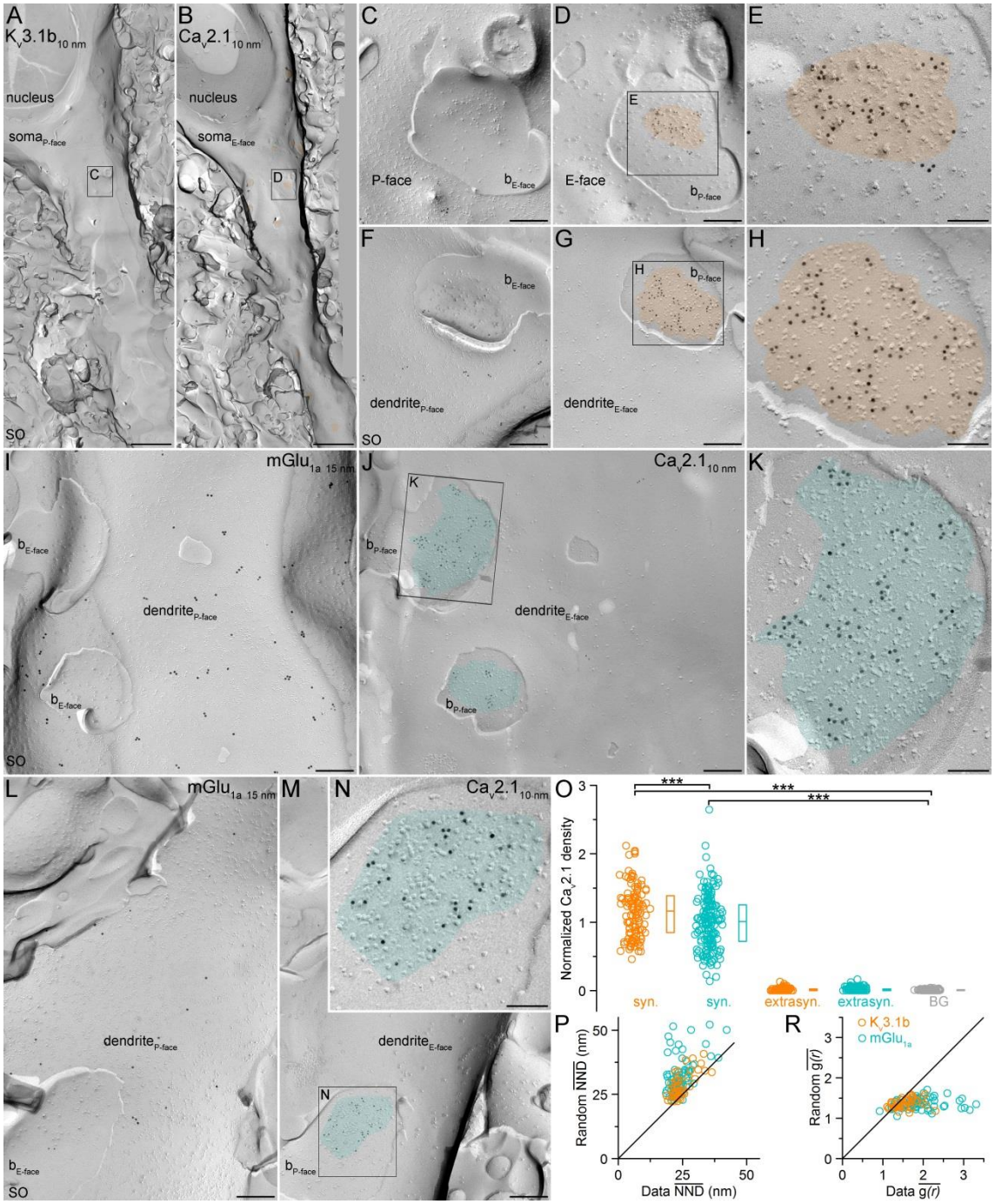

Figure 15. The density of $Ca_v2.1$ subunit is 1.15 times larger in the AZs of $K_v3.1b^+$ compared with $mGlu_{1a}^+$ dendrite-targeting boutons. (A and B) Corresponding electron microscopic P-face and E-face images of a $K_v3.1b^+$ (expressed in PV^+ cells) cell receiving several excitatory inputs (orange in B). (C and D) Higher-magnification images of the boxed areas in (A) and (B) show a perisomatic E-face membrane with attached P-face fragments of boutons ($b_{P\text{-face}}$) containing AZs (orange in D). AZs are indicated by the loose cluster of IMPs. (E) Higher-magnification view of the boxed areas in (D). (F–H) Another example of an intensely $Ca_v2.1$ labeled AZ attached to a $K_v3.1b^+$ dendrite. (I and J) P-face and E-face images of an $mGlu_{1a}$-immunoreactive dendrite contacted by axon terminals with AZs (cyan in J). (K) Higher-magnification

image of the boxed area in (J). (L–N) Another $mGlu_{1a}$ dendrite-attached AZ with intense $Ca_v2.1$ labeling. (O) Normalized densities of gold particles labeling the $Ca_v2.1$ subunit within presynaptic AZs (syn.), extrasynaptic bouton membranes (extrasyn.), and surrounding E-face membranes (background: BG, gray) obtained from five rats. *Post hoc* Mann-Whitney *U* test tests with Bonferroni correction after Kruskal–Wallis test ($P < 0.0001$) demonstrated a significant difference between the synaptic and background labeling ($P < 0.0001$), and between the synaptic compartments of $K_v3.1b^+$ and $mGlu_{1a}^+$ dendrite-targeting boutons ($P < 0.001$). Circles indicate individual measurements of AZs, boxes indicate IQRs, and horizontal bars indicate medians. (P) NND was calculated for each gold particle within an AZ and the mean value ($\overline{NND}$) is plotted against the $\overline{NND}$ of randomly placed gold particles (repeated 1000 times) for each AZ contacting $K_v3.1b^+$ (n = 43) or $mGlu_{1a}^+$ (n = 72) dendrites. Wilcoxon signed rank test revealed a significant difference ($P < 0.0001$) between the data and the random distributions for both AZ populations. (R) Comparison of the mean 2D spatial autocorrelation functions ($\overline{g(r)}$) measured in individual $K_v3.1b^+$ (n = 43) or $mGlu_{1a}^+$ (n = 72) dendrite-targeting AZs to their simulated random controls (repeated 1000 times). Wilcoxon signed-rank test revealed significant differences ($P < 0.0001$) *between the* data and the random distributions for both AZ populations. *Scale bars, 2 μm (A and B); 250 nm (C, D, F, G, I, J, L and M); 100 nm (E, H, K and N).*

whereas the $Ca_v2.1$ subunit density in extrasynaptic bouton membranes was similar to that of the background ($P < 0.0001$ Kruskal–Wallis test, $P > 0.05$ *post hoc* Mann-Whitney *U* test tests with Bonferroni correction; Figure 15O). I performed these experiments in five animals and analyzed a total of 112 and 172 AZs attached to $K_v3.1b^+$ and $mGlu_{1a}^+$ dendrites, respectively, in the SO of the CA3 area. Quantitative comparison of the two AZ populations revealed an overall 1.15 times higher density in $K_v3.1b^+$ dendrite-targeting AZs ($P < 0.0001$ Kruskal–Wallis test, $P < 0.001$ *post hoc* Mann-Whitney *U* test tests with Bonferroni correction; Figure 15O; for non-normalized gold densities see Table 3) Next, I conducted the same investigation for the other major Ca_v subunit ($Ca_v2.2$; Figure 16).

Presynaptic P-face plasma membranes attached to $K_v3.1b^+$ (n = 52) or $mGlu_{1a}^+$ (n = 114) dendrites were also heavily labeled for the $Ca_v2.2$ subunit (Figure 16A–I). Gold particles were confined to the AZs, where their densities were significantly higher than the background ($P < 0.0001$ Kruskal–Wallis test, $P < 0.0001$ *post hoc* Mann-Whitney *U* test tests with Bonferroni correction; Figure 16J). $Ca_v2.2$ subunit densities also showed a 1.20-fold higher value in $K_v3.1b^+$ compared with $mGlu_{1a}^+$ dendrite-targeting AZs, but the difference did not reach significance ($P < 0.0001$ Kruskal–Wallis test, $P > 0.02$ *post hoc* Mann-Whitney *U* test tests with Bonferroni correction; Figure 16J; for non-normalized gold densities, see Table 3).

DOI:10.14753/SE.2018.2123

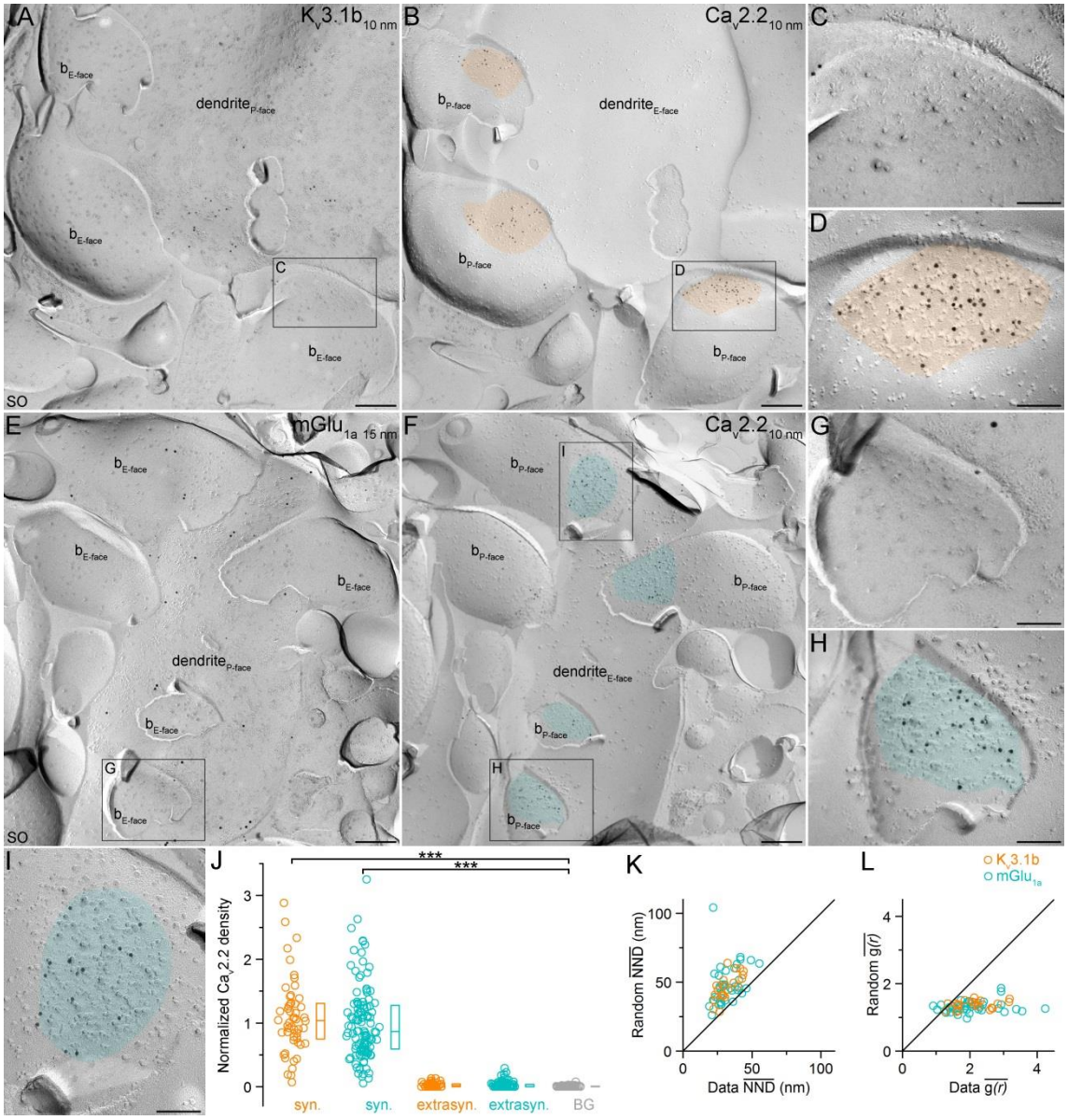

Figure 16. The densities of $Ca_v2.2$ subunit in AZs of PC boutons targeting $K_v3.1b^+$ and $mGlu_{1a}^+$ dendrites. (*A* and *B)* A $K_v3.1b$ dendrite ($dendrite_{P\text{-}face}$ in A) is contacted by boutons with P-face ($b_{P\text{-}face}$) membranes that show strong $Ca_v2.2$ subunit reactivity in their AZs (orange in B). (C and D) High-magnification images of the boxed areas shown in (A) and (B), respectively. (E and F) P-face bouton membranes contacting an $mGlu_{1a}^+$ dendrite ($dendrite_{P\text{-}face}$ in E) contain $Ca_v2.2$ subunit immunolabeled AZs (cyan in F). (G–I) Enlarged views of the boxed areas in (E) and (F). (J) Normalized densities of gold particles labeling the $Ca_v2.2$ subunit within presynaptic AZs (syn.) and extrasynaptic membranes (extrasyn.) of boutons contacting $K_v3.1b^+$ or $mGlu_{1a}^+$ profiles and in surrounding E-face membranes (background: BG, gray). *Post hoc* Mann-Whitney *U* tests with Bonferroni correction after Kruskal–Wallis test ($P < 0.0001$) demonstrated a significant difference between the synaptic and background labeling ($P < 0.0001$).Circles indicate individual measurements of AZs, boxes indicate IQRs, and horizontal bars indicate medians. (K) Comparison of $\overline{NND}$'s measured in 21 $K_v3.1b^+$ and 40 $mGlu_{1a}^+$ dendrite-contacting AZs to their random controls (repeated 1000 times).

Wilcoxon signed-rank test revealed significant difference ($P < 0.0001$) between the data and the random distributions for both AZ populations. (L) $\overline{g(r)}$ of individual $K_v3.1b^+$ (n = 21) or $mGlu_{1a}^+$ (n = 40) dendrite-targeting AZs is plotted against the $\overline{g(r)}$ of their random controls (repeated 1000 times). Wilcoxon signed-rank test revealed significant differences ($P < 0.0001$) between the data and the random distributions for both AZ populations. *Scale bars, 250 nm (A, B, E and F); 100 nm (C, D, G, H and I).*

5.2.2. Non-random distribution of the $Ca_v2.1$ and $Ca_v2.2$ subunits in presynaptic AZs contacting $K_v3.1b$ and $mGlu_{1a}$ immunopositive dendrites

Finally, I investigated whether the sub-AZ distribution of the gold particles labeling the Ca_v subunits is compatible with a random process. To test this, I computed the $\overline{\mathrm{NND}}$ and the $\overline{g(r)}$ then compared the real anti-$Ca_v2.1$ immunogold distribution data in 43 $K_v3.1b^+$ and 72 $mGlu_{1a}^+$ dendrite-targeting AZs (fractured in their completeness) with their corresponding random distributions (same number of gold particle placed randomly in the same area, 1000 repetitions). Both measures revealed that the actual data were significantly different from random distributions ($P < 0.0001$ Wilcoxon signed-rank test; Figure 15P and R). A similar result was obtained for the $Ca_v2.2$ subunit in 21 ($K_v3.1b$) and 40 ($mGlu_{1a}$) AZs ($P < 0.0001$ Wilcoxon signed-rank test; Figure 16K and L). The significantly lower mean $\overline{\mathrm{NND}}$s and the $\overline{g(r)} > 1$ in both $K_v3.1b^+$ and $mGlu_{1a}^+$ dendrite-innervating AZs demonstrate spatial inhomogeneities of gold particles within these AZs.

DOI:10.14753/SE.2018.2123

Table 3. Properties of Ca_v immunoreactivities in $K_v3.1b^+$ and $mGlu_{1a}^+$ dendrite-innervating axon terminals. Density values are calculated from the medians of 5 ($Ca_v2.1$) and 4 ($Ca_v2.2$) rats. For the NND calculations AZs fractured in their completeness were subselected and pooled together from the same rats.

	$K_v3.1b^+$ dendrite-targeting boutons				$mGlu_{1a}^+$ dendrite-targeting boutons			
	Mean	SD	Median	n	Mean	SD	Median	n
$Ca_v2.1$ subunit density in AZs (gold/μm^2)	373	47	370	112	321	46	325	172
$Ca_v2.2$ subunit density in AZs (gold/μm^2)	151	30	139	52	130	39	130	114
$Ca_v2.1$ subunit density in extrasynaptic membranes (gold/μm^2)	2.14	2.46	2.21	93	2.88	2.64	2.23	174
$Ca_v2.2$ subunit density in extrasynaptic membranes (gold/μm^2)	2.69	3.15	2.35	48	1.02	1.26	0.75	113
Background $Ca_v2.1$ subunit density (gold/μm^2)	2.27	1.93	2.94	132	2.27	1.93	2.94	132
Background $Ca_v2.2$ subunit density (gold/μm^2)	0.66	0.33	0.62	104	0.66	0.33	0.62	104
$Ca_v2.1$ NND distance (nm)	24.7	4.0	23.3	43	24.3	4.6	23.1	72
$Ca_v2.2$ NND distance (nm)	32.1	7.2	30.3	21	32.0	8.3	28.7	40

5.3. Input cell type-dependent localization of voltage-gated Ca^{2+} channels in basket cell axon terminals of the hippocampal CA3 area

5.3.1. Segregation of presynaptic Ca_v channels in CCK^+ and PV^+ axon terminals targeting the somatic region of CA3 PCs

In the final part of my work, I examined the distribution of Ca_v channels in IN axon terminals targeting the soma of CA3 PCs. The somatic region of PCs is contacted almost exclusively by basket cells expressing either PV or CCK/CB_1[111,295]. Previous experiments employing subtype-specific Ca_v channel blockers indicated that GABA release from CCK/CB_1^+ neurons is almost exclusively mediated by N-type channels, whereas PV^+ INs rely on P/Q-type channels[274,275,296]. However, direct experimental data is not available concerning the localization of these subunits on these terminals. Therefore, I carried out high-resolution SDS-FRL of the $Ca_v2.1$ and $Ca_v2.2$ subunits in axon terminals targeting the soma of CA3 PCs in adult rats. As the antibodies against the Ca_v subunits recognize intracellular domains of the target molecules, I focused on P-face segments of axon terminals attached to E-face somatic membranes. To differentiate between the two populations of axon terminals contacting the somatic region of PCs, I identified the axon terminals as CCK-containing boutons if they were immunolabeled for CB_1, and PV^+ if they were CB_1 immunonegative. To prove this assumption, first I preformed double-labeling experiments for CB_1 and VGAT, to show that the P-face membrane segments attached to E-face somatic membranes are GABAergic, while a subset of them is CB_1 immunoreactive (Figure 17A and B). Secondly, I colocalized of CB_1 with synaptotagmin-2, the Ca^{2+} sensor specific to PV^+ axon terminals in the hippocampus and cortex[297-299]. As expected, the axon terminals segregated into two non-overlapping populations: the CB_1 and the synaptotagmin-2 immunopositive profiles (Figure 17C and D), confirming that immunolabeling for CB_1 in itself is enough to distinguish between CCK^+ and PV^+ boutons. The specificity of the CB_1 immunosignal was validated in replicas from $CB_1^{+/+}$ and $CB_1^{-/-}$ mice. In mice, the antibodies raised against the CB_1 also labeled VGAT immunopositive profiles in the SP (Figure 18A and B), and the CB_1 signal completely disappeared in brain section obtained from $CB_1^{-/-}$ mice (Figure 18C–F).

DOI:10.14753/SE.2018.2123

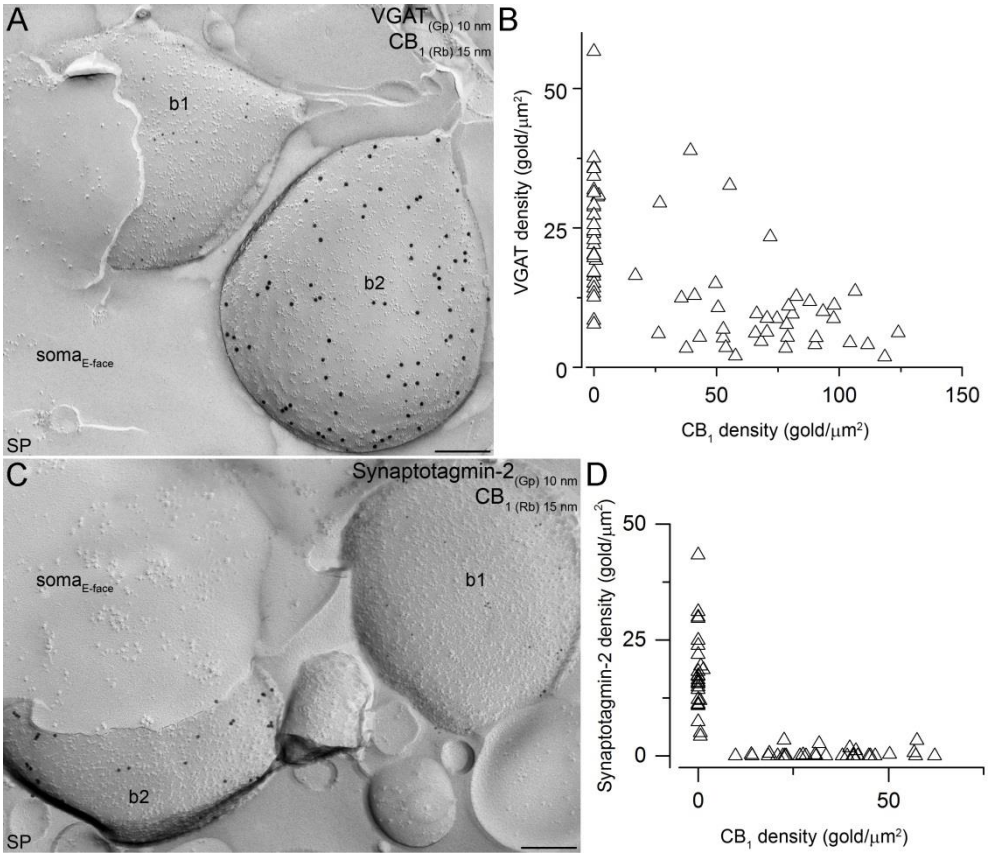

Figure 17. Segregation of soma-targeting GABAergic boutons based on CB_1 immunoreactivity in the rat CA3 area. (A) Double-labeling experiment for CB_1 (15 nm gold) and VGAT (10 nm gold) demonstrates that the CB_1 immunopositive P-face profile is a GABAergic axon terminal (b2). Note that not all VGAT labeled terminals contain CB_1 (b1). (B) Background-subtracted density values for CB_1 and VGAT in VGAT immunopositive axon terminals are shown. (C) Colocalization of CB_1 (15 nm gold) and synaptotagmin-2 (10 nm gold) revealed that these proteins are fully exclusive on soma-tageting axon terminals. (D) Background-subtracted density values for CB_1 and synaptotagmin-2 in P-face segments of axon terminals attached to E-face somatic membranes are shown. In (B) and (D) each symbol represents an individual bouton (n = 1 rat). Gp: guinea pig; Rb: rabbit. *Scale bars: 200 nm.*

When I performed colocalization of CB_1 and $Ca_v2.2$, I found that many CB_1 immunopositive terminals attached to E-face somatic membranes contained the $Ca_v2.2$ subunit, but the $Ca_v2.2^+$ profiles were almost always CB_1^+ (94%; Figure 19A–D). Double-labeling experiments for the CB_1 and $Ca_v2.1$ subunit revealed that the CB_1 immunopositive boutons almost never contained the $Ca_v2.1$ subunit (95% were $Ca_v2.1$ immunonegative; Figure 19E–G). Finally, double immunolabeling for the $Ca_v2.1$ and $Ca_v2.2$ subunits further confirmed the segregation of these Ca_v subunits in axon terminal membrane segments fractured onto PC somata: 89% of the fractured membranes had

either $Ca_v2.1$ or $Ca_v2.2$ labeling (Figure 19H–K). Taken together, these experiments provide morphological evidence for the exclusive role of these Ca_v subunits in PV^+ and CCK^+ basket cell axon terminals. It is important to note that the segregation of Ca_v channels could also be observed in mice (92% of the fractured membranes had either $Ca_v2.1$ or $Ca_v2.2$ labeling; Figure 20) where the specificity of the Ca_v antibodies was tested (see chapter 5.2.1.).

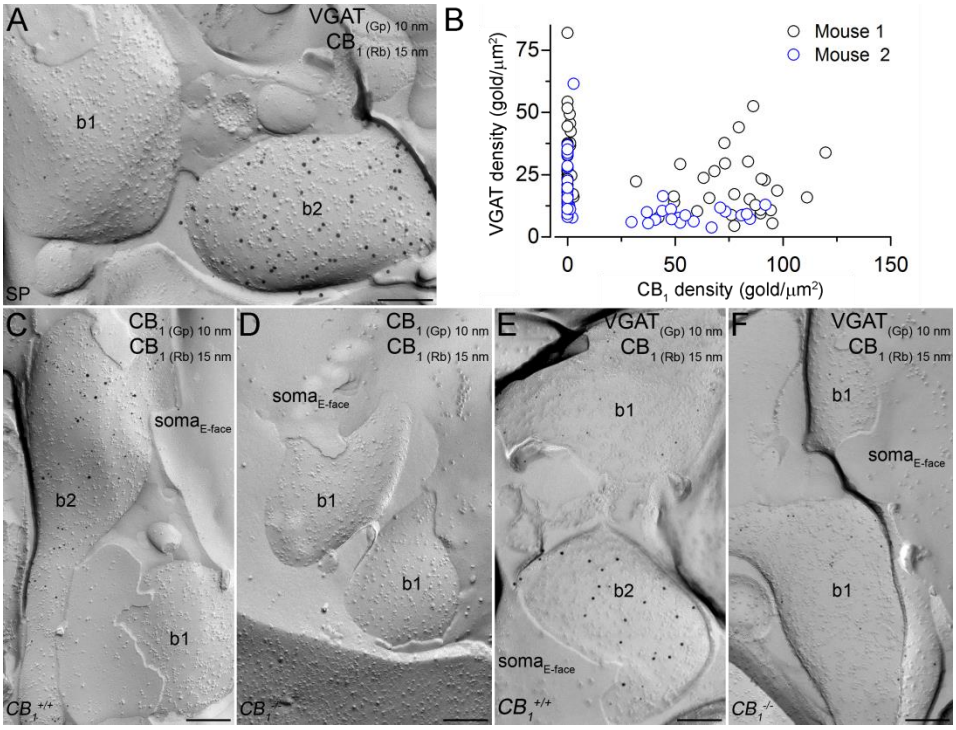

Figure 18. Testing the specificity of the CB_1 immunolabeling with SDS-FRL. (A) Double-labeling experiments for CB_1 (15 nm gold) and (VGAT, 10 nm gold) reveal that the CB_1-immunolabeled profiles are GABAergic axon terminals (b2), but not all VGAT-labeled terminals contain CB_1 (b1). (B) Background-subtracted density values for CB_1 and VGAT of VGAT immunopositive axon terminals are shown from two mice. Symbols represent individual boutons. (C–F) The CB_1 immunolabeling is abolished in $CB_1^{-/-}$ mice. A perisomatic axon terminal is co-labeled with two CB_1 antibodies in a $CB_1^{+/+}$ mouse (b2 in C), while another is unlabeled (presumed PV^+ axon terminals, b1 in C). In $CB_1^{-/-}$ mice only unlabeled profiles could be observed in the SP (b1 in D). A VGAT (10 nm gold) immunolabeled axon terminal is strongly CB_1 immunopositive (15 nm gold, b2 in E) in a $CB_1^{+/+}$ mouse, but all $VGAT^+$ boutons are immunonegative in the $CB_1^{-/-}$ tissue (b1 in F). Rb, rabbit; Gp, guinea pig. *Scale bars, 200nm.*

DOI:10.14753/SE.2018.2123

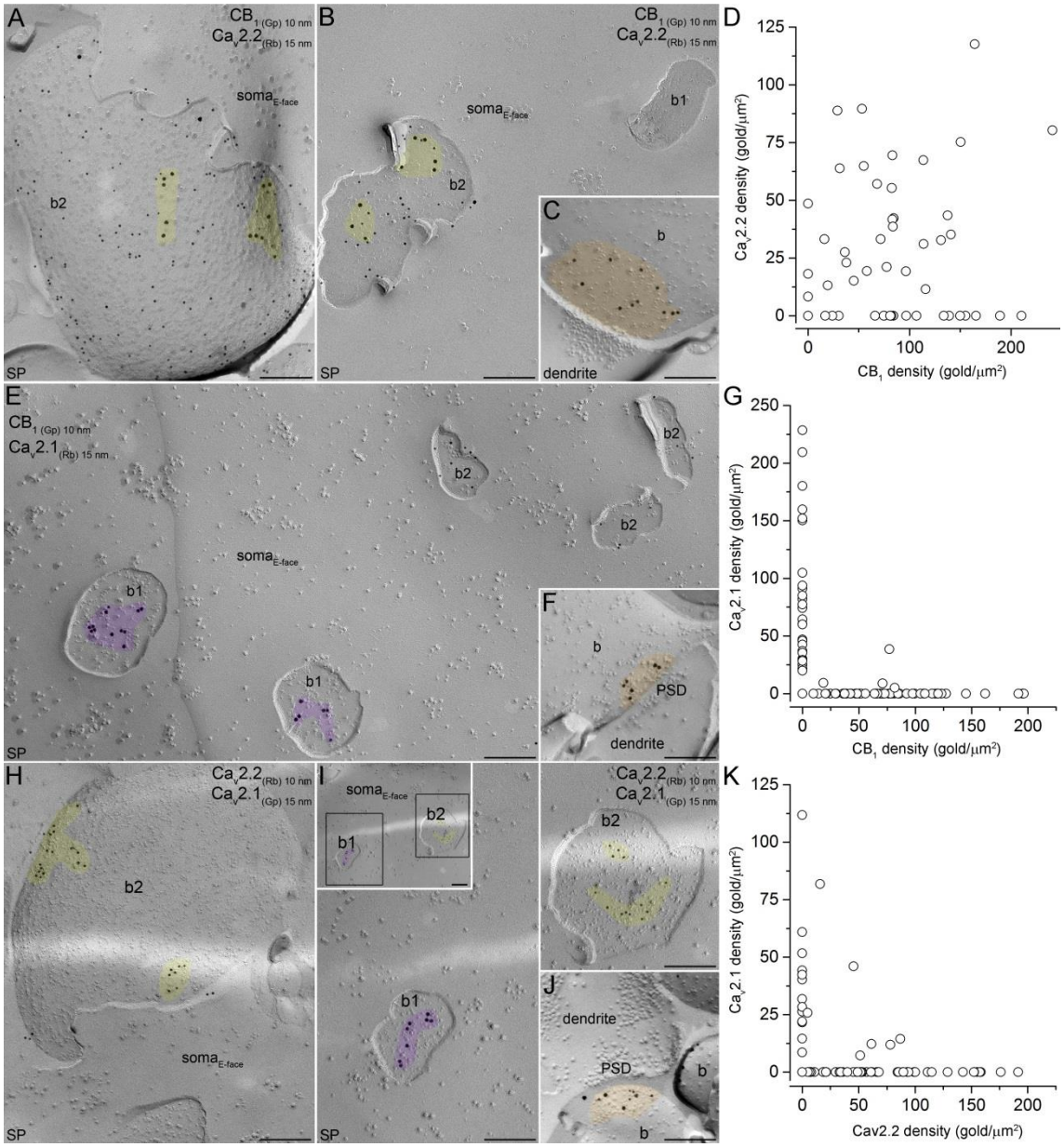

Figure 19. CB_1 immunopositive axon terminals contain the $Ca_v2.2$, but not the $Ca_v2.1$ subunit in the rat hippocampus. (A and B) A perisomatic axon terminal (b2 in A) and a P-face section of an axon terminal (b2 in B) attached to somatic E-face membrane are co-labeled for CB_1 (10 nm gold) and $Ca_v2.2$ subunit (15 nm gold), while another one is unlabeled (b1). (C) An excitatory axon terminal contains only $Ca_v2.2$ subunit, but not the CB_1 (orange). (D) Background-subtracted gold particle densities for CB_1 and $Ca_v2.2$ of P-face fragments attached to somatic E-face membranes are shown (n = 1 rat). (E) CB_1 (10 nm gold, b2) or $Ca_v2.1$ subunit (15 nm gold, b1) containing P-face axon terminal fragments are attached to a somatic plasma membrane. (F) The AZ of an excitatory axon terminal contains $Ca_v2.1$ subunit (orange). (G) Background-subtracted gold particle densities for CB_1 and $Ca_v2.1$ subunit of P-face axon terminal sections attached to the E-face somatic membranes (n = 1 rat). (H–J) Perisomatic axon terminals contain either $Ca_v2.2$ (b2 in H and I) or $Ca_v2.1$ (b1 in I) subunit, while an excitatory axon terminal contains both subunits (orange in J). Enlarged views of boxed

areas of (I) are shown on the bottom and on the right. (K) Background-subtracted gold particle densities for $Ca_v2.2$ and $Ca_v2.1$ subunits measured in axon terminal fragments attached to E-face somatic membranes. In panels (A–C), (E), (F), (H–J) putative AZs are pseudocolored for illustrative purposes. In (D), (G) and (K) every symbol represents a P-face fragment with an area between 0.010 μm^2 and 0.207 μm^2 (n= 1 rat). Gp: guinea pig; Rb: rabbit. *Scale bars: 200 nm.*

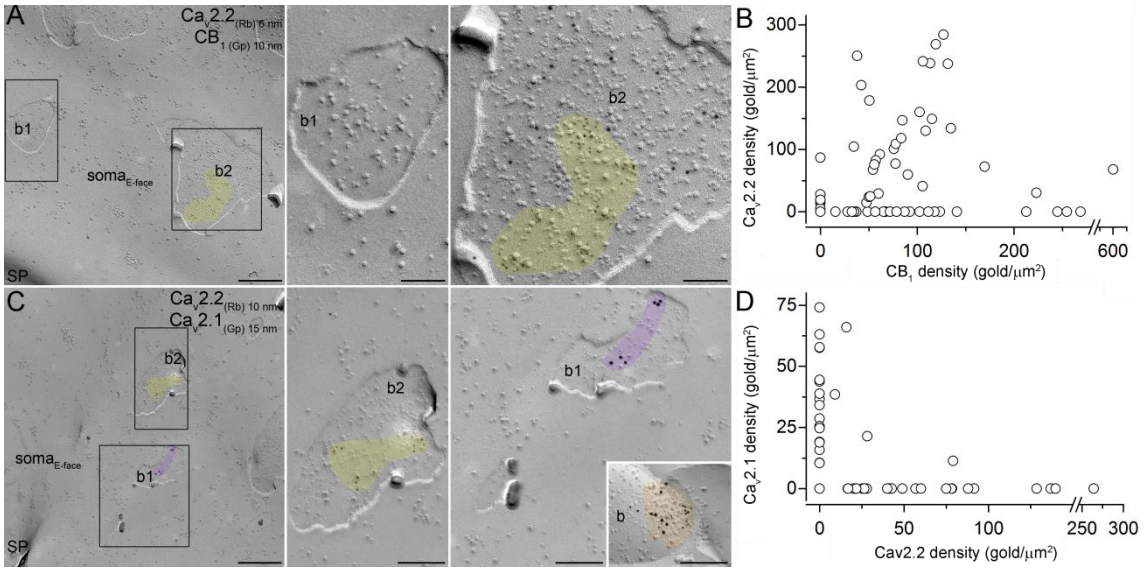

Figure 20. CB_1-immunopositive axon terminals express the $Ca_v2.2$, but not the $Ca_v2.1$ subunit in the mouse hippocampus. (A) A P-face axon terminal fragment attached to an E-face somatic membrane is co-labeled for CB_1 and $Ca_v2.2$ subunit (b2), while another is unlabeled (b1). (B) Background-subtracted densities for CB_1 and $Ca_v2.2$ subunit in P-face axon terminal sections. The CB_1 immunopositive profiles were either $Ca_v2.2$ positive or negative, but the majority (84.2%) of the $Ca_v2.2$ subunit immunopositive profiles containe the CB_1. (C) Double-labeling experiments reveal that the P-face axon terminal fragments attached to E-face somatic membranes are labeled for either $Ca_v2.2$ (b2) or $Ca_v2.1$ (b1) subunit. The AZ of an excitatory axon terminal (b) contains large number of gold particles for both $Ca_v2.2$ and $Ca_v2.1$ subunits (orange, inset). (D) Background-subtracted density values for $Ca_v2.2$ and $Ca_v2.1$ of P-face bouton fragments. Enlarged views of boxed areas of (A) and (C) are shown on the right. In (A) and (C) panels putative AZs are pseudocolored for illustrative purposes. In (B) and (D) every symbol represents a P-face fragment with an area between 0.010 μm^2 and 0.207 μm^2 (pooled from n= 2 mouse). Gp: guinea pig; Rb: rabbit. *Scale bars: 500 nm (A and C); 100 nm (enlarged views of A); 200 nm (enlarged views and inset in C).*

DOI:10.14753/SE.2018.2123

5.3.2. $Ca_v2.2$ and $Ca_v2.1$ subunits are enriched in putative AZs of CCK^+ and PV^+ axon terminals of the CA3 area

The gold particles labeling the $Ca_v2.2$ and $Ca_v2.1$ subunits were restricted to sub-areas of the axon terminal segments, which might correspond to AZs. In contrast to excitatory AZs, where these Ca_v subunits were enriched in AZs identified by the high density of IMPs[79] (Figure 19C, F and J, Figure 20B inset), in soma-targeting GABAergic axon terminals this morphological feature was absent. This observation entails that AZs on these boutons can only be identified by using molecular markers for

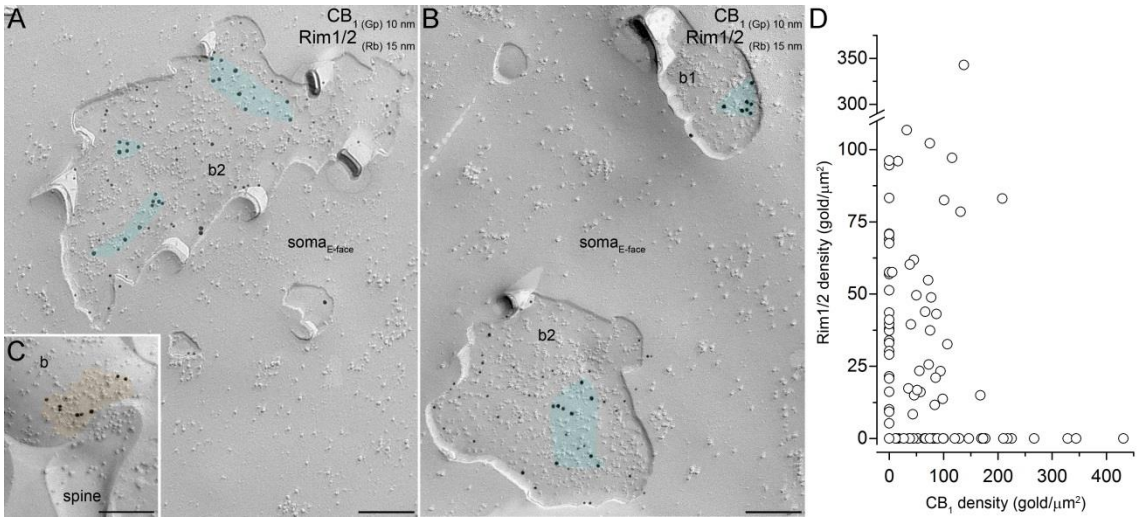

Figure 21 P-face sections of axon terminals attached to E-face somatic membranes contain AZs in the rat CA3 area. (A and B) CB_1 immunopositive (b2, 10 nm) and negative (b1) axon terminals are attached to an E-face somatic plasma membrane. Both axon terminals contain a $Rim1/2^+$ AZ (blue). (C) The AZ of an excitatory terminal (orange) also contains gold particles labeling Rim1/2. In (A–C) panels AZs are pseudocolored for illustrative purposes. (D) Background-subtracted density values for CB_1 and Rim1/2 measured in P-face axon terminal sections attached to the E-face membrane of PC somata. A total of 52% of axon terminal fragments were double negative, while 14.4% were only Rim1/2 immunopositive, 16.3% were only CB_1^+ and the remaining 17.3% contained both Rim1/2 and CB_1 labeling. In (D) every symbol represents a P-face fragment with an area between 0.010 μm^2 and 0.207 μm^2 (n= 1 rat). Gp: guinea pig; Rb: rabbit. *Scale bars: 200 nm.*

AZ proteins. For this reason, I performed labeling of Rim1/2, a protein restricted to excitatory and inhibitory AZs[235]. My results show that 32% of P-face membranes fractured to large E-face somatic membranes contained AZs (n = 1 rat; this ratio was 24% in mice, data pooled from n =2 mice); in all cases without underlying high density of IMPs (Figure 21A and B). Furthermore, the Rim1/2 immunolabeled AZs showed

DOI:10.14753/SE.2018.2123

great variability in size, shape and number, similarly to the $Ca_v2.2$-enriched areas (Figure 21A and B). This finding is consistent with the shapes, sizes and number of AZs obtained from 3D electron microscopic reconstructions of CCK^+ perisomatic boutons performed by Noémi Holderith in our laboratory[290]. In $Ca_v2.1$ and $Ca_v2.2$ double-labeling experiments, the proportion of labeled profiles was similar to the Rim1/2 experiments (43% in rats and 20% mice), further supporting the notion that Ca_v subunits are localized within AZs on these boutons.

Finally, the double-labeling experiments for CB_1 and the presynaptic AZ marker Rim1/2 also revealed an extensive colocalization of the two proteins in rats (Figure 21A and B and Figure 22) and mice (not shown), providing evidence for the presence of CB_1 in presynaptic AZs. My immunoreactions also revealed heterogeneity in the CB_1 content of AZs; some $Rim1/2^+$ AZs were strongly labeled, whereas others were apparently immunonegative.

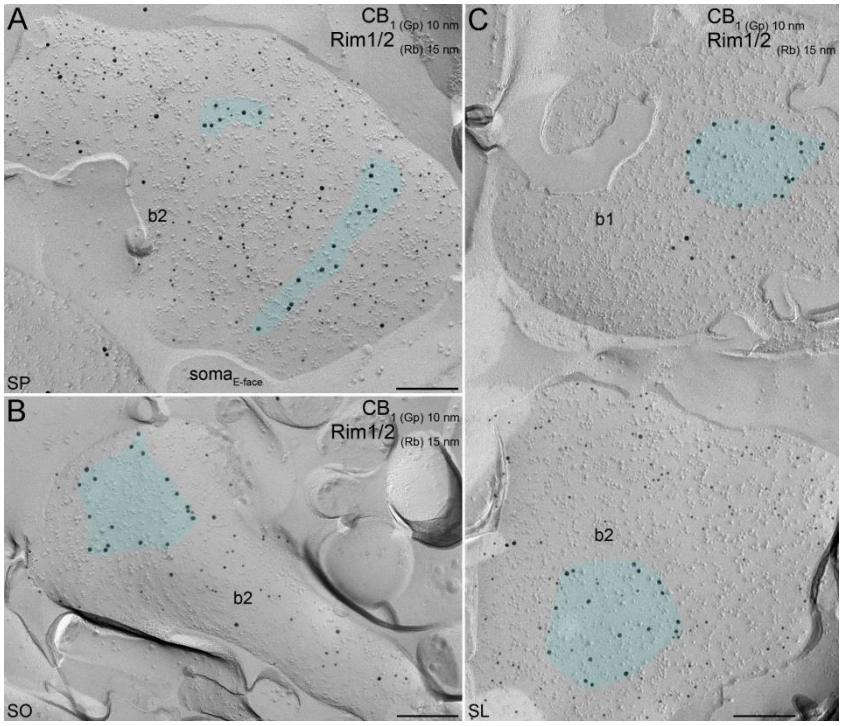

Figure 22. Variability in the CB_1 content in AZs of CB_1 immunoreactive axon terminals in the rat hippocampus. (A–C) Axon terminals contain a variable number of immunogold particles for CB_1 (10 nm gold, b2) in their AZs (blue, labeled by Rim1/2 with 15 nm gold). Around the CB_1^+ axon terminals, CB_1^+ boutons (b1) also contain $Rim1/2^+$ (15 nm gold) AZs. In all panels putative AZs are pseudocolored for illustrative purposes. Gp: guinea pig; Rb: rabbit. *Scale bars: 200 nm.*

DOI:10.14753/SE.2018.2123

6. Discussion

In my dissertation, I investigated the distribution of different voltage-gated ion channels in the hippocampus. I employed the highly sensitive, high-resolution quantitative electron microscopic immunogold method SDS-FRL to address my aims, and exploited the potential of this method to localize my proteins in small subcellular compartments, usually unresolvable and inaccessible with traditional light microscopic immunohistochemical and electrophysiological methods.

In the first part of the study I provided a quantitative surface map of two delayed-rectifier K_v channel subunits on hippocampal CA1 PCs. Afterwards, I revealed target cell type-dependent differences in Ca_v densities in presynaptic AZs of CA3 PC axon terminals contacting two distinct types of INs. Finally, I provided morphological evidence for the exclusive expression of $Ca_v2.2$ and $Ca_v2.1$ Ca^{2+} channel subunits by CCK/CB_1^+ and PV^+ basket cell boutons contacting CA3 PCs.

6.1. The $K_v1.1$ subunit is restricted to axonal compartments of CA1 PCs

In the first part of the study, I revealed a novel distribution pattern of the $K_v1.1$ delayed-rectifier K_v channel subunit on the surface of hippocampal CA1 PCs. Using SDS-FRL, I detected the highest gold particle density for the $K_v1.1$ subunit in AISs of CA1 PCs, in accordance with my immunofluorescent reactions and previous reports using light microscopy. Immunofluorescent labeling of $K_v1.1$ revealed an intense, homogeneous neuropil labeling in SO and SR that could originate from axonal or dendritic profiles. Although K_v1 channels are generally considered ‘axonal’ channels, associating the neuropil labeling with axons without experimental evidence might be premature because K_v1 subunits could also be present in somato-dendritic compartments as shown in, e.g., the ventral cochlear nucleus[199]. Therefore, I used the highly sensitive SDS-FRL method to assess the origin of the neuropil labeling. I could not detect any $K_v1.1$ subunit in the somato-dendritic compartments of CA1 PCs, but found immunogold particles in axon terminals. It is important to note that glutamatergic axon terminals in SR mainly originate from CA3 PCs and those in the SLM from layer 3 PCs of the entorhinal cortex. In SO, there is a mixture of local collaterals of CA1 PCs and Schaffer collaterals of CA3 PCs. Thus my result regarding the axonal labeling of SR and SLM does not directly prove that this ion channel is present in the same density

in CA1 PCs. However, the similar gold densities in axon terminals of SO and SR suggest that the $K_v1.1$ density of local axon collaterals of CA1 PCs is similar to that of Schaffer collaterals. Nevertheless, within SNAP-25 immunopositive axon terminals, the $K_v1.1$ subunit is apparently homogeneously distributed without any preferential accumulation within or nearby the AZs. The density of $K_v1.1$ in axon terminals was approximately eightfold lower than in AISs. This eightfold difference in the density might not be the only difference in these two axonal compartments, because a potential differential distribution of associated β subunits[300] that alter the kinetic properties of K_v1 channels could add another layer of complexity. In addition, the subunit composition of heteromeric K_v1 channels might also be different in these two axonal compartments. Homomeric $K_v1.1$ channels are retained in endoplasmic reticulum[301], suggesting the presence of heteromeric functional channels in the plasma membranes. In CA1 PCs, $K_v1.1$, $K_v1.2$ and $K_v1.4$ are the most abundantly expressed K_v1 subunits (http://brain-map.org). In AISs[169] and juxta-paranodal regions of myelinated axons[302], immunolabeling for the $K_v1.1$ and $K_v1.2$ subunits showed a very similar distribution pattern, suggesting that they might form heteromeric channels in these compartments. The neuropil of the CA1 area is strongly labeled for the $K_v1.1$ and $K_v1.4$, but not the $K_v1.2$ subunit[169,197], indicating that in presynaptic glutamatergic terminals the $K_v1.1$ subunit might be co-assembled with the $K_v1.4$ subunit, similar to other axon terminals containing fast-inactivating, α-dendrotoxin-sensitive outward currents[50].

6.2. Axo-somato-dendritic distribution of the $K_v2.1$ subunit

I also determined the distribution of the $K_v2.1$ subunit, which is the most ubiquitously expressed K_v channel subunit in the brain. It is responsible for mediating the majority of the delayed-rectifier K^+ current in various types of neurons and it is thought to shape AP trains during high frequency firing[171,180,303]. In agreement with previous traditional light microscopic results[181-187], I detected the highest density of gold particles labeling the $K_v2.1$ subunit in AISs, somatic and proximal dendritic plasma membranes. These compartments contained the $K_v2.1$ subunit at similar densities. $K_v2.1$ subunits have been shown to form clusters in neuronal plasma membranes[181,188]. Altered neuronal activity induces calcineurin-mediated dephosphorylation and dispersion of the clustered channels, which is paralleled by changes in their biophysical

properties[181,188,304]. In my immunogold reactions, both clustered and scattered $K_v2.1$ subunits were present in the axo-somato-dendritic plasma membranes, suggesting the presence of $K_v2.1$ channels in differential phosphorylated states. Due to its high sensitivity, SDS-FRL allows the detection of proteins in compartments where they are expressed at low densities. I was able to detect the scattered $K_v2.1$ subunits in AISs, somata and proximal dendrites, where their average density is moderate (~ 10 gold/μm^2) but their out-of-cluster density is very low. However, I was still unable to detect this subunit in other dendritic compartments (e.g. oblique dendrites and spines). Pre-embedding immunogold experiments localized the $K_v2.1$ subunit adjacent to inhibitory PSDs[184]. I was not able to detect gold particles inside the NL-2-containing GABAergic PSDs, but $K_v2.1$ clusters were often formed within less than a micrometer distance from perisomatic GABAergic synapses. Somato-dendritic $K_v2.1$ clusters have been found over subsurface cysternal organelles and their role in Ca^{2+} signaling has been proposed[184], but whether and how they affect neighboring $K_v2.1$ channel function remain to be determined.

6.3. $K_v2.1$ and $K_v1.1$ subunits are segregated within the AIS of CA1 PCs

An intriguing finding of the first part of my work is that the $K_v1.1$ subunits and the clustered $K_v2.1$ subunits occupy discrete, non-overlapping subdomains within the AISs of CA1 PCs. The AIS is a highly specialized subcellular compartment, accumulating voltage-gated ion channels at high densities, especially Na_v channels, thereby ensuring the lowest threshold for AP generation[10,11]. Various mechanisms control the expression of ion channels in the AIS. Ank-G anchors Na_v channels as well as K_v7 channels in the AIS via direct binding[292,305,306]. Expression of the K_v1 channels in the AIS depends on different mechanisms involving PSD-93[192], Caspr2[307] and recently the contribution of the cytoskeletal linker protein 4.1B has also been proposed[308]. Interestingly, although anchored by different proteins in the AISs, the $K_v1.1$ and $K_v1.2$ subunits occupy the same plasma membrane areas as the $Na_v1.6$ subunit (Figure 7 and Figure 8; see also [169]). Previously, nonhomogeneous labeling for Ank-G, NF and the $Na_v1.6$ subunit was found within the AIS of CA1 PCs, where discrete patches remained unlabeled, and were identified as PSDs of axo-axonic synapses[69]. Similarly, here I found that small clusters of the $K_v2.1$ subunits avoided

plasma membrane areas rich in the $Na_v1.6$ (Figure 9E–K and Figure 12A and B) and $K_v1.1$ (Figure 12C and D) subunits. However, my reactions also demonstrated that these $K_v2.1$ clusters are also distinct from GABAergic axo-axonic synapses. They were not only morphologically different, but often separated by $Na_v1.6$- and $K_v1.1$-rich membrane areas. AISs are also polarized along the proximo-distal axis, having high density of $Na_v1.1$ and $Na_v1.2$ subunits in the proximal regions and $Na_v1.6$, $K_v1.1$ and $K_v1.2$ subunits in the more distal part[69,169]. The distribution of the $K_v2.1$ subunit does not seem to follow such a tendency, as clusters are uniformly distributed along the entire length of the AIS of CA1 PCs. We hypothesize that these compartments are not necessarily electrically distinct, but these channels might require differential regulation and association with intracellular signaling cascades, which could underlie their sub-micrometer segregation.

6.4. Unique distribution patterns of distinct ion channels in CA1 PCs.

Hippocampal CA1 PCs have been the subject of many functional, structural and molecular investigations. There is a large body of experimental data revealing the presence of voltage- and ligand-gated ionic currents in different subcellular compartments. Electrophysiological recordings detected a similar increase in the density of the hyperpolarization-activated mixed cation current (I_H) and I_A in the main apical dendrites of CA1 PCs[40,41], suggesting a very similar distribution of the underlying HCN1/2 and $K_v4.2$ subunits. However, electron microscopic immunogold studies performed by my colleagues revealed that the subcellular distribution of the HCN1[309] and $K_v4.2$[179] subunits are markedly different. Consistent with the electrophysiological findings, a distance-dependent increase in the density of the HCN1 subunit was found in distal dendritic shafts[309]. In contrast, the $K_v4.2$ subunit showed only a moderate (70%) increase in the density in the SR[179]. Neither the HCN1, nor the $K_v4.2$ subunit was detected in the axonal compartments of CA1 PCs. SDS-FRL localization of the $Na_v1.6$ subunit revealed a completely different distribution pattern[69]. The $Na_v1.6$ subunit was identified in both somato-dendritic and axonal compartments. The highest density was found in nodes of Ranvier and in AISs, and only a low density was detected in somata and proximal apical dendrites. In the main apical dendrites, the density of Nav1.6

subunit decreased as a function of distance from the soma, and dendritic spines were always immunonegative.

SDS-FRL localization of the G-protein coupled inwardly rectifying K^+ channel $K_{ir}3.2$ subunit was also performed by my colleague, Katalin Kerti-Szigeti[310]. She found that the distribution of gold particles labeling the $K_{ir}3.2$ was different again, showing a quasi-linear increase from the soma towards the distal dendrites, with no significant difference between the main apical dendrites, oblique dendrites and dendritic spines at approximately the same distance from the soma. This is in good agreement with the work of Chen and Johnston (2005)[311], who reported an enhanced spontaneous activity of $K_{ir}3$ channels at resting membrane potential in the apical dendrites of CA1 PCs as compared to somata, which might be the result of increased channel number or increased open probability of the channels.

Among the ion channels studied in CA1 PCs with quantitative EM, including the $K_v1.1$ and $K_v2.1$ subunits presented here and the HCN1, $Na_v1.6$, $K_v4.2$, and $K_{ir}3.2$ analyzed by my colleagues, so far we found that each ion channel subunit has its own unique distribution pattern on the surface of a given neuron type, and likely to help produce the remarkable neuronal diversity present in the CNS[24,25]. It remains to be seen whether this is a general rule or eventually we will find two distinct subunits with identical distribution pattern.

6.5. Target cell type-dependent differential modulation of voltage-gated Ca^{2+} channel function

In the third part of the study, I determined the densities of Ca_v channels in presynaptic AZs of CA3 PCs contacting two distinct types of INs to test the hypothesis that different Ca_v channel densities in presynaptic AZs underlie different P_r[271]. I performed SDS-FRL of the $Ca_v2.1$ and $Ca_v2.2$ Ca_v subunits, and found that high *Pr*, PV^+ dendrite-innervating terminals exhibited only a 1.15 times higher Ca_v channel subunit density than low *Pr*, $mGlu_{1a}{}^+$ dendrite-contacting synapses.

In parallel, my colleagues Tímea Éltes and Noémi Holderith used independent techniques to estimate the Ca_v channel densities in the AZs of CA3 PCs targeting PV^+ and $mGlu_{1a}{}^+$ dendrites[294]. By performing two-photon Ca^{2+} imaging in hippocampal CA3 PC axon terminals, *post hoc* immunohistochemical identification of their postsynaptic

target cells, followed by 3D electron microscopic reconstructions of the imaged boutons, they estimated the amount of Ca^{2+} entering the bouton (peak concentration × the bouton volume) and divided it by the AZ area, which they called 'functional Ca^{2+} channel density' estimate. Assuming similar Ca_v channel properties in different *Pr* boutons, their data predicted a 1.7–1.9 times higher density of Ca_v channels in high *Pr* AZs.

A potential explanation for the discrepancy between their functional channel density and the SDS-FRL Ca_v subunit density estimates is a preferential enrichment of $Ca_v2.3$/Ca_v1/Ca_v3 subunits in PV^+ dendrite-innervating boutons[222,312]. Tímea Éltes and Noémi Holderith excluded this possibility by showing that 1 μM ω-CTX MVIIC (a selective N- and P/Q-type Ca^{2+} channel blocker at a concentration that almost fully blocked the evoked EPSCs in both IN types) causes an almost identical block of [Ca^{2+}] transients in boutons targeting these distinct IN types, arguing against differential contribution of R-, T-, and L-type Ca_v channels to the [Ca^{2+}] transients[294]. Another possible explanation for this discrepancy is a differential fixed Ca^{2+} buffer concentration in these two bouton populations. However, the similar decay of the [Ca^{2+}] transients (recorded with either 300 or 100 μM Fluo5F) recorded by Tímea Éltes and Noémi Holderith in these bouton populations argues against this possibility[294]. We suggest that differential target cell type-dependent regulation of Ca_v channel function is the most likely mechanism underlying the differences. There are a number of ways to regulate Ca_v channel function. Association with different β subunits promotes different voltage-dependent activation and inactivation (reviewed in [313]). Interactions with SNARE proteins such as syntaxin and SNAP-25 at the so-called 'synprint' motif reduce the channel open probability, whereas additional coexpression of synaptotagmin reverses this effect[314]. This suggests a regulatory switch by which presynaptic Ca_v channels bound to Ca^{2+} sensors are functionally enabled, whereas Ca_v channels decoupled from Ca^{2+} sensors are disabled[250]. The AZ protein Munc13, which is involved in vesicle priming processes, has also been found to alter Ca^{2+} inflow by modulating the kinetic properties of Ca_v channels without changing their density[315]. Probably the most widely studied modulation of Ca_v channel function is its regulation by presynaptic G-protein-coupled receptors (*e.g.*, mGluRs, A_1 adenosine-α_2 noradrenergic, $GABA_B$, or endocannabinoid receptors[296,316-321]). P/Q- and N-type Ca_v channel function is reduced

via direct binding of G-protein β/γ-subunits to Ca_v channel β subunits. In a recent study, Anderson *et al*. (2015)[322] demonstrated that presynaptic neurexins can reduce tonic endocannabinoid production transsynaptically and increase the *Pr* of CA1 PC axons by alleviating presynaptic [Ca^{2+}] from CB_1-mediated inhibition. Another way of modulating Ca_v channel function is phosphorylation: CDK5 (kinase)/calcineurin (phosphatase) equilibrium has been shown to set the phosphorylation state of the $Ca_v2.2$ channels, which influences the voltage dependence of the open probability of the channel[323,324]. Whatever the mechanisms are, they must be able to modulate the function of presynaptic Ca_v channels in a postsynaptic target cell type-dependent manner. The amount of Ca^{2+} entering through presynaptic voltage-gated Ca_v channels is very sensitive to the shape/waveform of the AP[50], so a postsynaptic target cell type-dependent difference in the AP waveform could also explain our results. It remains to be seen whether the AP waveform in boutons[52] that are segregated by only a few micrometers along the same axon could be sufficiently different to account for the 30% difference in the [Ca^{2+}] transient observed in Tímea Éltes and Noémi Holderith's experiments[294]. Rozov *et al.* (2001)[271] tested the transmission between cortical PCs and two distinct IN types (multipolar PV^+ and bitufted somatostatin$^+$) with fast and slow Ca^{2+} buffers. The more robust effect of EGTA (slow buffer) on neurotransmitter release from PC to bitufted compared with multipolar cells predicted a larger physical distance between the Ca_v channels and Ca^{2+} sensors (larger coupling distance) in the low *Pr* synapse. My collegues'[294] functional Ca_v channel density estimate is consistent with this prediction and supports the hypothesis that the mechanisms underlying the low initial *Pr* and the subsequent short-term facilitation is a large Ca_v channel to Ca^{2+} sensor distance[18,250,325]. Another level of complexity might arise from the potential target cell type-dependent differences in the sub-AZ distribution of Ca_v channels[18,253,235,236]. Our NND and ACF analysis revealed that $Ca_v2.1$ and $Ca_v2.2$ subunits show within-AZ distributions that are significantly different from random distributions. However, the fact that the distribution of gold particles in both AZ populations differ from random does not mean that the sub-AZ distribution of Ca_v channels is identical in both AZ populations.

DOI:10.14753/SE.2018.2123

6.6. Target cell type-dependent molecular differences in presynaptic axon terminals

So far, the only known protein with a dramatic difference in its density between low- and high-*Pr* synapses of a single PC axon is $mGlu_7$[97], making it an ideal candidate through which a low initial *Pr* and a consequent short-term facilitation could be achieved. The pharmacological blockade of group III mGluRs (including $mGlu_7$) increases the amplitude of evoked EPSCs, but does not change the facilitating phenotype of EPSCs recorded from CA1 $mGlu_1$ INs[269], suggesting a tonic, mGluR-mediated reduction of transmitter release from these axon terminals. Similarly, knocking down Elfn1 from somatostatin expressing INs also led to an increase in the amplitude of the first EPSC of a train and a reduction in the degree of short-term facilitation[270], consistent with the results of pharmacological block of $mGlu_7$. Indeed, it has been shown recently that the postsynaptically located Elfn1 has a key role in the selective recruitment of $mGlu_7$ to the presynaptic AZs of PC axons that contact somatostatin/$mGlu_1^+$ INs[326] (Figure 23). However, the short-term plasticity of the $mGlu_1$

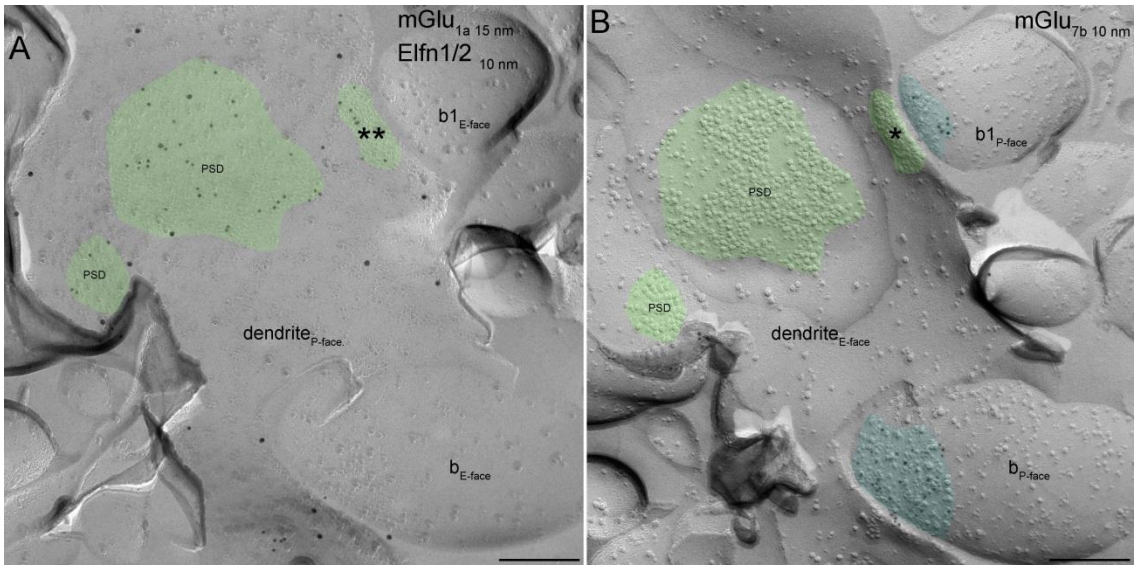

Figure 23. Expression of $mGlu_{7b}$ in the presynaptic AZs of axon terminals targeting a $mGlu_{1a}$ immunopositive dendrite. (A and B) Mirror replica images of a $mGlu_{1a}$ immunolabeled dendrite (15 nm gold on A), which is contacted by two axon terminals ($b_{E\text{-face}}$). The P-face of the boutons shows strong $mGlu_{7b}$ reactivity in their AZs (cyan on B). For one bouton ($b1_{P\text{-face}}$), the fracturing plane traversed from the pre- to the postsynaptic plasma membrane within the synapse, resulting a $mGlu_{7b}$ immunoreactive AZ opposed to a partial PSD (* on B), which contains gold particles for Efn1/2 on the P-face (10 nm gold and ** on A). On the E-face of the dendrite two

additional PSDs can be delinated based on the underlying IMP clusters. The complementary P-face these PSDs are enriched in Elfn1/2. On both panels PSDs are pseudocolred green. *Scale bars, 200 nm.*

dendrite-targeting boutons in $mGlu_7$ antagonist or after Elfn1 knock-down is still facilitating, very different from that observed in PV^+ IN-targeting boutons, suggesting that other mechanisms must be involved. These might include the regulation of Ca_v channel function mentioned above or the selective presence of molecules that might impose facilitation on synapses (e.g., NMDA receptors[327], kainate receptors[270], or synaptotagmin-7[328]). Additional factors could contribute to differences in initial *Pr* by changing the sensitivity of the release machinery to Ca^{2+}. Proteins such as Rab3A-D and Munc13–3 increase *Pr*[329-331], whereas others such as mover decrease *Pr*[332] without affecting the readily releasable pool. Unc13 isoforms have been implicated in the preferential targeting of vesicles to docking sites that are formed at varying distances from the Ca_v channels[333]. Any of these mechanisms may also contribute to the differences in initial *Pr* in addition to the above described differences in $[Ca^{2+}]$; thereby explain the discrepancy between our functional and SDS-FRL data.

6.7. Input-specific expression of Ca_v subunits in PV^+ and CCK^+ basket cell axon terminals in the CA3 area

In the final part of my dissertation, I investigated the Ca_v channel distribution in basket cell axon terminals targeting the somatic region of CA3 PCs, which originate from either PV^+ or CCK/CB_1^+ INs[295]. Here, I provided direct morphological evidence for the segregation of $Ca_v2.1$ and $Ca_v2.2$ Ca^{2+}channel subunits in CCK^+ and PV^+ IN axon terminals. My SDS-FRL data is consistent with the results of Hefft and Jonas (2005)[274], who used blockers of specific types of Ca^{2+} channels to show that CCK^+ INs use N-type Ca^{2+} channels ($Ca_v2.2$) for transmitter release, whereas PV^+ INs rely on P/Q-type channels ($Ca_v2.1$). They also found that PV^+ output synapses release GABA in a tightly synchronized manner in response to presynaptic APs, while CCK^+ axon terminals release GABA in a more asynchronous manner, for up to several hundred milliseconds after high-frequency stimulation. They suggested that the asynchronous release at CCK^+ IN output synapses could be a consequence of loose coupling between Ca^{2+} source and sensor that is to say a larger diffusional distance between the Ca_v channels (source) and synaptotagmins (Ca^{2+} sensor) that triggers GABA release[274]. The

loose coupling at these synapses was confirmed by the fact that the diffusional process of Ca^{2+} from Ca_vs to synaptotagmins is sufficiently long-lasting that the slow Ca^{2+} chelator, EGTA could interfere with the coupling[274]. In contrast, the synchronous release from PV^+ IN axon terminals was not affected by the EGTA[274]. Based on these results, they hypothesized that $Ca_v2.1$ channels must be located in AZs, as they are tightly coupled to release, whereas $Ca_v2.2$ channels should be distributed throughout the presynaptic terminals[274], similarly to the young calyx of Held[334].

In contrast, I found that both Ca_v subunits are concentrated in presynaptic AZs, despite the fact that these channels are differentially coupled to the release. However, this does not exclude the possibility that within the AZ the two types of Ca_v channels are not localized at different distances form docked vesicles. Unfortunately for the time being, there are no techniques available which would allow the concurrent visualization of docked vesicles and Ca_v channels.

6.8. Variability in the CB_1 content in the AZs of CB_1 immunoreactive axon terminals in the CA3 area

My SDS-FRL reactions clearly demonstrated the presence of CB_1 in AZs in addition to peri- and extrasynaptic locations, in agreement with the results of a previous study applying post-embedding immunogold localization[335]. My data also revealed heterogeneity in the CB_1 content of AZs; some Rim1/2 immunopositive AZs were strongly labeled, whereas some were apparently immunonegative.

Previously, substantial heterogeneity has been reported in the degree of CB_1 modulation of GABA release from distinct CCK^+ IN subtypes[336-338], similar to that of glutamatergic boutons of the cerebellum[339]. In addition, the CB_1 content of individual boutons also seems to be variable[335,340]. Despite this, no correlation was found between the total CB_1 content of boutons and the degree of CB_1-mediated control of presynaptic $[Ca^{2+}]$ transients, in a study done by my colleague, Nóra Lenkey[290].

These findings raise the possibility that only a subpopulation of CB_1 receptors, within nanometer distances from their target $Ca_v2.2$ channels, might be responsible for endocannabinoid-mediated modulation of GABA release. The different amounts of CB_1 in AZs could be achieved by the rapid diffusion of receptors in and out of synapses as shown with single-molecule tracking after agonist induced desensitization[341].

DOI:10.14753/SE.2018.2123

7. Conclusions

My results from the first part of the dissertation reveal that the two studied delayed-rectifier K^+ channel subunits take up different subcellular locations in CA1 PCs, resulting in unique, subunit-specific labeling patterns. The $K_v1.1$ subunit is only present in significant amounts in axons, particularly at the AIS, which has an approximately eightfold higher density than axon terminals. In contrast, the $K_v2.1$ subunit is detected at similar densities in AISs, somata and proximal dendrites, but not elsewhere. This subunit has a non-uniform plasma membrane distribution; Kv2.1 clusters are frequently adjacent to, but never overlap with, GABAergic synapses. Within the AIS the $K_v1.1$/$Na_v1.6$ and $K_v2.1$ subunits are segregated into distinct subdomains, all separate from GABAergic synapses, demonstrating that the surface of the AIS is molecularly more complex than previously anticipated. These results suggest that K^+ channels modulate neuronal excitability in a compartment-specific manner.

In the second part of the study, I found that both $Ca_v2.1$ (P/Q-type) and $Ca_v2.2$ (N-type) Ca^{2+} channel subunits are present in functionally distinct CA3 PC axon terminals targeting the $K_v3.1b^+$ and $mGlu_{1a}{}^+$ dendrites. In both populations, the studied Ca_v subunits are restricted to putative AZs, and their within-AZ distribution is significantly different from random distributions. Furthermore, high *Pr* $K_v3.1b^+$ dendrite-innervating AZs contain 15% higher Ca_v subunit density than low *Pr* $mGlu_{1a}{}^+$ dendrite-contacting AZs. This target-dependent difference in Ca_v channel density is much smaller than the almost twofold (70–90%) difference implied by functional experiments of my colleagues[294]. Their experiments excluded the preferential enrichment of $Ca_v2.3$ (R-type)/Ca_v1 (L-type)/Ca_v3 (T-type) subunits in PV^+ dendrite-innervating boutons and the differential fixed Ca^{2+} buffer concentration in these two bouton populations[294]. These results, taken together, suggest that differential target cell type-dependent regulation of Ca_v channel function is the most likely mechanism underlying the functional differences between these two bouton populations, which can also dissolve the discrepancy between our data.

Finally, I provide morphological evidence for the segregation of distinct Ca_v channel subunits in CCK/$CB_1{}^+$ and PV^+ basket cell boutons contacting the somatic region of CA3 PCs. The $Ca_v2.2$ subunit is restricted to CCK/$CB_1{}^+$ axon terminals, while the $Ca_v2.1$ subunit is almost exclusively expressed by PV^+ boutons. In addition, Ca_v

channels are enriched over subareas of axon terminals, which also contain the Rim1/2 indicating their localization within AZs. As both Ca_v subunits are restricted to putative AZs, the well-known differences in synaptic transmission between these boutons are likely to be the consequence of slight, but crucial within-AZs differences in the arrangement of synaptic vesicles and Ca^{2+} channels. Moreover, AZs of CCK/CB_1^+ axon terminals contain the CB_1 in various quantities. This raises the possibility that CB_1 modulation of $Ca_v2.2$ channels and consequently neurotransmitter release might depend on the amount of CB_1 in the presynaptic AZ close to N-type channels. This would also offer a potential explanation of why the degree of CB_1 modulation does not depend on the total amount of CB_1 on the entire axon terminal[290].

These findings reveal previously unseen cell-surface distribution patterns of two delayed-rectifier K^+ channel subunits, as well as input- and target cell type-dependent differences in Ca_v channel distribution in axon terminals. These data furthers our understanding of ion channel localization and functional consequences of distinct distribution patterns.

DOI:10.14753/SE.2018.2123

8. Summary

The functional impact of ion channels depends on their molecular structure as well as their exact subcellular distribution on the surface of neurons, emphasizing the necessity of quantitative determination of ion channel distributions. Special attention has been paid to K^+ channels due to their impact on neuronal excitability, and to Ca^{2+} channels for their role in synaptic transmission. Nonetheless, the precise distribution of most of these ion channels is still lacking. Here, I used the high-resolution SDS-FRL technique to determine ion channel distributions in the rat hippocampus, and to reveal input- and target cell type-dependent differences that might underlie distinct functions.

First, I showed that the $K_v1.1$ K^+ channel subunit is present in axon initial segments (AISs) and axon terminals of CA1 pyramidal cells (PCs), with an eightfold lower density in boutons. The $K_v2.1$ subunit was found in somatic, proximal dendritic and AIS plasma membranes at similar densities. This subunit has a non-uniform distribution; $K_v2.1$ clusters can be close to, but never overlap with GABAergic synapses. These results identify novel K^+ channel distribution patterns in CA1 PCs, and predict their compartment-specific function.

Next, I revealed target cell type-specific differences in the densities of $Ca_v2.2$ and $Ca_v2.1$ Ca^{2+} channel subunits in functionally distinct presynaptic active zones (AZs) of CA3 PCs contacting $K_v3.1b^+$ or $mGlu_{1a}{}^+$ dendrites. SDS-FRL detected a ~15% higher Ca^{2+} channel density in $K_v3.1b^+$ dendrite-targeting AZs, which is much smaller than the twofold difference implied by functional experiments of T. Éltes and N. Holderith. My results suggest a target cell type-dependent regulation of Ca^{2+} channel function or distinct subunit composition as the mechanism underlying the functional differences.

Finally, I provided morphological evidence for the exclusive expression of $Ca_v2.2$ and $Ca_v2.1$ subunits by cholecystokinin/$CB_1{}^+$ and parvalbumin$^+$ basket cell boutons contacting CA3 PCs. As both Ca_v subunits are restricted to putative AZs, the well-known differences in synaptic transmission between these boutons are likely to be the consequence of slight, but crucial within-AZs differences in the arrangement of synaptic vesicles and Ca^{2+} channels. AZs of $CB_1{}^+$ boutons also contain various quantities of CB_1 within nanometer distances from their target $Ca_v2.2$ channels, which I propose to be the basis of the heterogeneity in endocannabinoid-mediated modulation of GABA release.

DOI:10.14753/SE.2018.2123

9. Összefoglaló

Az ioncsatornák funkcionális hatása molekuláris összetételüktől és szubcelluláris sejtfelszíni eloszlásuktól függ. Az utóbbi időben az ioncsatornák közül a K^+ és Ca^{2+} csatornák különös figyelmet kaptak az idegsejtek serkenthetőségének szabályozásában, illetve a szinaptikus transzmisszióban betöltött szerepük miatt. A disszertációmban a nagyfelbontású SDS-maratott fagyasztva-tört replika jelölés (SDS-FRL) módszerét használtam, hogy meghatározzam a kérdéses ioncsatornák eloszlását patkány hippokampuszban, illetve, hogy az ioncsatornák eloszlásában bemenet és célsejtfüggő különbségeket tárjak fel, amelyek különböző funkciókért lehetnek felelősek.

Kimutattam, hogy a $K_v1.1$ K^+ csatorna alegység jelen van CA1 piramissejtek (PS) axon iniciális szegmentumában és ahhoz viszonyítva nyolcszor kisebb sűrűségben axonvégződésekben. A $K_v2.1$ alegység hasonló sűrűségben található meg CA1 PS-ek sejttestén, proximális apikális dendritjein és axon iniciális szegmentumaiban. Ez az alegység inhomogén eloszlást mutat, de a fellelhető $K_v2.1$ klaszterek nem fedtek át gátló szinapszisokkal. Összességében, feltártam két funkcionálisan eltérő K^+ csatorna alegység egyedi, kompartmentfüggő eloszlását CA1 PS-ekben.

Ezt követően céljsetfüggő különbségeket írtam le a $Ca_v2.1$ és $Ca_v2.2$ Ca^{2+} csatorna alegységek sűrűségében olyan funkcionálisan eltérő axonvégződések aktív zónájában, amelyek $K_v3.1b^+$ vagy $mGlu_{1a}{}^+$ dendritekre adnak szinapszist. Az SDS-FRL 15% nagyobb Ca^{2+} csatorna sűrűsséget detektált $K_v3.1b^+$ dendritre menő aktív zónákban, ami jóval kisebb, mint az Éltes T. és Holderith N. funkcionális kísérletei által perdiktált kétszeres eltérés. Összességében eredményeink arra utalnak, hogy a két axonvégződés között levő funkcionális különbségek hátterében vagy a csatornák funkciójának céljsetfüggő modulálása vagy pedig eltérő alegység összetétele áll.

Végül leírtam, hogy a CA3 PS-re szinapszist adó $CCK/CB_1{}^+$ kosársejtek axonvégződéseiben a $Ca_v2.2$ alegység, míg $parvalbumin^+$ kosársejtekében a $Ca_v2.1$ van jelen. Mindkét alegység az aktív zónában fordul elő, arra utalva, hogy az axonvégződés típusok közötti szinaptikus transzmisszióban felellhető különbségekért az aktív zónán belüli Ca^{2+} csatorna elrendeződésében előforduló apró, de fontos különbségek lehetnek felelősek. A $CB_1{}^+$ kosársejtek aktív zónái tartalmazzák a CB_1-et változó mennyiségben nanométerekre az ők célmolekulájuktól, a $Ca_v2.2$ alegységtől, ami az endokannabinoid-mediálta GABA felszabadulás modulációjában fellelhető heterogenitás alapja lehet.

10. Bibliography

1. Golgi C. (1989) On the structure of nerve cells. 1898. J Microsc, 155: 3–7.
2. Ramon y Cajal S. Histologie du systéme nerveux de l'homme et des vertébrés. Maloine, Paris, 1911.
3. Lorente de No R. (1934) Studies on the structure of the cerebral cortex. II. Continuation of the study of the ammonic system. J für Psychol und Neurol, 46: 113–177.
4. Gutman GA, Chandy KG, Adelman JP, Aiyar J, Bayliss DA, Clapham DE, Covarriubias M, Desir GV, Furuichi K, Ganetzky B, Garcia ML, Grissmer S, Jan LY, Karschin A, Kim D, Kuperschmidt S, Kurachi Y, Lazdunski M, Lesage F, Lester HA, McKinnon D, Nichols CG, O'Kelly I, Robbins J, Robertson GA, Rudy B, Sanguinetti M, Seino S, Stuehmer W, Tamkun MM, Vandenberg CA, Wei A, Wulff H, Wymore RS. (2003) International Union of Pharmacology. XLI. Compendium of voltage-gated ion channels: potassium channels. Pharmacol Rev, 55: 583–6.
5. Hille B. Ionic channels of excitable membranes. Sinauer Associates Inc., Sunderland, 2001.
6. Bean BP. (2007) The action potential in mammalian central neurons. Nat Rev Neurosci, 8: 451–65.
7. Hodgkin AL, Huxley AF. (1952) A quantitative description of membrane current and its application to conduction and excitation in nerve. J Physiol, 117: 500–44.
8. Neher E, Sakmann B. (1976) Single-channel currents recorded from membrane of denervated frog muscle fibres. Nature, 260: 799–802.
9. Armstrong CM, Hille B. (1998) Voltage-gated ion channels and electrical excitability. Neuron, 20: 371–80.
10. Rasband MN. (2010) The axon initial segment and the maintenance of neuronal polarity. Nat Rev Neurosci, 11: 552–62.
11. Kole MHP, Stuart GJ. (2012) Signal processing in the axon initial segment. Neuron, 73: 235–47.
12. Bender KJ, Trussell LO. (2012) The physiology of the axon initial segment. Annu Rev Neurosci, 35: 249–65.
13. Hollmann M, Heinemann S. (1994) Cloned glutamate receptors. Annu Rev

Neurosci, 17: 31–108.

14. Macdonald RL, Olsen RW. (1994) GABAA receptor channels. Annu Rev Neurosci, 17: 569–602.
15. Sieghart W. (1995) Structure and pharmacology of gamma-aminobutyric acidA receptor subtypes. Pharmacol Rev, 47: 181–234.
16. Traynelis SF, Wollmuth LP, McBain CJ, Menniti FS, Vance KM, Ogden KK, Hansen KB, Yuan H, Myers SJ, Dingledine R. (2010) Glutamate receptor ion channels: structure, regulation, and function. Pharmacol Rev, 62: 405–96.
17. Greger IH, Watson JF, Cull-Candy SG. (2017) Structural and Functional Architecture of AMPA-Type Glutamate Receptors and Their Auxiliary Proteins. Neuron, 94: 713–730.
18. Atwood HL, Karunanithi S. (2002) Diversification of synaptic strength: presynaptic elements. Nat Rev Neurosci, 3: 497–516.
19. Stuart G, Spruston N, Häusser M. Principles of dendritic integration. In: Stuart G, Spruston N & Häusser M (editors), Dendrites. Oxford University Press, Oxford, 2016: 351–398.
20. Magee JC. (2000) Dendritic integration of excitatory synaptic input. Nat Rev Neurosci, 1: 181–90.
21. Stuart GJ, Spruston N. (2015) Dendritic integration: 60 years of progress. Nat Neurosci, 18: 1713–21.
22. Stuart GJ, Sakmann B. (1994) Active propagation of somatic action potentials into neocortical pyramidal cell dendrites. Nature, 367: 69–72.
23. Lai HC, Jan LY. (2006) The distribution and targeting of neuronal voltage-gated ion channels. Nat Rev Neurosci, 7: 548–62.
24. Nusser Z. (2009) Variability in the subcellular distribution of ion channels increases neuronal diversity. Trends Neurosci, 32: 267–74.
25. Nusser Z. (2012) Differential subcellular distribution of ion channels and the diversity of neuronal function. Curr Opin Neurobiol, 22: 366–71.
26. Trimmer JS. (2015) Subcellular localization of K+ channels in mammalian brain neurons: remarkable precision in the midst of extraordinary complexity. Neuron, 85: 238–56.
27. Indriati DW, Kamasawa N, Matsui K, Meredith AL, Watanabe M, Shigemoto R.

(2013) Quantitative localization of Cav2.1 (P/Q-type) voltage-dependent calcium channels in Purkinje cells: somatodendritic gradient and distinct somatic coclustering with calcium-activated potassium channels. J Neurosci, 33: 3668–78.

28. Davie JT, Clark BA, Häusser M. (2008) The origin of the complex spike in cerebellar Purkinje cells. J Neurosci, 28: 7599–609.
29. Rancz EA, Häusser M. (2006) Dendritic calcium spikes are tunable triggers of cannabinoid release and short-term synaptic plasticity in cerebellar Purkinje neurons. J Neurosci, 26: 5428–37.
30. De Schutter E, Bower JM. (1994) Simulated responses of cerebellar Purkinje cells are independent of the dendritic location of granule cell synaptic inputs. Proc Natl Acad Sci U S A, 91: 4736–4740.
31. Mintz IM, Sabatini BL, Regehr WG. (1995) Calcium control of transmitter release at a cerebellar synapse. Neuron, 15: 675–88.
32. Marder E, Goaillard J-M. (2006) Variability, compensation and homeostasis in neuron and network function. Nat Rev Neurosci, 7: 563–74.
33. Aradi I, Soltesz I. (2002) Modulation of network behaviour by changes in variance in interneuronal properties. J Physiol, 538: 227–251.
34. Aradi I, Santhakumar V, Chen K, Soltesz I. (2002) Postsynaptic effects of GABAergic synaptic diversity: Regulation of neuronal excitability by changes in IPSC variance. Neuropharmacology, 43: 511–522.
35. Aradi I, Santhakumar V, Soltesz I. (2004) Impact of heterogeneous perisomatic IPSC populations on pyramidal cell firing rates. J Neurophysiol, 91: 2849–58.
36. Földy C, Aradi I, Howard A, Soltesz I. (2004) Diversity beyond variance: Modulation of firing rates and network coherence by GABAergic subpopulations. Eur J Neurosci, 19: 119–130.
37. Santhakumar V, Soltesz I. (2004) Plasticity of interneuronal species diversity and parameter variance in neurological diseases. Trends Neurosci, 27: 504–510.
38. Stuart GJ, Dodt HU, Sakmann B. (1993) Patch-clamp recordings from the soma and dendrites of neurons in brain slices using infrared video microscopy. Pflugers Arch, 423: 511–8.
39. Magee J, Johnston D. (1995) Characterization of single voltage-gated Na+ and

Ca2+ channels in apical dendrites of rat CA1 pyramidal neurons. J Physiol, 487: 67–90.

40. Hoffman DA, Magee JC, Colbert CM, Johnston D. (1997) K+ channel regulation of signal propagation in dendrites of hippocampal pyramidal neurons. Nature, 387: 869–875.
41. Magee JC. (1998) Dendritic hyperpolarization-activated currents modify the integrative properties of hippocampal CA1 pyramidal neurons. J Neurosci, 18: 7613–24.
42. Poolos NP, Johnston D. (1999) Calcium-activated potassium conductances contribute to action potential repolarization at the soma but not the dendrites of hippocampal CA1 pyramidal neurons. J Neurosci, 19: 5205–5212.
43. Bekkers JM. (2000) Distribution and activation of voltage-gated potassium channels in cell-attached and outside-out patches from large layer 5 cortical pyramidal neurons of the rat. J Physiol, 525 Pt 3: 611–20.
44. Korngreen A, Sakmann B. (2000) Voltage-gated K+ channels in layer 5 neocortical pyramidal neurones from young rats: subtypes and gradients. J Physiol, 525 Pt 3: 621–39.
45. Harnett MT, Magee JC, Williams SR. (2015) Distribution and function of HCN channels in the apical dendritic tuft of neocortical pyramidal neurons. J Neurosci, 35: 1024–37.
46. Srinivas KV, Buss EW, Sun Q, Santoro B, Takahashi H, Nicholson DA, Siegelbaum SA. (2017) The Dendrites of CA2 and CA1 Pyramidal Neurons Differentially Regulate Information Flow in the Cortico-Hippocampal Circuit. J Neurosci, 37: 3276–3293.
47. Stuart G, Häusser M. (1994) Initiation and spread of sodium action potentials in cerebellar Purkinje cells. Neuron, 13: 703–12.
48. Forsythe ID. (1994) Direct patch recording from identified presynaptic terminals mediating glutamatergic EPSCs in the rat CNS, in vitro. J Physiol, 381–7.
49. Southan AP, Robertson B. (1998) Patch-clamp recordings from cerebellar basket cell bodies and their presynaptic terminals reveal an asymmetric distribution of voltage-gated potassium channels. J Neurosci, 18: 948–55.
50. Geiger JRP, Jonas P. (2000) Dynamic control of presynaptic Ca2+ inflow by

fast-inactivating K+ channels in hippocampal mossy fiber boutons. Neuron, 28: 927–939.

51. Kawaguchi S, Sakaba T. (2015) Control of inhibitory synaptic outputs by low excitability of axon terminals revealed by direct recording. Neuron, 85: 1273–1288.
52. Rowan MJM, DelCanto G, Yu JJ, Kamasawa N, Christie JM. (2016) Synapse-level determination of action potential duration by K(+) channel clustering in axons. Neuron, 91: 370–83.
53. Rowan MJM, Christie JM. (2017) Rapid state-dependent dlteration in Kv3 cChannel dvailability drives flexible synaptic signaling dependent on somatic subthreshold depolarization. Cell Rep, 18: 2018–2029.
54. Maglione M, Sigrist SJ. (2013) Seeing the forest tree by tree: super-resolution light microscopy meets the neurosciences. Nat Neurosci, 16: 790–7.
55. Godin AG, Lounis B, Cognet L. (2014) Super-resolution microscopy approaches for live cell imaging. Biophys J, 107: 1777–1784.
56. Oddone A, Vilanova IV, Tam J, Lakadamyali M. (2014) Super-resolution imaging with stochastic single-molecule localization: concepts, technical developments, and biological applications. Microsc Res Tech, 77: 502–9.
57. Yamanaka M, Smith NI, Fujita K. (2014) Introduction to super-resolution microscopy. Microscopy, 63: 177–192.
58. Sydor AM, Czymmek KJ, Puchner EM, Mennella V. (2015) Super-resolution microscopy: from single molecules to supramolecular assemblies. Trends Cell Biol, 25: 730–48.
59. Amiry-Moghaddam M, Ottersen OP. (2013) Immunogold cytochemistry in neuroscience. Nat Neurosci, 16: 798–804.
60. Bernard V, Somogyi P, Bolam JP. (1997) Cellular, subcellular, and subsynaptic distribution of AMPA-type glutamate receptor subunits in the neostriatum of the rat. J Neurosci, 17: 819–833.
61. Luján R. (2004) Electron microscopic studies of receptor localization. Methods Mol Biol, 259: 123–36.
62. Nusser Z. (1999) A new approach to estimate the number, density and variability of receptors at central synapses. Eur J Neurosci, 11: 745–752.

63. Shida H, Ohga R. (1990) Effect of resin use in the post-embedding procedure on immunoelectron microscopy of membranous antigens, with special reference to sensitivity. J Histochem Cytochem, 38: 1687–1691.
64. Matsubara A, Laake JH, Davanger S, Usami S, Ottersen OP. (1996) Organization of AMPA receptor subunits at a glutamate synapse: a quantitative immunogold analysis of hair cell synapses in the rat organ of Corti. J Neurosci, 16: 4457–4467.
65. Fujimoto K. (1997) SDS-digested freeze-fracture replica labeling electron microscopy to study the two dimensional distribution of intgral membrane proteins and phospholipids in biomembranes; practical proceedure, interpretation and application. Histochem Cell Biol, 107: 87.
66. Robenek H, Severs NJ. (2008) Recent advances in freeze-fracture electron microscopy: the replica immunolabeling technique. Biol Proced Online, 10: 9–19.
67. Severs NJ, Robenek H. (2008) Freeze-fracture cytochemistry in cell biology. Methods Cell Biol, 88: 181–204.
68. Fujimoto K. (1995) Freeze-fracture replica electron microscopy combined with SDS digestion for cytochemical labeling of integral membrane proteins. Application to the immunogold labeling of intercellular junctional complexes. J Cell Sci, 3443–9.
69. Lorincz A, Nusser Z. (2010) Molecular identity of dendritic voltage-gated sodium channels. Science, 328: 906–9.
70. Tanaka J, Matsuzaki M, Tarusawa E, Momiyama A, Molnar E, Kasai H, Shigemoto R. (2005) Number and density of AMPA receptors in single synapses in immature cerebellum. J Neurosci, 25: 799–807.
71. Schönherr S, Seewald A, Kasugai Y, Bosch D, Ehrlich I, Ferraguti F. (2016) Combined optogenetic and freeze-fracture replica immunolabeling to examine input-specific arrangement of glutamate receptors in the mouse amygdala. J Vis Exp, 110:1–14.
72. Masugi-Tokita M, Shigemoto R. (2007) High-resolution quantitative visualization of glutamate and GABA receptors at central synapses. Curr Opin Neurobiol, 17: 387–93.

73. Landis DMD, Reese TS. (1974) Differences in membrane structure between excitatory and inhibitory synapses in the cerebellar cortex. J Comp Neurol, 155: 93–125.
74. Harris KM, Landis DM. (1986) Membrane structure at synaptic junctions in area CA1 of the rat hippocampus. Neuroscience, 19: 857–72.
75. Masugi-Tokita M, Tarusawa E, Watanabe M, Molnár E, Fujimoto K, Shigemoto R. (2007) Number and density of AMPA receptors in individual synapses in the rat cerebellum as revealed by SDS-digested freeze-fracture replica labeling. J Neurosci, 27: 2135–44.
76. Goodenough DA, Revel JP. (1970) A fine structural analysis of intercellular junctions in the mouse liver. J Cell Biol, 45: 272–90.
77. Rash JE, Duffy HS, Dudek FE, Bilhartz BL, Whalen LR, Yasumura T. (1997) Grid-mapped freeze-fracture analysis of gap junctions in gray and white matter of adult rat central nervous system, with evidence for a 'panglial syncytium' that is not coupled to neurons. J Comp Neurol, 388: 265–92.
78. Rash JE, Yasumura T, Dudek FE. (1998) Ultrastructure, histological distribution, and freeze-fracture immunocytochemistry of gap junctions in rat brain and spinal cord. Cell Biol Int, 22: 731–49.
79. Hagiwara A, Fukazawa Y, Deguchi-Tawarada M, Ohtsuka T, Shigemoto R. (2005) Differential distribution of release-related proteins in the hippocampal CA3 area as revealed by freeze-fracture replica labeling. J Comp Neurol, 489: 195–216.
80. Kerti-Szigeti K, Nusser Z. (2016) Similar GABA $_A$ receptor subunit composition in somatic and axon initial segment synapses of hippocampal pyramidal cells. Elife, 5: 1–23.
81. Scoville WB, Milner B. (1957) Loss of recent memory after bilateral hippocampal lesions. J Neurol Neurosurg Psychiatry, 20: 11–21.
82. Zola-Morgan S, Squire LR, Amaral DG. (1986) Human amnesia and the medial temporal region: enduring memory impairment following a bilateral lesion limited to field CA1 of the hippocampus. J Neurosci, 6: 2950–67.
83. Andersen P, Bliss T V, Skrede KK. (1971) Unit analysis of hippocampal polulation spikes. Exp brain Res, 13: 208–21.

84. Blackstad TW. (1958) On the termination of some afferents to the hippocampus and fascia dentata; an experimental study in the rat. Acta Anat (Basel), 35: 202–14.
85. Witter MP. (1993) Organization of the entorhinal-hippocampal system: a review of current anatomical data. Hippocampus, 3 Spec No: 33–44.
86. Claiborne BJ, Amaral DG, Cowan WM. (1986) A light and electron microscopic analysis of the mossy fibers of the rat dentate gyrus. J Comp Neurol, 246: 435–58.
87. Tamamaki N, Watanabe K, Nojyo Y. (1984) A whole image of the hippocampal pyramidal neuron revealed by intracellular pressure-injection of horseradish peroxidase. Brain Res, 307: 336–40.
88. Ishizuka N, Weber J, Amaral DG. (1990) Organization of intrahippocampal projections originating from CA3 pyramidal cells in the rat. J Comp Neurol, 295: 580–623.
89. Li XG, Somogyi P, Ylinen A, Buzsáki G. (1994) The hippocampal CA3 network: an in vivo intracellular labeling study. J Comp Neurol, 339: 181–208.
90. Scharfman HE. (1994) Evidence from simultaneous intracellular recordings in rat hippocampal slices that area CA3 pyramidal cells innervate dentate hilar mossy cells. J Neurophysiol, 72: 2167–80.
91. Storm-Mathisen J. (1981) Glutamate in hippocampal pathways. Adv Biochem Psychopharmacol, 27: 43–55.
92. Liu CJ, Grandes P, Matute C, Cuénod M, Streit P. (1989) Glutamate-like immunoreactivity revealed in rat olfactory bulb, hippocampus and cerebellum by monoclonal antibody and sensitive staining method. Histochemistry, 90: 427–45.
93. Grandes P, Streit P. (1991) Effect of perforant path lesion on pattern of glutamate-like immunoreactivity in rat dentate gyrus. Neuroscience, 41: 391–400.
94. Südhof TC. (2012) Calcium control of neurotransmitter release. Cold Spring Harb Perspect Biol, 4:
95. Magee JC, Cook EP. (2000) Somatic EPSP amplitude is independent of synapse location in hippocampal pyramidal neurons. Nat Neurosci, 3: 895–903.
96. Pin JP, Duvoisin R. (1995) The metabotropic glutamate receptors: structure and

functions. Neuropharmacology, 34: 1–26.

97. Shigemoto R, Kulik A, Roberts JD, Ohishi H, Nusser Z, Kaneko T, Somogyi P. (1996) Target-cell-specific concentration of a metabotropic glutamate receptor in the presynaptic active zone. Nature, 381: 523–5.
98. Shigemoto R, Kinoshita A, Wada E, Nomura S, Ohishi H, Takada M, Flor PJ, Neki A, Abe T, Nakanishi S, Mizuno N. (1997) Differential presynaptic localization of metabotropic glutamate receptor subtypes in the rat hippocampus. J Neurosci, 17: 7503–22.
99. Pinheiro PS, Mulle C. (2008) Presynaptic glutamate receptors: physiological functions and mechanisms of action. Nat Rev Neurosci, 9: 423–36.
100. del Castillo J, Katz B. (1954) Quantal components of the end-plate potential. J Physiol, 124: 560–73.
101. Bekkers JM, Richerson GB, Stevens CF. (1990) Origin of variability in quantal size in cultured hippocampal neurons and hippocampal slices. Proc Natl Acad Sci U S A, 87: 5359–62.
102. Dobrunz LE, Stevens CF. (1997) Heterogeneity of release probability, facilitation, and depletion at central synapses. Neuron, 18: 995–1008.
103. Shepherd GM, Harris KM. (1998) Three-dimensional structure and composition of CA3-->CA1 axons in rat hippocampal slices: implications for presynaptic connectivity and compartmentalization. J Neurosci, 18: 8300–10.
104. Hanse E, Gustafsson B. (2001) Vesicle release probability and pre-primed pool at glutamatergic synapses in area CA1 of the rat neonatal hippocampus. J Physiol, 531: 481–93.
105. del Castillo J, Katz B. (1954) Statistical factors involved in neuromuscular facilitation and depression. J Physiol, 124: 574–85.
106. Zucker RS, Regehr WG. (2002) Short-term synaptic plasticity. Annu Rev Physiol, 64: 355–405.
107. Jackman SL, Regehr WG. (2017) The mechanisms and functions of synaptic facilitation. Neuron, 94: 447–464.
108. Bliss T V, Gardner-Medwin AR. (1973) Long-lasting potentiation of synaptic transmission in the dentate area of the unanaestetized rabbit following stimulation of the perforant path. J Physiol, 232: 357–74.

109. Bliss T V, Lomo T. (1973) Long-lasting potentiation of synaptic transmission in the dentate area of the anaesthetized rabbit following stimulation of the perforant path. J Physiol, 232: 331–56.
110. Abbott LF, Nelson SB. (2000) Synaptic plasticity: taming the beast. Nat Neurosci, 3 Suppl: 1178–83.
111. Freund TF, Buzsáki G. (1998) Interneurons of the hippocampus. Hippocampus, 6: 347–470.
112. McBain CJ, Fisahn A. (2001) Interneurons unbound. Nat Rev Neurosci, 2: 11–23.
113. Woodson W, Nitecka L, Ben-Ari Y. (1989) Organization of the GABAergic system in the rat hippocampal formation: a quantitative immunocytochemical study. J Comp Neurol, 280: 254–71.
114. Aika Y, Ren JQ, Kosaka K, Kosaka T. (1994) Quantitative analysis of GABA-like-immunoreactive and parvalbumin-containing neurons in the CA1 region of the rat hippocampus using a stereological method, the disector. Exp brain Res, 99: 267–76.
115. Somogyi P, Klausberger T. (2005) Defined types of cortical interneurone structure space and spike timing in the hippocampus. J Physiol, 562: 9–26.
116. Klausberger T, Somogyi P. (2008) Neuronal diversity and temporal dynamics: the unity of hippocampal circuit operations. Science, 321: 53–7.
117. Klausberger T, Magill PJ, Márton LF, Roberts JDB, Cobden PM, Buzsáki G, Somogyi P. (2003) Brain-state- and cell-type-specific firing of hippocampal interneurons in vivo. Nature, 421: 844–8.
118. Tukker JJ, Fuentealba P, Hartwich K, Somogyi P, Klausberger T. (2007) Cell type-specific tuning of hippocampal interneuron firing during gamma oscillations in vivo. J Neurosci, 27: 8184–9.
119. Tukker JJ, Lasztóczi B, Katona L, Roberts JDB, Pissadaki EK, Dalezios Y, Márton L, Zhang L, Klausberger T, Somogyi P. (2013) Distinct dendritic arborization and in vivo firing patterns of parvalbumin-expressing basket cells in the hippocampal area CA3. J Neurosci, 33: 6809–25.
120. Lasztóczi B, Tukker JJ, Somogyi P, Klausberger T. (2011) Terminal field and firing selectivity of cholecystokinin-expressing interneurons in the hippocampal

CA3 area. J Neurosci, 31: 18073–93.

121. Lapray D, Lasztoczi B, Lagler M, Viney TJ, Katona L, Valenti O, Hartwich K, Borhegyi Z, Somogyi P, Klausberger T. (2012) Behavior-dependent specialization of identified hippocampal interneurons. Nat Neurosci, 15: 1265–71.
122. Gulyás AI, Szabó GG, Ulbert I, Holderith N, Monyer H, Erdélyi F, Szabó G, Freund TF, Hájos N. (2010) Parvalbumin-containing fast-spiking basket cells generate the field potential oscillations induced by cholinergic receptor activation in the hippocampus. J Neurosci, 30: 15134–45.
123. Hájos N, Karlócai MR, Németh B, Ulbert I, Monyer H, Szabó G, Erdélyi F, Freund TF, Gulyás AI. (2013) Input-output features of anatomically identified CA3 neurons during hippocampal sharp wave/ripple oscillation in vitro. J Neurosci, 33: 11677–91.
124. Freund TF, Katona I. (2007) Perisomatic inhibition. Neuron, 56: 33–42.
125. Armstrong C, Soltesz I. (2012) Basket cell dichotomy in microcircuit function. J Physiol, 590: 683–94.
126. Bartos M, Elgueta C. (2012) Functional characteristics of parvalbumin- and cholecystokinin-expressing basket cells. J Physiol, 590: 669–81.
127. Klausberger T, Marton LF, O'Neill J, Huck JHJ, Dalezios Y, Fuentealba P, Suen WY, Papp E, Kaneko T, Watanabe M, Csicsvari J, Somogyi P. (2005) Complementary roles of cholecystokinin- and parvalbumin-expressing GABAergic neurons in hippocampal network oscillations. J Neurosci, 25: 9782–93.
128. Hu H, Gan J, Jonas P. (2014) Fast-spiking, parvalbumin+ GABAergic interneurons: From cellular design to microcircuit function. Science, 345: 1255263–1255263.
129. Somogyi P, Nunzi MG, Gorio A, Smith AD. (1983) A new type of specific interneuron in the monkey hippocampus forming synapses exclusively with the axon initial segments of pyramidal cells. Brain Res, 259: 137–42.
130. Buhl EH, Han ZS, Lörinczi Z, Stezhka VV, Karnup SV, Somogyi P. (1994) Physiological properties of anatomically identified axo-axonic cells in the rat hippocampus. J Neurophysiol, 71: 1289–307.

131. Gulyás AI, Megías M, Emri Z, Freund TF. (1999) Total number and ratio of excitatory and inhibitory synapses converging onto single interneurons of different types in the CA1 area of the rat hippocampus. J Neurosci, 19: 10082–10097.
132. Kosaka T, Katsumaru H, Hama K, Wu JY, Heizmann CW. (1987) GABAergic neurons containing the Ca2+-binding protein parvalbumin in the rat hippocampus and dentate gyrus. Brain Res, 419: 119–30.
133. Katsumaru H, Kosaka T, Heizmann CW, Hama K. (1988) Immunocytochemical study of GABAergic neurons containing the calcium-binding protein parvalbumin in the rat hippocampus. Exp brain Res, 72: 347–62.
134. Weiser M, Bueno E, Sekirnjak C, Martone ME, Baker H, Hillman D, Chen S, Thornhill W, Ellisman M, Rudy B. (1995) The potassium channel subunit KV3.1b is localized to somatic and axonal membranes of specific populations of CNS neurons. J Neurosci, 15: 4298–314.
135. Du J, Zhang L, Weiser M, Rudy B, McBain CJ. (1996) Developmental expression and functional characterization of the potassium-channel subunit Kv3.1b in parvalbumin-containing interneurons of the rat hippocampus. J Neurosci, 16: 506–518.
136. Pawelzik H, Hughes DI, Thomson AM. (2002) Physiological and morphological diversity of immunocytochemically defined parvalbumin- and cholecystokinin-positive interneurones in CA1 of the adult rat hippocampus. J Comp Neurol, 443: 346–67.
137. Nunzi MG, Gorio A, Milan F, Freund TF, Somogyi P, Smith AD. (1985) Cholecystokinin-immunoreactive cells form symmetrical synaptic contacts with pyramidal and nonpyramidal neurons in the hippocampus. J Comp Neurol, 237: 485–505.
138. Katona I, Sperlágh B, Sík A, Käfalvi A, Vizi ES, Mackie K, Freund TF. (1999) Presynaptically located CB1 cannabinoid receptors regulate GABA release from axon terminals of specific hippocampal interneurons. J Neurosci, 19: 4544–4558.
139. Freund TF, Katona I, Piomelli D. (2003) Role of endogenous cannabinoids in synaptic signaling. Physiol Rev, 83: 1017–66.

140. Kawaguchi Y, Katsumaru H, Kosaka T, Heizmann CW, Hama K. (1987) Fast spiking cells in rat hippocampus (CA1 region) contain the calcium-binding protein parvalbumin. Brain Res, 416: 369–74.
141. Cope DW, Maccaferri G, Márton LF, Roberts JDB, Cobden PM, Somogyi P. (2002) Cholecystokinin-immunopositive basket and Schaffer collateral-associated interneurones target different domains of pyramidal cells in the CA1 area of the rat hippocampus. Neuroscience, 109: 63–80.
142. Lee S-H, Marchionni I, Bezaire M, Varga C, Danielson N, Lovett-Barron M, Losonczy A, Soltesz I. (2014) Parvalbumin-positive basket cells differentiate among hippocampal pyramidal cells. Neuron, 82: 1129–44.
143. Glickfeld LL, Roberts JD, Somogyi P, Scanziani M. (2009) Interneurons hyperpolarize pyramidal cells along their entire somatodendritic axis. Nat Neurosci, 12: 21–3.
144. Szabadics J, Varga C, Molnár G, Oláh S, Barzó P, Tamás G. (2006) Excitatory effect of GABAergic axo-axonic cells in cortical microcircuits. Science, 311: 233–5.
145. McBain CJ, DiChiara TJ, Kauer JA. (1994) Activation of metabotropic glutamate receptors differentially affects two classes of hippocampal interneurons and potentiates excitatory synaptic transmission. J Neurosci, 14: 4433–45.
146. Baude A, Nusser Z, Roberts JDB, Mulvihill E, Mcllhinney RAJ, Somogyi P. (1993) The metabotropic glutamate receptor (mGluR1 alpha) is concentrated at perisynaptic membrane of neuronal subpopulations as detected by immunogold reaction. Neuron, 11: 771–787.
147. Somogyi P, Dalezios Y, Luján R, Roberts JDB, Watanabe M, Shigemoto R. (2003) High level of mGluR7 in the presynaptic active zones of select populations of GABAergic terminals innervating interneurons in the rat hippocampus. Eur J Neurosci, 17: 2503–2520.
148. Buhl EH, Halasy K, Somogyi P. (1994) Diverse sources of hippocampal unitary inhibitory postsynaptic potentials and the number of synaptic release sites. Nature, 368: 823–8.
149. Buhl EH, Szilágyi T, Halasy K, Somogyi P. (1996) Physiological properties of

anatomically identified basket and bistratified cells in the CA1 area of the rat hippocampus in vitro. Hippocampus, 6: 294–305.

150. Klausberger T, Márton LF, Baude A, Roberts JDB, Magill PJ, Somogyi P. (2004) Spike timing of dendrite-targeting bistratified cells during hippocampal network oscillations in vivo. Nat Neurosci, 7: 41–7.
151. Maccaferri G, Roberts JD, Szucs P, Cottingham CA, Somogyi P. (2000) Cell surface domain specific postsynaptic currents evoked by identified GABAergic neurones in rat hippocampus in vitro. J Physiol, 524 Pt 1: 91–116.
152. Losonczy A, Zhang L, Shigemoto R, Somogyi P, Nusser Z. (2002) Cell type dependence and variability in the short-term plasticity of EPSCs in identified mouse hippocampal interneurones. J Physiol, 542: 193–210.
153. Ribak CE, Vaughn JE, Saito K. (1978) Immunocytochemical localization of glutamic acid decarboxylase in neuronal somata following colchicine inhibition of axonal transport. Brain Res, 140: 315–32.
154. Krnjević K, Schwartz S. (1967) The action of gamma-aminobutyric acid on cortical neurones. Exp brain Res, 3: 320–36.
155. Somogyi P, Hodgson AJ. (1985) Antisera to gamma-aminobutyric acid. III. Demonstration of GABA in Golgi-impregnated neurons and in conventional electron microscopic sections of cat striate cortex. J Histochem Cytochem, 33: 249–257.
156. Chalifoux JR, Carter AG. (2012) GABAB receptor modulation of synaptic function. Curr Opin Neurobiol, 21: 339–344.
157. Gassmann M, Bettler B. (2012) Regulation of neuronal GABA(B) receptor functions by subunit composition. Nat Rev Neurosci, 13: 380–94.
158. Padgett CL, Slesinger PA. (2010) GABAB receptor coupling to G-proteins and ion channels. Adv Pharmacol, 58: 123–47.
159. Pin J-P, Bettler B. (2016) Organization and functions of mGlu and GABAB receptor complexes. Nature, 540: 60–68.
160. Farrant M, Nusser Z. (2005) Variations on an inhibitory theme: phasic and tonic activation of GABA(A) receptors. Nat Rev Neurosci, 6: 215–29.
161. Migliore M, Shepherd GM. (2002) Emerging rules for the distributions of active dendritic conductances. Nat Rev Neurosci, 3: 362–70.

162. Caldwell JH, Schaller KL, Lasher RS, Peles E, Levinson SR. (2000) Sodium channel Na(v)1.6 is localized at nodes of ranvier, dendrites, and synapses. Proc Natl Acad Sci U S A, 97: 5616–20.
163. Stuart G, Spruston N, Sakmann B, Hausser M. (1997) Action potential initiation and back propagation in neurons of the mammalian central nervous system. Trends Neurosci, 20: 125–131.
164. Kamondi A, Acsády L, Buzsáki G. (1998) Dendritic spikes are enhanced by cooperative network activity in the intact hippocampus. J Neurosci, 18: 3919–28.
165. Losonczy A, Magee JC. (2006) Integrative properties of radial oblique dendrites in hippocampal CA1 pyramidal neurons. Neuron, 50: 291–307.
166. Gasparini S, Magee JC. (2006) State-dependent dendritic computation in hippocampal CA1 pyramidal neurons. J Neurosci, 26: 2088–100.
167. Losonczy A, Makara JK, Magee JC. (2008) Compartmentalized dendritic plasticity and input feature storage in neurons. Nature, 452: 436–441.
168. Beckh S, Noda M, Lübbert H, Numa S. (1989) Differential regulation of three sodium channel messenger RNAs in the rat central nervous system during development. EMBO J, 8: 3611–6.
169. Lorincz A, Nusser Z. (2008) Cell-type-dependent molecular composition of the axon initial segment. J Neurosci, 28: 14329–40.
170. Wu RL, Barish ME. (1992) Two pharmacologically and kinetically distinct transient potassium currents in cultured embryonic mouse hippocampal neurons. J Neurosci, 12: 2235–46.
171. Du J, Haak LL, Phillips-Tansey E, Russell JT, McBain CJ. (2000) Frequency-dependent regulation of rat hippocampal somato-dendritic excitability by the K+ channel subunit Kv2.1. J Physiol, 522 Pt 1: 19–31.
172. Chen X, Yuan L-L, Zhao C, Birnbaum SG, Frick A, Jung WE, Schwarz TL, Sweatt JD, Johnston D. (2006) Deletion of Kv4.2 gene eliminates dendritic A-type K+ current and enhances induction of long-term potentiation in hippocampal CA1 pyramidal neurons. J Neurosci, 26: 12143–51.
173. Migliore M, Hoffman DA, Magee JC, Johnston D. (1999) Role of an A-type K+ conductance in the back-propagation of action potentials in the dendrites of hippocampal pyramidal neurons. J Comput Neurosci, 7: 5–15.

174. Margulis M, Tang CM. (1998) Temporal integration can readily switch between sublinear and supralinear summation. J Neurophysiol, 79: 2809–13.
175. Cash S, Yuste R. (1999) Linear summation of excitatory inputs by CA1 pyramidal neurons. Neuron, 22: 383–94.
176. Watanabe S, Hoffman DA, Migliore M, Johnston D. (2002) Dendritic K+ channels contribute to spike-timing dependent long-term potentiation in hippocampal pyramidal neurons. Proc Natl Acad Sci U S A, 99: 8366–71.
177. Frick A, Magee J, Johnston D. (2004) LTP is accompanied by an enhanced local excitability of pyramidal neuron dendrites. Nat Neurosci, 7: 126–35.
178. Makara JK, Losonczy A, Wen Q, Magee JC. (2009) Experience-dependent compartmentalized dendritic plasticity in rat hippocampal CA1 pyramidal neurons. Nat Neurosci, 12: 1485–7.
179. Kerti K, Lorincz A, Nusser Z. (2012) Unique somato-dendritic distribution pattern of Kv4.2 channels on hippocampal CA1 pyramidal cells. Eur J Neurosci, 35: 66–75.
180. Murakoshi H, Trimmer JS. (1999) Identification of the Kv2.1 K+ channel as a major component of the delayed rectifier K+ current in rat hippocampal neurons. J Neurosci, 19: 1728–35.
181. Misonou H, Mohapatra DP, Park EW, Leung V, Zhen D, Misonou K, Anderson AE, Trimmer JS. (2004) Regulation of ion channel localization and phosphorylation by neuronal activity. Nat Neurosci, 7: 711–8.
182. Trimmer JS. (1991) Immunological identification and characterization of a delayed rectifier K+ channel polypeptide in rat brain. Proc Natl Acad Sci U S A, 88: 10764–10768.
183. Maletic-Savatic M, Lenn N, Trimmer J. (1995) Differential spatiotemporal expression of K+ channel polypeptides in rat hippocampal neurons developing in situ and in vitro. J Neurosci, 15:
184. Du J, Tao-Cheng JH, Zerfas P, McBain CJ. (1998) The K+ channel, Kv2.1, is apposed to astrocytic processes and is associated with inhibitory postsynaptic membranes in hippocampal and cortical principal neurons and inhibitory interneurons. Neuroscience, 84: 37–48.
185. Lim ST, Antonucci DE, Scannevin RH, Trimmer JS. (2000) A novel targeting

signal for proximal clustering of the Kv2.1 K+ channel in hippocampal neurons. Neuron, 25: 385–97.

186. Rhodes KJ, Trimmer JS. (2006) Antibodies as valuable neuroscience research tools versus reagents of mass distraction. J Neurosci, 26: 8017–20.
187. Sarmiere PD, Weigle CM, Tamkun MM. (2008) The Kv2 . 1 K + channel targets to the axon initial segment of hippocampal and cortical neurons in culture and in situ. BMC Neurosci, 9:112.
188. Misonou H, Mohapatra DP, Menegola M, Trimmer JS. (2005) Calcium- and metabolic state-dependent modulation of the voltage-dependent Kv2.1 channel regulates neuronal excitability in response to ischemia. J Neurosci, 25: 11184–93.
189. Dodson PD, Forsythe ID. (2004) Presynaptic K+ channels: electrifying regulators of synaptic terminal excitability. Trends Neurosci, 27: 210–7.
190. Kole MHP, Letzkus JJ, Stuart GJ. (2007) Axon initial segment Kv1 channels control axonal action potential waveform and synaptic efficacy. Neuron, 55: 633–47.
191. Shu Y, Yu Y, Yang J, McCormick DA. (2007) Selective control of cortical axonal spikes by a slowly inactivating K+ current. Proc Natl Acad Sci, 104: 11453–11458.
192. Ogawa Y, Horresh I, Trimmer JS, Bredt DS, Peles E, Rasband MN. (2008) Postsynaptic density-93 clusters Kv1 channels at axon initial segments independently of Caspr2. J Neurosci, 28: 5731–9.
193. Zuberi SM, Eunson LH, Spauschus A, De Silva R, Tolmie J, Wood NW, McWilliam RC, Stephenson JB, Stephenson JP, Kullmann DM, Hanna MG. (1999) A novel mutation in the human voltage-gated potassium channel gene (Kv1.1) associates with episodic ataxia type 1 and sometimes with partial epilepsy. Brain, 122: 817–25.
194. Storm JF. (1988) Temporal integration by a slowly inactivating K+ current in hippocampal neurons. Nature, 336: 379–81.
195. Chiu SY, Ritchie JM. (1981) Evidence for the presence of potassium channels in the paranodal region of acutely demyelinated mammalian single nerve fibres. J Physiol, 313: 415–37.

196. Veh RW, Lichtinghagen R, Sewing S, Wunder F, Grumbach IM, Pongs O. (1995) Immunohistochemical localization of five members of the Kv1 channel subunits: contrasting subcellular locations and neuron-specific co-localizations in rat brain. Eur J Neurosci, 7: 2189–205.
197. Rhodes KJ, Strassle BW, Monaghan MM, Bekele-Arcuri Z, Matos MF, Trimmer JS. (1997) Association and colocalization of the Kvbeta1 and Kvbeta2 beta-subunits with Kv1 alpha-subunits in mammalian brain K+ channel complexes. J Neurosci, 17: 8246–8258.
198. Monaghan MM, Trimmer JS, Rhodes KJ. (2001) Experimental localization of Kv1 family voltage-gated K+ channel alpha and beta subunits in rat hippocampal formation. J Neurosci, 21: 5973–5983.
199. Oertel D, Shatadal S, Cao X-J. (2008) In the ventral cochlear nucleus Kv1.1 and subunits of HCN1 are colocalized at surfaces of neurons that have low-voltage-activated and hyperpolarization-activated conductances. Neuroscience, 154: 77–86.
200. Sekirnjak C, Martone ME, Weiser M, Deerinck T, Bueno E, Rudy B, Ellisman M. (1997) Subcellular localization of the K+ channel subunit Kv3.1b in selected rat CNS neurons. Brain Res, 766: 173–87.
201. Rudy B, Chow A, Lau D, Amarillo Y, Ozaita A, Saganich M, Moreno H, Nadal MS, Hernandez-Pineda R, Hernandez-Cruz A, Erisir A, Leonard C, Vega-Saenz de Miera E. (1999) Contributions of Kv3 channels to neuronal excitability. Ann N Y Acad Sci, 868: 304–43.
202. Martina M, Schultz JH, Ehmke H, Monyer H, Jonas P. (1998) Functional and molecular differences between voltage-gated K+ channels of fast-spiking interneurons and pyramidal neurons of rat hippocampus. J Neurosci, 18: 8111–25.
203. Lien C-C, Jonas P. (2003) Kv3 potassium conductance is necessary and kinetically optimized for high-frequency action potential generation in hippocampal interneurons. J Neurosci, 23: 2058–68.
204. Baranauskas G, Tkatch T, Nagata K, Yeh JZ, Surmeier DJ. (2003) Kv3.4 subunits enhance the repolarizing efficiency of Kv3.1 channels in fast-spiking neurons. Nat Neurosci, 6: 258–66.

205. Vacher H, Mohapatra DP, Trimmer JS. (2008) Localization and targeting of voltage-dependent ion channels in mammalian central neurons. Physiol Rev, 88: 1407–47.
206. Fricker D, Miles R. (2000) EPSP amplification and the precision of spike timing in hippocampal neurons. Neuron, 28: 559–69.
207. Hu H, Martina M, Jonas P. (2010) Dendritic mechanisms underlying rapid synaptic activation of fast-spiking hippocampal interneurons. Science, 327: 52–8.
208. Chang SY, Zagha E, Kwon ES, Ozaita A, Bobik M, Martone ME, Ellisman MH, Heintz N, Rudy B. (2007) Distribution of Kv3.3 potassium channel subunits in distinct neuronal populations of mouse brain. J Comp Neurol, 502: 953–72.
209. Catterall WA. (2000) Structure and regulation of voltage-gated Ca2+ channels. Annu Rev Cell Dev Biol, 16: 521–55.
210. Catterall WA. (2011) Voltage-gated calcium channels. Cold Spring Harb Perspect Biol, 3: a003947.
211. Catterall WA, Perez-Reyes E, Snutch TP, Striessnig J. Voltage-gated calcium channels. Available at: http://www.guidetopharmacology.org/GRAC/FamilyDisplayForward?familyId=80.
212. Magee J, Hoffman D, Colbert C, Johnston D. (1998) Electrical and calcium signaling in dendrites of hippocampal pyramidal neurons. Annu Rev Physiol, 60: 327–46.
213. Christie BR, Eliot LS, Ito K, Miyakawa H, Johnston D. (1995) Different Ca2+ channels in soma and dendrites of hippocampal pyramidal neurons mediate spike-induced Ca2+ influx. J Neurophysiol, 73: 2553–7.
214. Gillessen T, Alzheimer C. (1997) Amplification of EPSPs by low Ni(2+)- and amiloride-sensitive Ca2+ channels in apical dendrites of rat CA1 pyramidal neurons. J Neurophysiol, 77: 1639–43.
215. Kavalali ET, Zhuo M, Bito H, Tsien RW. (1997) Dendritic Ca2+ channels characterized by recordings from isolated hippocampal dendritic segments. Neuron, 18: 651–63.
216. McKay BE, McRory JE, Molineux ML, Hamid J, Snutch TP, Zamponi GW, Turner RW. (2006) Ca(V)3 T-type calcium channel isoforms differentially

distribute to somatic and dendritic compartments in rat central neurons. Eur J Neurosci, 24: 2581–94.

217. Vinet J, Sík A. (2006) Expression pattern of voltage-dependent calcium channel subunits in hippocampal inhibitory neurons in mice. Neuroscience, 143: 189–212.
218. Tippens AL, Pare J-F, Langwieser N, Moosmang S, Milner TA, Smith Y, Lee A. (2008) Ultrastructural evidence for pre- and postsynaptic localization of Cav1.2 L-type Ca2+ channels in the rat hippocampus. J Comp Neurol, 506: 569–83.
219. Leitch B, Szostek A, Lin R, Shevtsova O. (2009) Subcellular distribution of L-type calcium channel subtypes in rat hippocampal neurons. Neuroscience, 164: 641–57.
220. Moreno CM, Dixon RE, Tajada S, Yuan C, Opitz-Araya X, Binder MD, Santana LF. (2016) Ca2+ entry into neurons is facilitated by cooperative gating of clustered Cav1.3 channels. Elife, 5: 1–26.
221. Timmermann DB, Westenbroek RE, Schousboe A, Catterall WA. (2002) Distribution of high-voltage-activated calcium channels in cultured gamma-aminobutyric acidergic neurons from mouse cerebral cortex. J Neurosci Res, 67: 48–61.
222. Parajuli LK, Nakajima C, Kulik A, Matsui K, Schneider T, Shigemoto R, Fukazawa Y. (2012) Quantitative regional and ultrastructural localization of the Ca(v)2.3 subunit of R-type calcium channel in mouse brain. J Neurosci, 32: 13555–67.
223. Yu Y, Maureira C, Liu X, McCormick D. (2010) P/Q and N channels control baseline and spike-triggered calcium levels in neocortical axons and synaptic boutons. J Neurosci, 30: 11858–69.
224. Callewaert G, Eilers J, Konnerth A. (1996) Axonal calcium entry during fast 'sodium' action potentials in rat cerebellar Purkinje neurones. J Physiol, 495 (Pt 3: 641–7.
225. Bender KJ, Trussell LO. (2009) Axon initial segment Ca2+ channels influence action potential generation and timing. Neuron, 61: 259–71.
226. Clapham DE. (2007) Calcium signaling. Cell, 131: 1047–58.
227. Schneggenburger R, Neher E. (2005) Presynaptic calcium and control of vesicle

fusion. Curr Opin Neurobiol, 15: 266–274.

228. Nadkarni S, Bartol TM, Sejnowski TJ, Levine H, Mcculloch AD. (2010) Modelling Vesicular Release at Hippocampal Synapses. PLoS Comput Biol, 6:
229. Wu LG, Saggau P. (1994) Pharmacological identification of two types of presynaptic voltage-dependent calcium channels at CA3-CA1 synapses of the hippocampus. J Neurosci, 14: 5613–22.
230. Wheeler D, Randall A, Tsien R. (1994) Roles of N-type and Q-type Ca2+ channels in supporting hippocampal synaptic transmission. Science, 264: 107–111.
231. Reid CA, Clements JD, Bekkers JM. (1997) Nonuniform distribution of Ca2+ channel subtypes on presynaptic terminals of excitatory synapses in hippocampal cultures. J Neurosci, 17: 2738–45.
232. Poncer JC, McKinney RA, Gähwiler BH, Thompson SM. (1997) Either N- or P-type calcium channels mediate GABA release at distinct hippocampal inhibitory synapses. Neuron, 18: 463–72.
233. Poncer JC, McKinney RA, Gahwiler BH, Thompson SM. (2000) Differential control of GABA release at synapses from distinct interneurons in rat hippocampus. J Physiol, 528 Pt 1: 123–30.
234. Ohno-Shosaku T, Hirata K, Sawada S, Yamamoto C. (1994) Contributions of multiple calcium channel types to GABAergic transmission in rat cultured hippocampal neurons. Neurosci Lett, 181: 145–8.
235. Holderith N, Lorincz A, Katona G, Rózsa B, Kulik A, Watanabe M, Nusser Z. (2012) Release probability of hippocampal glutamatergic terminals scales with the size of the active zone. Nat Neurosci, 15: 988–97.
236. Althof D, Baehrens D, Watanabe M, Suzuki N, Fakler B, Kulik Á. (2015) Inhibitory and excitatory axon terminals share a common nano-architecture of their Cav2.1 (P/Q-type) Ca2+ channels. Front Cell Neurosci, 9: 1–11.
237. Gasparini S, Kasyanov AM, Pietrobon D, Voronin LL, Cherubini E. (2001) Presynaptic R-type calcium channels contribute to fast excitatory synaptic transmission in the rat hippocampus. J Neurosci, 21: 8715–21.
238. Wormuth C, Lundt A, Henseler C, Müller R, Broich K, Papazoglou A, Weiergräber M. (2016) Review: Cav2.3 R-type voltage-gated Ca(2+) channels -

functional implications in convulsive and non-convulsive seizure activity. Open Neurol J, 10: 99–126.

239. Kimm T, Bean BP. (2014) Inhibition of A-type potassium current by the peptide toxin SNX-482. J Neurosci, 34: 9182–9.
240. Kamiya H, Sawada S, Yamamoto C. (1988) Synthetic omega-conotoxin blocks synaptic transmission in the hippocampus in vitro. Neurosci Lett, 91: 84–8.
241. Helton TD, Xu W, Lipscombe D. (2005) Neuronal L-type calcium channels open quickly and are inhibited slowly. J Neurosci, 25: 10247–51.
242. Tang A-H, Karson MA, Nagode DA, McIntosh JM, Uebele VN, Renger JJ, Klugmann M, Milner TA, Alger BE. (2011) Nerve terminal nicotinic acetylcholine receptors initiate quantal GABA release from perisomatic interneurons by activating axonal T-type (Cav3) Ca^{2+} channels and Ca^{2+} release from stores. J Neurosci, 31: 13546–61.
243. Huang Z, Lujan R, Kadurin I, Uebele VN, Renger JJ, Dolphin AC, Shah MM. (2011) Presynaptic HCN1 channels regulate Cav3.2 activity and neurotransmission at select cortical synapses. Nat Neurosci, 14: 478–86.
244. Fujiyama F, Kuramoto E, Okamoto K, Hioki H, Furuta T, Zhou L, Nomura S, Kaneko T. (2004) Presynaptic localization of an AMPA-type glutamate receptor in corticostriatal and thalamostriatal axon terminals. Eur J Neurosci, 20: 3322–30.
245. Tarusawa E, Matsui K, Budisantoso T, Molnar E, Watanabe M, Matsui M, Fukazawa Y, Shigemoto R. (2009) Input-Specific Intrasynaptic Arrangements of Ionotropic Glutamate Receptors and Their Impact on Postsynaptic Responses. J Neurosci, 29: 12896–12908.
246. Franks KM, Stevens CF, Sejnowski TJ. (2003) Independent sources of quantal variability at single glutamatergic synapses. J Neurosci, 23: 3186–3195.
247. Tang A-H, Chen H, Li TP, Metzbower SR, MacGillavry HD, Blanpied TA. (2016) A trans-synaptic nanocolumn aligns neurotransmitter release to receptors. Nature, 536: 210–4.
248. Nusser Z, Lujan R, Laube G, Roberts JD, Molnar E, Somogyi P. (1998) Cell type and pathway dependence of synaptic AMPA receptor number and variability in the hippocampus. Neuron, 21: 545–59.

249. Nusser Z. (2000) AMPA and NMDA receptors: similarities and differences in their synaptic distribution. Curr Opin Neurobiol, 10: 337–41.
250. Eggermann E, Bucurenciu I, Goswami SP, Jonas P. (2011) Nanodomain coupling between Ca^{2+} channels and sensors of exocytosis at fast mammalian synapses. Nat Rev Neurosci, 13: 7–21.
251. Scimemi A, Diamond JS. (2012) The number and organization of Ca2+ channels in the active zone shapes neurotransmitter release from Schaffer collateral synapses. J Neurosci, 32: 18157–76.
252. Sheng J, He L, Zheng H, Xue L, Luo F, Shin W, Sun T, Kuner T, Yue DT, Wu L-G. (2012) Calcium-channel number critically influences synaptic strength and plasticity at the active zone. Nat Neurosci, 15: 998–1006.
253. Keller D, Babai N, Kochubey O, Han Y, Markram H, Schürmann F, Schneggenburger R. (2015) An exclusion zone for Ca2+ channels around docked vesicles explains release control by multiple channels at a CNS synapse. PLoS Comput Biol, 11: e1004253.
254. Nakamura Y, Harada H, Kamasawa N, Matsui K, Rothman JS, Shigemoto R, Silver RA, DiGregorio DA, Takahashi T. (2015) Nanoscale distribution of presynaptic Ca(2+) channels and its impact on vesicular release during development. Neuron, 85: 145–58.
255. Fogelson AL, Zucker RS. (1985) Presynaptic calcium diffusion from various arrays of single channels. Implications for transmitter release and synaptic facilitation. Biophys J, 48: 1003–1017.
256. Simon SM, Llinás RR. (1985) Compartmentalization of the submembrane calcium activity during calcium influx and its significance in transmitter release. Biophys J, 48: 485–98.
257. Naraghi M, Neher E. (1997) Linearized buffered Ca2+ diffusion in microdomains and its implications for calculation of [Ca2+] at the mouth of a calcium channel. J Neurosci, 17: 6961–73.
258. Tóth K, McBain CJ. (2000) Target-specific expression of pre- and postsynaptic mechanisms. J Physiol, 525 Pt 1: 41–51.
259. Pelkey KA, McBain CJ. (2007) Differential regulation at functionally divergent release sites along a common axon. Curr Opin Neurobiol, 17: 366–373.

260. Branco T, Staras K. (2009) The probability of neurotransmitter release: variability and feedback control at single synapses. Nat Rev Neurosci, 10: 373–83.
261. Koester HJ, Johnston D. (2005) Target cell-dependent normalization of transmitter release at neocortical synapses. Science, 308: 863–6.
262. Biró AA, Holderith NB, Nusser Z. (2005) Quantal size is independent of the release probability at hippocampal excitatory synapses. J Neurosci, 25: 223–32.
263. Mercer A, Eastlake K, Trigg HL, Thomson AM. (2012) Local circuitry involving parvalbumin-positive basket cells in the CA2 region of the hippocampus. Hippocampus, 22: 43–56.
264. Reyes A, Lujan R, Rozov A, Burnashev N, Somogyi P, Sakmann B. (1998) Target-cell-specific facilitation and depression in neocortical circuits. Nat Neurosci, 1: 279–285.
265. Gupta A, Wang Y, Markram H. (2000) Organizing principles for a diversity of GABAergic interneurons and synapses in the neocortex. Science, 287: 273–8.
266. Markram H, Wang Y, Tsodyks M. (1998) Differential signaling via the same axon of neocortical pyramidal neurons. Proc Natl Acad Sci U S A, 95: 5323–8.
267. Markram H, Gupta A, Uziel A, Wang Y, Tsodyks M. (1998) Information processing with frequency-dependent synaptic connections. Neurobiol Learn Mem, 70: 101–12.
268. Pouille F, Scanziani M. (2004) Routing of spike series by dynamic circuits in the hippocampus. Nature, 429: 717–23.
269. Losonczy A, Somogyi P, Nusser Z. (2003) Reduction of excitatory postsynaptic responses by persistently active metabotropic glutamate receptors in the hippocampus. J Neurophysiol, 89: 1910–1919.
270. Sylwestrak EL, Ghosh A. (2012) Elfn1 regulates target-specific release probability at CA1-interneuron synapses. Science, 338: 536–40.
271. Rozov A, Burnashev N, Sakmann B, Neher E. (2001) Transmitter release modulation by intracellular Ca 2+ buffers in facilitating and depressing nerve terminals of pyramidal cells in layer 2/3 of the rat neocortex indicates a target cell-specific difference in presynaptic calcium dynamics. J Physiol, 531: 807–826.

272. Reyes A, Sakmann B. (1999) Developmental switch in the short-term modification of unitary EPSPs evoked in layer 2/3 and layer 5 pyramidal neurons of rat neocortex. J Neurosci, 19: 3827–3835.
273. Xu-Friedman MA, Harris KM, Regehr WG. (2001) Three-dimensional comparison of ultrastructural characteristics at depressing and facilitating synapses onto cerebellar Purkinje cells. J Neurosci, 21: 6666–72.
274. Hefft S, Jonas P. (2005) Asynchronous GABA release generates long-lasting inhibition at a hippocampal interneuron-principal neuron synapse. Nat Neurosci, 8: 1319–28.
275. Wilson RI, Kunos G, Nicoll RA. (2001) Presynaptic specificity of endocannabinoid signaling in the hippocampus. Neuron, 31: 453–462.
276. Zimmer AM, Zimmer AM, Hohmann AG, Herkenham M, Bonner TI. (1999) Increased mortality, hypoactivity, and hypoalgesia in cannabinoid CB1 receptor knockout mice. Proc Natl Acad Sci U S A, 96: 5780–5.
277. Berod A, Hartman BK, Pujol JF. (1981) Importance of fixation in immunohistochemistry: use of formaldehyde solutions at variable pH for the localization of tyrosine hydroxylase. J Histochem Cytochem, 29: 844–50.
278. Ino M, Yoshinaga T, Wakamori M, Miyamoto N, Takahashi E, Sonoda J, Kagaya T, Oki T, Nagasu T, Nishizawa Y, Tanaka I, Imoto K, Aizawa S, Koch S, Schwartz A, Niidome T, Sawada K, Mori Y. (2001) Functional disorders of the sympathetic nervous system in mice lacking the alpha 1B subunit (Cav 2.2) of N-type calcium channels. Proc Natl Acad Sci U S A, 98: 5323–8.
279. Iwakura A, Uchigashima M, Miyazaki T, Yamasaki M, Watanabe M. (2012) Lack of molecular-anatomical evidence for GABAergic influence on axon initial segment of cerebellar Purkinje cells by the pinceau formation. J Neurosci, 32: 9438–48.
280. Tiffany AM, Manganas LN, Kim E, Hsueh YP, Sheng M, Trimmer JS. (2000) PSD-95 and SAP97 exhibit distinct mechanisms for regulating K(+) channel surface expression and clustering. J Cell Biol, 148: 147–58.
281. Antonucci DE, Lim ST, Vassanelli S, Trimmer JS. (2001) Dynamic localization and clustering of dendritic Kv2.1 voltage-dependent potassium channels in developing hippocampal neurons. Neuroscience, 108: 69–81.

282. Barry J, Xu M, Gu Y, Dangel AW, Jukkola P, Shrestha C, Gu C. (2013) Activation of conventional kinesin motors in clusters by Shaw voltage-gated K+ channels. J Cell Sci, 126: 2027–2041.
283. Mansouri M, Kasugai Y, Fukazawa Y, Bertaso F, Raynaud F, Perroy J, Fagni L, Kaufmann WA, Watanabe M, Shigemoto R, Ferraguti F. (2015) Distinct subsynaptic localization of type 1 metabotropic glutamate receptors at glutamatergic and GABAergic synapses in the rodent cerebellar cortex. Eur J Neurosci, 41: 157–167.
284. Briatore F, Patrizi A, Viltono L, Sassoè-Pognetto M, Wulff P. (2010) Quantitative organization of GABAergic synapses in the molecular layer of the mouse cerebellar cortex. PLoS One, 5: e12119.
285. Schafer DP, Bansal R, Hedstrom KL, Pfeiffer SE, Rasband MN. (2004) Does paranode formation and maintenance require partitioning of neurofascin 155 into lipid rafts? J Neurosci, 24: 3176–85.
286. Van Wart A, Trimmer JS, Matthews G. (2007) Polarized distribution of ion channels within microdomains of the axon initial segment. J Comp Neurol, 500: 339–52.
287. Von Kriegstein K, Schmitz F, Link E, Südhof TC. (1999) Distribution of synaptic vesicle proteins in the mammalian retina identifies obligatory and facultative components of ribbon synapses. Eur J Neurosci, 11: 1335–48.
288. Johnson SL, Franz C, Kuhn S, Furness DN, Rüttiger L, Münkner S, Rivolta MN, Seward EP, Herschman HR, Engel J, Knipper M, Marcotti W. (2010) Synaptotagmin IV determines the linear Ca2+ dependence of vesicle fusion at auditory ribbon synapses. Nat Neurosci, 13: 45–52.
289. Gallart-Palau X, Tarabal O, Casanovas A, Sábado J, Correa FJ, Hereu M, Piedrafita L, Calderó J, Esquerda JE. (2014) Neuregulin-1 is concentrated in the postsynaptic subsurface cistern of C-bouton inputs to α-motoneurons and altered during motoneuron diseases. FASEB J, 28: 3618–32.
290. Lenkey N, Kirizs T, Holderith N, Máté Z, Szabó G, Vizi ES, Hájos N, Nusser Z. (2015) Tonic endocannabinoid-mediated modulation of GABA release is independent of the CB1 content of axon terminals. Nat Commun, 6: 6557.
291. Veatch SL, Machta BB, Shelby SA, Chiang EN, Holowka DA, Baird BA. (2012)

Correlation functions quantify super-resolution images and estimate apparent clustering due to over-counting. PLoS One, 7: e31457.

292. Kordeli E, Lambert S, Bennett V. (1995) AnkyrinG: A new ankyrin gene with neural-specific isoforms localized at the axonal initial segment and node of ranvier. *Journal of Biological Chemistry* 270: 2352–2359.
293. Kasugai Y, Swinny JD, Roberts JDB, Dalezios Y, Fukazawa Y, Sieghart W, Shigemoto R, Somogyi P. (2010) Quantitative localisation of synaptic and extrasynaptic GABAA receptor subunits on hippocampal pyramidal cells by freeze-fracture replica immunolabelling. Eur J Neurosci, 32: 1868–1888.
294. Éltes T, Kirizs T, Nusser Z, Holderith N. (2017) Target cell type-dependent differences in Ca(2+) channel function underlie distinct release probabilities at hippocampal glutamatergic terminals. J Neurosci, 37: 1910–1924.
295. Takács VT, Szőnyi A, Freund TF, Nyiri G, Gulyás AI. (2015) Quantitative ultrastructural analysis of basket and axo-axonic cell terminals in the mouse hippocampus. Brain Struct Funct, 220: 919–940.
296. Szabó GG, Lenkey N, Holderith N, Andrási T, Nusser Z, Hájos N. (2014) Presynaptic calcium channel inhibition underlies CB_1 cannabinoid receptor-mediated suppression of GABA release. J Neurosci, 34: 7958–63.
297. Kerr AM, Reisinger E, Jonas P. (2008) Differential dependence of phasic transmitter release on synaptotagmin 1 at GABAergic and glutamatergic hippocampal synapses. Proc Natl Acad Sci U S A, 105: 15581–6.
298. Bragina L, Fattorini G, Giovedí S, Melone M, Bosco F, Benfenati F, Conti F. (2011) Analysis of synaptotagmin, SV2, and Rab3 expression in cortical glutamatergic and GABAergic axon terminals. Front Cell Neurosci, 5: 32.
299. Sommeijer JP, Levelt CN. (2012) Synaptotagmin-2 is a reliable marker for parvalbumin positive inhibitory boutons in the mouse visual cortex. PLoS One, 7: 1–12.
300. McIntosh P, Southan AP, Akhtar S, Sidera C, Ushkaryov Y, Dolly JO, Robertson B. (1997) Modification of rat brain Kv1.4 channel gating by association with accessory Kvbeta1.1 and beta2.1 subunits. Pflugers Arch, 435: 43–54.
301. Manganas LN, Trimmer JS. (2000) Subunit composition determines Kv1

potassium channel surface expression. J Biol Chem, 275: 29685–93.

302. Wang H, Kunkel DD, Martin TM, Schwartzkroin PA, Tempel BL. (1993) Heteromultimeric K+ channels in terminal and juxtaparanodal regions of neurons. Nature, 365: 75–79.
303. Malin SA, Nerbonne JM. (2002) Delayed rectifier K+ currents, IK, are encoded by Kv2 alpha-subunits and regulate tonic firing in mammalian sympathetic neurons. J Neurosci, 22: 10094–105.
304. Mulholland PJ, Carpenter-Hyland EP, Hearing MC, Becker HC, Woodward JJ, Chandler LJ. (2008) Glutamate transporters regulate extrasynaptic NMDA receptor modulation of Kv2.1 potassium channels. J Neurosci, 28: 8801–9.
305. Garrido JJ, Giraud P, Carlier E, Fernandes F, Moussif A, Fache M-P, Debanne D, Dargent B. (2003) A targeting motif involved in sodium channel clustering at the axonal initial segment. Science, 300: 2091–4.
306. Pan Z, Kao T, Horvath Z, Lemos J, Sul J-Y, Cranstoun SD, Bennett V, Scherer SS, Cooper EC. (2006) A common ankyrin-G-based mechanism retains KCNQ and NaV channels at electrically active domains of the axon. J Neurosci, 26: 2599–613.
307. Inda MC, DeFelipe J, Muñoz A. (2006) Voltage-gated ion channels in the axon initial segment of human cortical pyramidal cells and their relationship with chandelier cells. Proc Natl Acad Sci U S A, 103: 2920–5.
308. Duflocq A, Chareyre F, Giovannini M, Couraud F, Davenne M. (2011) Characterization of the axon initial segment (AIS) of motor neurons and identification of a para-AIS and a juxtapara-AIS, organized by protein 4.1B. BMC Biol, 9: 66.
309. Lörincz A, Notomi T, Tamás G, Shigemoto R, Nusser Z. (2002) Polarized and compartment-dependent distribution of HCN1 in pyramidal cell dendrites. Nat Neurosci, 5: 1185–93.
310. Kirizs T, Kerti-Szigeti K, Lorincz A, Nusser Z. (2014) Distinct axo-somato-dendritic distributions of three potassium channels in CA1 hippocampal pyramidal cells. Eur J Neurosci, 39: 1771–1783.
311. Chen X, Johnston D. (2005) Constitutively active G-protein-gated inwardly rectifying K+ channels in dendrites of hippocampal CA1 pyramidal neurons. J

Neurosci, 25: 3787–92.

312. Carbone E, Calorio C, Vandael DHF. (2014) T-type channel-mediated neurotransmitter release. Pflugers Arch, 466: 677–87.
313. Buraei Z, Yang J. (2010) The ß subunit of voltage-gated Ca2+ channels. Physiol Rev, 90: 1461–506.
314. Zhong H, Yokoyama CT, Scheuer T, Catterall WA. (1999) Reciprocal regulation of P/Q-type Ca2+ channels by SNAP-25, syntaxin and synaptotagmin. Nat Neurosci, 2: 939–41.
315. Calloway N, Gouzer G, Xue M, Ryan TA. (2015) The active-zone protein Munc13 controls the use-dependence of presynaptic voltage-gated calcium channels. Elife, 4: 1–15.
316. Bean BP. (1989) Neurotransmitter inhibition of neuronal calcium currents by changes in channel voltage dependence. Nature, 340: 153–6.
317. Dittman JS, Regehr WG. (1996) Contributions of calcium-dependent and calcium-independent mechanisms to presynaptic inhibition at a cerebellar synapse. J Neurosci, 16: 1623–33.
318. Takahashi T, Forsythe ID, Tsujimoto T, Barnes-Davies M, Onodera K. (1996) Presynaptic calcium current modulation by a metabotropic glutamate receptor. Science, 274: 594–7.
319. Leão RM, Von Gersdorff H. (2002) Noradrenaline increases high-frequency firing at the calyx of Held synapse during development by inhibiting glutamate release. J Neurophysiol, 87: 2297–306.
320. Brown SP, Safo PK, Regehr WG. (2004) Endocannabinoids inhibit transmission at granule cell to Purkinje cell synapses by modulating three types of presynaptic calcium channels. J Neurosci, 24: 5623–31.
321. Kupferschmidt DA, Lovinger DM. (2015) Inhibition of presynaptic calcium transients in cortical inputs to the dorsolateral striatum by metabotropic GABA $_B$ and mGlu2/3 receptors. J Physiol, 593: 2295–2310.
322. Anderson GR, Aoto J, Tabuchi K, Földy C, Covy J, Yee AX, Wu D, Lee S-J, Chen L, Malenka RC, Südhof TC. (2015) β-Neurexins control neural circuits by regulating synaptic endocannabinoid signaling. Cell, 162: 593–606.
323. Su SC, Seo J, Pan JQ, Samuels BA, Rudenko A, Ericsson M, Neve RL, Yue DT,

Tsai L-H. (2012) Regulation of N-type voltage-gated calcium channels and presynaptic function by cyclin-dependent kinase 5. Neuron, 75: 675–87.

324. Kim SH, Ryan TA. (2013) Balance of calcineurin Aα and CDK5 activities sets release probability at nerve terminals. J Neurosci, 33: 8937–50.
325. Neher E. (1998) Vesicle pools and Ca2+ microdomains: New tools for understanding their roles in neurotransmitter release. Neuron, 20: 389–399.
326. Tomioka NH, Yasuda H, Miyamoto H, Hatayama M, Morimura N, Matsumoto Y, Suzuki T, Odagawa M, Odaka YS, Iwayama Y, Won Um J, Ko J, Inoue Y, Kaneko S, Hirose S, Yamada K, Yoshikawa T, Yamakawa, Aruga J. (2014) Elfn1 recruits presynaptic mGluR7 in trans and its loss results in seizures. Nat Commun, 5: 4501.
327. Buchanan KA, Blackman A V., Moreau AW, Elgar D, Costa RP, Lalanne T, Tudor Jones AA, Oyrer J, Sjöström PJ. (2012) Target-specific expression of presynaptic NMDA receptors in neocortical microcircuits. Neuron, 75: 451–66.
328. Jackman SL, Turecek J, Belinsky JE, Regehr WG. (2016) The calcium sensor synaptotagmin 7 is required for synaptic facilitation. Nature, 529: 88–91.
329. Schlüter OM, Schmitz F, Jahn R, Rosenmund C, Südhof TC. (2004) A complete genetic analysis of neuronal Rab3 function. J Neurosci, 24: 6629–37.
330. Schlüter OM, Basu J, Südhof TC, Rosenmund C. (2006) Rab3 superprimes synaptic vesicles for release: implications for short-term synaptic plasticity. J Neurosci, 26: 1239–46.
331. Ishiyama S, Schmidt H, Cooper BH, Brose N, Eilers J. (2014) Munc13-3 superprimes synaptic vesicles at granule cell-to-basket cell synapses in the mouse cerebellum. J Neurosci, 34: 14687–96.
332. Körber C, Horstmann H, Venkataramani V, Herrmannsdörfer F, Kremer T, Kaiser M, Schwenger DB, Ahmed S, Dean C, Dresbach T, Kuner T. (2015) Modulation of presynaptic release probability by the Vvertebrate-specific protein Mover. Neuron, 87: 521–33.
333. Böhme MA, Beis C, Reddy-Alla S, Reynolds E, Mampell MM, Grasskamp AT, Lützkendorf J, Bergeron DD, Driller JH, Babikir H, Göttfert F, Robinson IM, O'Kane CJ, Hell SW, Wahl MC, Stelzl U, Loll B, Walter AM, Sigrist SJ. (2016) Active zone scaffolds differentially accumulate Unc13 isoforms to tune Ca(2+)

channel-vesicle coupling. Nat Neurosci, 19: 1311–20.

334. Wu LG, Westenbroek RE, Borst JG, Catterall WA, Sakmann B. (1999) Calcium channel types with distinct presynaptic localization couple differentially to transmitter release in single calyx-type synapses. J Neurosci, 19: 726–36.
335. Nyíri G, Cserép C, Szabadits E, Mackie K, Freund TF. (2005) CB1 cannabinoid receptors are enriched in the perisynaptic annulus and on preterminal segments of hippocampal GABAergic axons. Neuroscience, 136: 811–822.
336. Losonczy A, Biró AA, Nusser Z. (2004) Persistently active cannabinoid receptors mute a subpopulation of hippocampal interneurons. Proc Natl Acad Sci U S A, 101: 1362–1367.
337. Lee S-H, Földy C, Soltesz I. (2010) Distinct endocannabinoid control of GABA release at perisomatic and dendritic synapses in the hippocampus. J Neurosci, 30: 7993–8000.
338. Ali AB. (2011) CB1 modulation of temporally distinct synaptic facilitation among local circuit interneurons mediated by N-type calcium channels in CA1. J Neurophysiol, 105: 1051–1062.
339. Zhang W, Linden DJ. (2009) Neuromodulation at single presynaptic boutons of cerebellar parallel fibers is determined by bouton size and basal action potential-evoked Ca transient amplitude. J Neurosci, 29: 15586–94.
340. Dudok B, Barna L, Ledri M, Szabó SI, Szabadits E, Pintér B, Woodhams SG, Henstridge CM, Balla GY, Nyilas R, Varga C, Lee S-H, Matolcsi M, Cervenak J, Kacskovics I, Watanabe M, Sagheddu C,Melis M, Pistis M, Soltesz I, Katona I. (2015) Cell-specific STORM super-resolution imaging reveals nanoscale organization of cannabinoid signaling. Nat Neurosci, 18: 75–86.
341. Mikasova L, Groc L, Choquet D, Manzoni OJ. (2008) Altered surface trafficking of presynaptic cannabinoid type 1 receptor in and out synaptic terminals parallels receptor desensitization. Proc Natl Acad Sci U S A, 105: 18596–601.

DOI:10.14753/SE.2018.2123

11. Bibliography of the candidate's publications

1. **Kirizs T**, Kerti-Szigeti K, Lorincz A, Nusser Z. (2014) Distinct axo-somato-dendritic distributions of three potassium channels in CA1 hippocampal pyramidal cells. Eur J Neurosci, 39: 1771–1783.

2. Lenkey N, **Kirizs T**, Holderith N, Máté Z, Szabó G, Vizi ESz, Hájos N, Nusser Z. (2015) Tonic endocannabinoid-mediated modulation of GABA release is independent of the CB1 content of axon terminals. Nat Commun, 6: 6557.

3. Éltes T[1], **Kirizs T**[1], Nusser Z, Holderith N. (2017) Target cell type-dependent differences in Ca(2+) channel function underlie distinct release probabilities at hippocampal glutamatergic terminals. J Neurosci, 37: 1910–1924.

[1] equal contribution

DOI:10.14753/SE.2018.2123

12. Acknowledgments

Above all, I would like to thank my supervisor, Prof. Zoltán Nusser for being a mentor for me. I would like to thank him for giving me the opportunity to join his research group, and for his patient guidance, constant encouragement and motivation over these years.

My deep appreciation goes out to Dr. Andrea Lőrincz for introducing me to the wonders of the 'SDS-digested freeze-fracture replica labeling' method, and for her valuable advice and inspiration. I am also indebted to Dr. Máté Sümegi for his teachings on molecular biology techniques.

I express my gratitude to present and former members of the Laboratory of Cellular Neurophysiology for providing a friendly and stimulating environment. Special thanks to my collaborators, Dr. Tímea Éltes, Dr. Noémi Holderith, Dr Kerti-Szigeti Katalin, Dr. Nóra Lenkey and Miklós Szoboszlay for the constant drive and the inspiring discussions. I am thankful to Éva Dóbai, Bence Kókay and Dóra Rónaszéki for their excellent technical assistance during many years.

Here I also would like to thank Prof. Tibor Szilágyi, who was my supervisor during my undergraduate years at the University of Medicine and Pharmacy Tirgu Mures, and who introduced me to the field of neuroscience.

I am grateful to my parents and my brother, Róbert, for their love and support in my choice. My greatest thanks goes to my mother, who always unconditionally believed in me.

Last but not least, I am especially grateful to my husband, Zsolt Szövérfi, for his encouragement, understanding and unceasing support throughout these years.